

Lateral Diffusion Processes in Biomimetic Polymer Membranes

Inauguraldissertation

zur Erlangung der Würde eines Doktors der Philosophie

vorgelegt der

Philosophisch-Naturwissenschaftlichen Fakultät

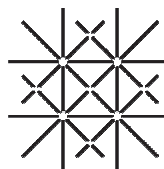
der Universität Basel

von

Fabian Itel

aus Basadingen, TG

Basel, 2015



**UNI
BASEL**

Originaldokument gespeichert auf dem Dokumentenserver der Universität Basel

edoc.unibas.ch



Dieses Werk ist unter dem Vertrag „Creative Commons Namensnennung-Keine kommerzielle Nutzung-Keine Bearbeitung 3.0 Schweiz“ (CC BY-NC-ND 3.0 CH) lizenziert. Die vollständige

Lizenz kann unter

creativecommons.org/licenses/by-nc-nd/3.0/ch/

eingesehen werden.

Genehmigt von der Philosophisch-Naturwissenschaftlichen Fakultät

auf Antrag von

Prof. Dr. Wolfgang P. Meier

(Universität Basel)

Fakultätsverantwortlicher / Dissertationsleiter

Prof. Dr. Nico Bruns

(Université Fribourg)

Korreferent

Basel, den 21. April 2015

Prof. Dr. Jörg Schibler

Dekan



Attribution-NonCommercial-NoDerivatives 4.0 International (CC BY-NC-ND 4.0)

You are free to:



Share — copy and redistribute the material in any medium or format.

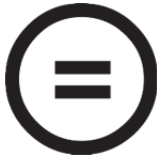
Under the following terms:



Attribution — You must give appropriate credit, provide a link to the license, and indicate if changes were made. You may do so in any reasonable manner, but not in any way that suggests the licensor endorses you or your use



Non Commercial — You may not use the material for commercial purposes.



No Derivatives — If you remix, transform, or build upon the material, you may not distribute the modified material.

No additional restrictions — You may not apply legal terms or technological measures that legally restrict others from doing anything the license permits

Notices:

You do not have to comply with the license for elements of the material in the public domain or where your use is permitted by an applicable exception or limitation

No warranties are given. The license may not give you all of the permissions necessary for your intended use. For example, other rights such as publicity, privacy, or moral rights may limit how you use the material

Summary

Molecular self-assembly offers an important bottom-up approach to generate new materials with great potential for applications in nano-, life- and medical- sciences and engineering. The interest in “soft” materials suitable for the generation of artificial, biomimetic membranes has increased rapidly over the last years. These membranes combine the advantages of specificity and efficiency found in nature and the robustness and stability of synthetic materials from polymer science. There are currently two approaches to design biomimetic membranes. One uses natural phospholipids, while the other one uses synthetic lipid mimics as the advanced alternative, which have shown great mechanical and chemical stability compared to their natural counterparts. This is important for technological application where durable devices are required. Biological membrane proteins, which provide selective and very efficient membrane transport, can be inserted into these synthetic block copolymer membranes. This combination of a synthetic membrane with biological membrane proteins is an intriguing phenomenon because the fundamental requirements for successful insertion are still matter of debate. One important issue is that polymeric membranes have thicknesses that exceed the height of the membrane proteins by several factors and the two lengths actually do not match. However, this significant height mismatch can be overcome by choosing a polymer with high flexibility, which has been shown to allow membrane proteins insertion in their active conformation. Flexibility and fluidity are essential membrane properties allowing successful generation of biomimetic membranes.

In this thesis, the fluid properties of synthetic membranes composed of synthetic amphiphiles are studied based on a large library of block copolymers. These consist of poly(2-methyloxazoline) (PMOXA) and poly(dimethylsiloxane) (PDMS) and are used as diblock (PMOXA-*b*-PDMS, AB) and triblock (PMOXA-*b*-PDMS-*b*-PMOXA, ABA) copolymers. Variation of the molecular weight induces changes in the membrane

thickness and thus the fluidity of the membrane. The diffusion of membrane proteins within synthetic triblock copolymer membranes was investigated. The study revealed that the membrane proteins are mobile even at hydrophobic mismatches of up to 7 nm, which is a factor of seven compared to mismatches existing in biological membranes. The advantage of PDMS-containing block copolymers is their enormous flexibility even at high molecular weights, which provides a similar membrane environment compared to biological phospholipid membranes. This explains and displays the ability of PDMS to compress in contact to membrane proteins. Their diffusion decreases steadily with increasing thickness mismatch.

The importance of a very flexible polymer for the generation of biomimetic membranes was elucidated for membrane protein insertion, such as PDMS, which offers high fluidity and high membrane stability within membranes with even large thicknesses. The properties of these synthetic membranes investigated here, *i.e.* fluidity, lateral diffusion and membrane thickness, are important for the generation of biomimetic membranes for technological applications.

Zusammenfassung

Molekulare Selbstorganisation bietet einen wichtigen Bottom-up-Ansatz, um neue Materialien mit grossem Potenzial für Anwendungen in der Nanowissenschaften, Lifesciences, Biomedizin und Ingenieurwissenschaften zu erzeugen. Das Interesse an "weichen" Materialien für die Herstellung von künstlichen, biomimetischen Membranen hat in den letzten Jahren stetig zugenommen. Diese Membranen kombinieren die Vorteile der Spezifität und Effizienz aus der Natur und der Widerstandsfähigkeit und Stabilität synthetischer Materialien aus den Polymerwissenschaften. Momentan gibt es verschiedene Ansätze zur Herstellung von biomimetischen Membranen. Einerseits werden biologische Lipide benutzt, zum anderen die synthetischen, lipid-imitierenden Polymere, welche durch ihre mechanischen und chemischen Eigenschaften immense Vorteile im Vergleich zu ihren natürlichen Gegenstücken bringen. Dies ist wichtig für technologische Anwendungen, wo langlebige Produkte gefordert sind. Die Möglichkeit, biologische Membranproteine, die einen selektiven und sehr effizienten Membrantransport erreichen, in diese synthetischen Membranen einzufügen ist ein faszinierendes Phänomen. Wenn solche Membranproteine, die optimal an ihre natürliche Phospholipid-Membran Umgebung angepasst sind, in dicken Polymermembranen eingebettet sind, entsteht ein grosser Unterschied zwischen der Höhe der Membranproteine und der Dicke der Membran auf. Um sich diesem erheblichen Höhenunterschied anzupassen, sind Flexibilität und Fluidität der Membran eine wesentliche Eigenschaft, welche es erst ermöglicht, biologische Membranproteine aufzunehmen.

In dieser Arbeit werden die Fluiditätseigenschaften von synthetischen Membranen aus selbstorganisierten amphiphilen Polymeren mittels einer grossen Anzahl an verschiedenen Blockcopolymeren untersucht. Diese bestehen aus Poly(2-methyloxazoline) (PMOXA und poly(dimethylsiloxane) (PDMS) und werden als Diblock- (PMOXA-b-PDMS, AB)

und Triblock- (PMOXA-*b*-PDMS-*b*-PMOXA, ABA) Copolymere benutzt. Durch das Variieren des Molekulargewichts der Amphiphile ändert sich die Membrandicke und damit die Fluidität der Membran. Der Vorteil der PDMS-Blockcopolymere ist deren hohe Flexibilität auch bei hohen Molekulargewichten, die eine ähnliche Membranumgebung bieten wie biologische Lipidmembranen. In einer zweiten Studie wurde die Diffusion von Membranproteinen in synthetischen Triblockcopolymermembranen untersucht. Die Studie zeigt, dass die Membranproteine trotz einem Dickeunterschied von bis zu sieben Nanometern immer noch mobil sind, allerdings nimmt deren Mobilität mit zunehmendem Dickeunterschied deutlich ab. Dies erläutert und zeigt die Fähigkeit von PDMS, sich in direktem Kontakt zu den Membranproteinen zu komprimieren.

Diese Arbeit zeigt, wie wichtig ein sehr flexibles Polymer, wie zum Beispiel PDMS, zur Einbringung von Membranproteinen ist, während es gleichzeitig eine hohe Membranstabilität durch die grossen Membrandicken erreicht. Die gezeigten Eigenschaften dieser synthetischen Membranen, das heisst deren Fluidität, laterale Diffusion, Membrandicke, *etc.*, sind wichtig für die Herstellung von biomimetischen Membranen für technologische Anwendungen.

Content

Summary	I
Zusammenfassung	III
Content	V
List of Figures	VIII
List of Tables	XI
Abbreviations	XII

Chapter 1

1 Introduction	1
1.1 Protein-polymer hybrid materials for technological and biomedical applications	1
1.2 Aim of the thesis	2
1.3 Structure of the thesis	3
1.4 Membranes	3
1.4.1 Building blocks of membranes	4
1.4.2 Biological membranes	5
1.4.3 Biomimetic membranes	7
1.4.4 Supramolecular assemblies to characterize biomimetic membranes	8
1.4.5 Amphiphilic block copolymers used in this thesis	8
1.4.6 Membrane protein insertion into block copolymer membranes	10
1.5 Self-assembly principle of amphiphilic macromolecules	13
1.5.1 Thermodynamic forces driving self-assembly	13
1.5.2 Geometrical considerations driving self-assembly	14
1.6 Block copolymer membrane properties	16
1.6.1 Membrane structure	16
1.6.2 Membrane thickness	17
1.6.3 Membrane stability	18

1.6.4	Membrane fluidity.....	18
1.6.5	Membrane permeability.....	19
1.7	Examples of biomimetic membranes.....	20
1.7.1	Membranes with selective permeability.....	21
1.7.2	Nanoreactors.....	22

Chapter 2

2	Fundamental theories and characterisation methods.....	25
2.1	Fundamentals of molecular diffusion.....	25
2.1.1	Brownian motion and diffusion.....	25
2.1.2	Anomalous diffusion.....	27
2.1.3	Saffman-Delbrück equation.....	28
2.2	Measuring lateral diffusion of macromolecules.....	29
2.2.1	Methods of lateral diffusion measurements.....	29
2.2.2	Fluorescence labelling.....	30
2.3	Fluorescence correlation spectroscopy (FCS).....	31
2.3.1	Basic principle of FCS.....	31
2.3.2	Molecule statistics.....	33
2.4	Z-scan FCS.....	36
2.4.1	Principle of z-scan FCS.....	36
2.4.2	FCS diffusion law.....	37

Chapter 3

3	Molecular organization and dynamics in polymersome membranes: A lateral diffusion study.....	39
3.1	Problem definition.....	39
3.2	Results and discussion.....	42
3.2.1	Amphiphilic block copolymers and self-assembly.....	42
3.2.2	Membrane thickness and molecular weight dependence.....	45
3.2.3	Fluorescent labelling of the polymers.....	50
3.2.4	GUV formation and immobilization.....	52
3.2.5	Z-scan FCS measurements.....	54
3.2.6	Molecular weight dependence of lateral diffusion.....	55

3.2.7	Existence of membrane inhomogeneities.....	59
3.2.8	Membrane viscosity.....	62
3.3	Conclusion.....	64

Chapter 4

4	Dynamics of membrane proteins within synthetic polymer membranes with large hydrophobic mismatch.....	67
4.1	Problem definition.....	67
4.2	Results and discussion.....	70
4.2.1	Lipids and amphiphilic block copolymers.....	70
4.2.2	Expected hydrophobic mismatch.....	71
4.2.3	Membrane proteins and labelling.....	73
4.2.4	GUV formation and immobilization.....	75
4.2.5	Membrane protein diffusion in lipid bilayers.....	77
4.2.6	Interaction of dye with polymer membrane.....	79
4.2.7	Membrane protein diffusion in block copolymer membranes.....	80
4.2.8	Membrane protein insertion efficiency.....	84
4.2.9	Structural meaning of membrane protein diffusion.....	86
4.3	Conclusion.....	89

Chapter 5

5	General conclusion and outlook.....	91
----------	--	-----------

Chapter 6

6	Experimental section.....	95
----------	----------------------------------	-----------

Chapter 7

7	Bibliography.....	105
----------	--------------------------	------------

Acknowledgments.....	121
-----------------------------	------------

List of Figures

Figure 1.1.	Amphiphilic block copolymer arrangements.....	5
Figure 1.2.	Schematic representation of a biological membrane.....	6
Figure 1.3.	Schematic representation of a biomimetic membrane.	8
Figure 1.4.	Chemical composition of the amphiphilic diblock and triblock copolymers, and the natural phospholipid POPC used in this thesis.....	9
Figure 1.5.	Hydrophobic mismatch between membrane proteins and block copolymer membrane.....	12
Figure 1.6.	Thermodynamic forces driving the self-assembly process of amphiphilic molecules.....	14
Figure 1.7.	Geometrical consideration of the self-assembly process.....	15
Figure 1.8.	Membrane conformation of AB, ABA and ABC block copolymers.....	17
Figure 1.9.	Applications of biomimetic membranes.....	21
Figure 2.1.	Simulated trajectories of random walks in a 2D system.....	26
Figure 2.2.	The hydrodynamic model proposed by Saffman and Delbrück.....	28
Figure 2.3.	Principle of lateral diffusion measurement of diffusing membrane components based on fluorescence correlation spectroscopy (FCS).....	31
Figure 2.4.	Principle of FCS.....	32
Figure 2.5.	Autocorrelation function of diffusing particles analysed by FCS.....	34
Figure 2.6.	Principle of z-scan FCS on a membrane to determine lateral diffusion coefficients.....	37
Figure 2.7.	Examples of the FCS diffusion law.....	38
Figure 3.1.	Schematic representation of lateral diffusion of amphiphilic block copolymer macromolecules that self-assemble into membranes.....	41
Figure 3.2.	Representative cryo-TEM images of all block copolymers.....	44
Figure 3.3.	Membrane thickness calculation.....	45
Figure 3.4.	Systematic view of membrane thicknesses.....	46

Figure 3.5.	Power law dependence of the membrane thickness on the hydrophobic molecular weight of the PDMS block.....	47
Figure 3.6.	Change in power law dependence of the membrane thickness on the hydrophobic molecular weight of the PDMS block.....	47
Figure 3.7.	Comparison of the membrane thickness of diblocks and triblock copolymer membrane.....	49
Figure 3.8.	Cryo-TEM images of lipid and diblock bilayer structures.....	49
Figure 3.9.	Excitation and emission spectra of the SRB-labelled block copolymers.....	51
Figure 3.10.	Visualization of polymeric GUVs on the example of $A_7B_{49}A_7$ triblock copolymer.....	53
Figure 3.11.	Z-scan FCS data plots of all block copolymers.....	56
Figure 3.12.	Log-log plots of diffusion coefficients D versus molecular weight of PDMS M_{PDMS} (A), membrane thickness d (B) and degree of polymerization Y (C).....	57
Figure 3.13.	Autocorrelation functions of a diblock (A_6B_{22}) and a triblock ($A_6B_{44}A_6$) copolymer.....	59
Figure 3.14.	Experimental FCS diffusion laws obtained for diblock and triblock copolymers.....	60
Figure 3.15.	Z-scan FCS data of Rhod-PE in a POPC phospholipid bilayer.....	61
Figure 4.1.	Schematic representation of the measurement principle and hydrophobic mismatch.....	70
Figure 4.2.	Theoretical hydrophobic mismatch existing in the membranes.	72
Figure 4.3.	Crystal-structures of the membrane proteins used in this study.....	73
Figure 4.4.	Membrane protein purification and labelling.....	74
Figure 4.5.	Imaging of block copolymers GUVs with inserted membrane proteins.....	76
Figure 4.6.	Protein aggregation in block copolymer membrane.....	77

Figure 4.7.	Membrane protein diffusion within lipid GUVs determined by z-scan FCS.....	78
Figure 4.8.	Saffman-Delbrück model (dashed line) of membrane protein diffusion within POPC GUVs.....	79
Figure 4.9.	Z-scan FCS data and FCS law of A ₇ B ₄₉ A ₇ membrane.....	80
Figure 4.10.	Z-scan FCS data of KcsA-, AqpZ- and OmpF-diffusion within polymeric GUVs.....	82
Figure 4.11.	Log-log plots of the diffusion coefficient D in relation to the membrane thickness d	83
Figure 4.12.	Size-dependent (radius) lateral diffusion of KcsA, AqpZ and OmpF within different membrane systems.....	84
Figure 4.13.	Dependence of the relative diffusion coefficients on the hydrophobic mismatch of membrane proteins diffusing within lipid and triblock copolymer membranes.....	86
Figure 6.1.	Determination of the LSM-FCS offset.....	102

List of Tables

Table 1.1.	Summary of published studies of membrane protein insertion into block copolymer membranes.....	11
Table 3.1.	Molecular characteristics of amphiphilic triblock and diblock copolymers.....	42
Table 3.2.	Statistical significance of membrane thickness determination for all block copolymer membranes.....	46
Table 3.3.	Absorption-, emission-, and diffusion analysis of the SRB-labelled triblock and diblock copolymers, and Rhodamine B labelled lipid (Rhod-PE).....	51
Table 3.4.	Molecular composition of the membranes mixtures used for the lateral diffusion measurements.....	52
Table 3.5.	Membrane properties of self-assembled triblock and diblock copolymers, and lipids.....	55
Table 3.6.	Overview of effective diffusion coefficient calculation.....	62
Table 3.7.	Calculation of membrane viscosities by the Saffman-Delbrück equation.....	63
Table 4.1.	Molecular characteristics of the triblock copolymers and lipid.....	71
Table 4.2.	Theoretical hydrophobic mismatch expected to exist in the different membranes.....	72
Table 4.3.	Diffusion coefficients of membrane proteins within POPC GUVs.....	78
Table 4.4.	Diffusion coefficients of membrane proteins within triblock copolymer GUVs.....	81
Table 4.5.	Calculation of membrane protein incorporation efficiencies into GUVs.....	85
Table 4.6.	Effective diffusion coefficient (D_{eff}) calculation using FCS diffusion law.....	87
Table 6.1.	List of amphiphilic block copolymers and lipids used in this thesis.....	97
Table 6.2.	List of labelled polymers and lipids used in this thesis.....	97

Abbreviations

%	Percent
°C	Degree Celsius
Å	Angstrom
a_0	Mean molecular area
AQP-0	Aquaporin0
AqpZ	AquaporinZ
ATP	Adenosine triphosphate
b	Segment length
Bodipy	Boron-dipyrromethene
bR	Purple membrane H ⁺ pump bacteriorhodopsin
C	Concentration
CHCl ₃	Chloroform
CLSM	Confocal laser scanning microscope
cmc	Critical micellar concentration
CPM	Counts per molecule
Cryo-TEM	Cryogenic-transmission electron microscopy
CTF	Contrast transfer function
D	Diffusion coefficient
D_{eff}	Effective diffusion coefficient
D_{MP}	Membrane protein diffusion coefficient
d	Membrane thickness
Da	Dalton
DMSO	Dimethyl sulfoxide
DNA	Desoxyribonucleic acid
ESR	Electron spin resonance
EtOH	Ethanol
f	Ratio
$f_{\text{hydrophilic}}$	Hydrophilic to hydrophobic weight ratio
$f_{\text{hydrophobic}}$	Hydrophobic to hydrophilic weight ratio
FhuA	Ferrichrome outer membrane transporter
fL	Femtoliter
FRAP	Fluorescence recovery after photobleaching
FCS	Fluorescence correlation spectroscopy
G	Autocorrelation amplitude
gA	Gramicidin
GFP	Green fluorescent protein
GPC	Gel permeation chromatography
GUV	Giant unilamellar vesicle
hAqp1	Human Aquaporin 1
He-Ne	Helium-Neon
Hepes	4-(2-hydroxyethyl)-1-piperazineethanesulfonic acid
Hz	Hertz
ITO	Indium tin oxide
k_B	Boltzmann constant
KcsA	Potassium crystallographically-sited activation channel
kDa	Kilo Dalton
kHz	Kilo Hertz

LamB	Maltoporin membrane protein
l_c	Critical length
LPR	Lipid to protein ratio
LSM	Laser scanning microscopy
M	Molar
MD	Molecular dynamics
M_h	Hydrophobic molecular weight
min	Minute
mL	Milliliter
MloK1	Cyclic nucleotide-gated potassium channel
mM	Millimolar
M_{PDMS}	PDMS molecular weight
ms	Millisecond
MSD	Mean square displacement
mW	Milliwatt
M_w	Mass weighted polymer molecular weight
N	Number of particles
n	Refractive index
NA	Numerical aperture
NADH	Nicotinamide adenine dinucleotide hydrogen
NHS	N-hydroxysuccinimide
nm	Nanometre
nM	Nanomolar
NMR	Nuclear magnetic resonance
Ni-NTA	Nickel-nitrilotriacetic acid
NtAqp1	Nicotiana tabacum L. aquaporin
OmpF	Outer membrane protein F
p	Packing parameter
P	Permeability
P_f	Water permeability
Pa	Pascal
PAGE	Polyacrylamide gel electrophoresis
PB	Poly(butadiene)
PBS	Phosphate buffered saline
PC	L- α -phosphatidylcholine
PDI	Polydispersity index
PDMS	Poly(dimethyl siloxane)
PEE	Poly(ethyl ethylene)
PEG	Poly(ethylene glycol)
PEO	Poly(ethylene oxide) = poly(ethylene glycol)
PEtOz	Poly(2-ethyl-2-oxazoline)
pH	Potential hydrogen
PIB	Poly(isobutylene)
PMOXA	Poly(2-methyloxazoline)
POPC	1-palmitoyl-2-oleoyl- <i>sn</i> -glycero-3-phosphocholine
POPE	1-Palmitoyl-2-oleoyl- <i>sn</i> -glycero-3-phosphoethanolamine
PoPR	Polymer to protein ratio
OG488	Oregon Green 488
R	Radius
R_g	Radius of gyration

R^2	Coefficient of determination
Rhod-PE	Rhodamine-PE
ROS	Reactive oxygen species
s	Second
SD	Saffman-Delbrück
SDS	Sodium dodecyl sulfate
SEC	Size exclusion chromatography
SPT	Single particle tracking
SRB	Sulforhodamine B
SSL	Strong segregation limit
T	Temperature
t	Time
T_c	Chain melting temperature
TEM	Transmission electron microscopy
T_g	Glass transition temperature
TIRF	Total internal reflection fluorescence
T_{trip}	Fraction of fluorophores in triplet state
V	Volt
v	Volume
Y	Degree of polymerization
α HL	Alpha hemolysin
β -OG	β -octylglucopyranoside
γ	Euler's constant
λ	Wavelength
λ_{em}	Emission wavelength
λ_{exc}	Excitation wavelength
η_m	Membrane viscosity
η_s	Surrounding medium viscosity
μ L	Microliter
μ m	Micrometre
μ M	Micromolar
μ s	Microsecond
ω	Beam waist radius
τ_D	Diffusion time
τ_{trip}	Triplet time

Chapter 1

1 Introduction

1.1 Protein-polymer hybrid materials for technological and biomedical applications

Nature provides a large pool of components to mimic structures and functions in the design of new materials and active assemblies that can be used in many domains including chemistry, material science, electronics and medicine [1]. Life sciences and nanoscience combines the advantages of both worlds: the specificity and efficiency of nature's biological molecules that have been perfected over millions of years and the robustness and high stability of newly developed synthetic materials that have been discovered mainly during the last century in the field of chemistry. In this respect, new, complex and robust bio-synthetic strategies for future technological applications became accessible in terms of activity, sensitivity, efficiency and rapid reply. One strategy involves the generation of biomimetic membranes based on the combination of synthetic membranes to realize high stability, and biological entities to achieve a desired function with exceptional efficiency [2,3].

Biomimetic membranes involve the implementation of sensitive biological elements, such as enzymes or membrane proteins. A key challenge for the generation of long-living technological materials is to protect these biological compounds, because they are delicate structures and prone to degradation/precipitation in harsh conditions. This protection can be achieved either by a compartmentalisation strategy, to encapsulate biological entities in a closed shell or by embedding the entities within a membrane on a surface. Synthetic membranes, mimicking natural phospholipid bilayers, have attracted strong interest for technical and biomedical applications over several years due to their

better chemical and mechanical stability compared to phospholipid bilayers [4–6]. These artificial membranes can be generated based on the self-assembly principle, a bottom-up approach. Polymeric amphiphiles, which mimic the properties of lipids, are used in aqueous solutions to spontaneously arrange into supramolecular assemblies. The molecular properties of these amphiphiles, synthesized to its specific need, dictate the self-assembled superstructure, which can yield several different types of supramolecular assemblies, either as 3D assemblies (micelles, rods, tubes, vesicles) or as 2D planar structures formed on solid supports [7]. Since these artificial membranes are fully synthetic, they must fulfil certain requirements to be able to embed biological entities in their active state within the synthetic membrane. Therefore, a better understanding of the synthetic membrane properties is of high importance for ongoing research or the generation of commercial applications such as biomimetic membranes for water desalination [8,9].

1.2 Aim of the thesis

At the molecular level of a biological membrane, everything is in motion. Since synthetic membranes are intended to mimic biological cell membranes, fluidity is an essential membrane property because it defines the motion at the molecular level. In this work, poly(dimethyl siloxane) (PDMS)-containing amphiphilic block copolymers are used as the membrane forming macromolecules and their fluid property within these synthetic membranes is analysed.

The aim of this thesis is, first, to investigate the membrane fluidity related to changing membrane parameters such as membrane thickness and polymer architecture and, second, to analyse the lateral diffusion of embedded biological channel proteins within synthetic block copolymer membranes with different thicknesses. Characterizing the fluidity of synthetic membranes is essential for the development of biomimetic membranes for future technological applications. It provides important information on the chemical type and molecular property of the amphiphilic block copolymers that can be used as the membrane forming element. The major advantage of block copolymer membranes is their high chemical and mechanical stability compared to lipid membrane systems. Thus, the fluidity is a kind of intermediate property between stability and fragility.

1.3 Structure of the thesis

This thesis is organized into an introduction providing an overview of biomimetic membranes, with their properties and examples for applications (chapter 1). Since the topic of this thesis is related to dynamics in block copolymer membranes, a brief summary on the fundamental theories and measurement techniques is given to describe lateral diffusion (chapter 2). The experimental work conducted for this dissertation on lateral diffusion within biomimetic membranes is presented in chapters 3 and 4. A general conclusion is given in the final chapter (chapter 5) with a brief reflection on the essential information obtained by the experimental work together with an outlook for its use on ongoing projects.

1.4 Membranes

In general, biological cell membranes provide a barrier separating two compartments. Membranes can protect and store active entities in a confined space and provide a selective filter for either rejecting and/or passing specific constituents in liquid. The membranes used here are supramolecular structures self-assembled from single building blocks [1]. There are many different types of building blocks that can be used for the generation of membranes and will be presented in this chapter. In addition, biological membranes have unique properties that are intended to be used in technological applications. Therefore, the general properties of biological membranes will be discussed in this chapter as well. In order to generate the combination of synthetic and biological components a brief introduction is given on the ideas and basic concepts behind these artificial structures needed for technological applications. The specific term “biomimetic membrane” is often used in this context. However, biomimetic does not necessarily mean the use of synthetic block copolymer for the generation of the membrane. Membranes can also be composed of natural phospholipids. Therefore, biomimetic membranes are artificially generated membranes via a bottom-up approach in order to mimic biological membranes, but with designed function. The reduction in complexity, compared to biological membranes, provides better data interpretation and improving experimental control.

1.4.1 Building blocks of membranes

Membranes are made from amphiphiles that have a hydrophilic/polar part, which is chemically linked to a hydrophobic/apolar part. This chemical architecture causes amphiphiles to spontaneously form supramolecular assemblies in aqueous environments. There are different building blocks to design artificial membranes, which can be based on natural phospholipids or synthetic- and biological polymers. Phospholipids are frequently used because of their origin from biological cell membranes. The self-assembly behaviour of lipids is well known and has been studied over centuries [10].

The class of polymers is defined as macromolecules that are composed of many repeat units. The large variety of arrangements and types of monomers results in a class of materials of an enormous range of properties [11]. Within biopolymers, three different types of natural biopolymers are distinguished: polysaccharides, polypeptides and polynucleotides. Polysaccharides, such as chitosan or cellulose, are used as supramolecular assemblies in biotechnical and biomedical applications [12]. Polypeptides and polynucleotides are biocompatible and biodegradable alternatives to synthetic polymers and can also be used for biomedical applications. The great variety of synthetic polymers can be categorized into homopolymers, polyelectrolytes, and block copolymers [13–16]. Homopolymers are composed of many repeating units synthesized in linear or branched form. Polyelectrolytes are polymers with charged functional groups. Block copolymers contain different types of homopolymers that are linked together.

In this thesis, the work has been focused on membranes based on amphiphilic block copolymers. They represent synthetic lipid-mimics and are composed of two or more different covalently connected homopolymers that possess different physical and chemical properties. As the term amphiphile already indicates, the physical difference relies on the different water solubility (hydrophilicity) of the two blocks. The physico-chemical principle of the self-assembly process will be discussed in section 1.4 in more detail. For simplification, the blocks are named with capital letters (A, B, C, ...) to classify the arrangement of the different blocks. When a hydrophilic block A is connected to a hydrophobic block B, diblock copolymers are formed. The combination of two hydrophilic and one hydrophobic block (ABA or ABC if one hydrophilic block has a different chemical structure) or two hydrophobic blocks and one hydrophilic (BAB), triblock copolymers are generated. Figure 1.1 shows examples of possible arrangements of amphiphilic block copolymers.

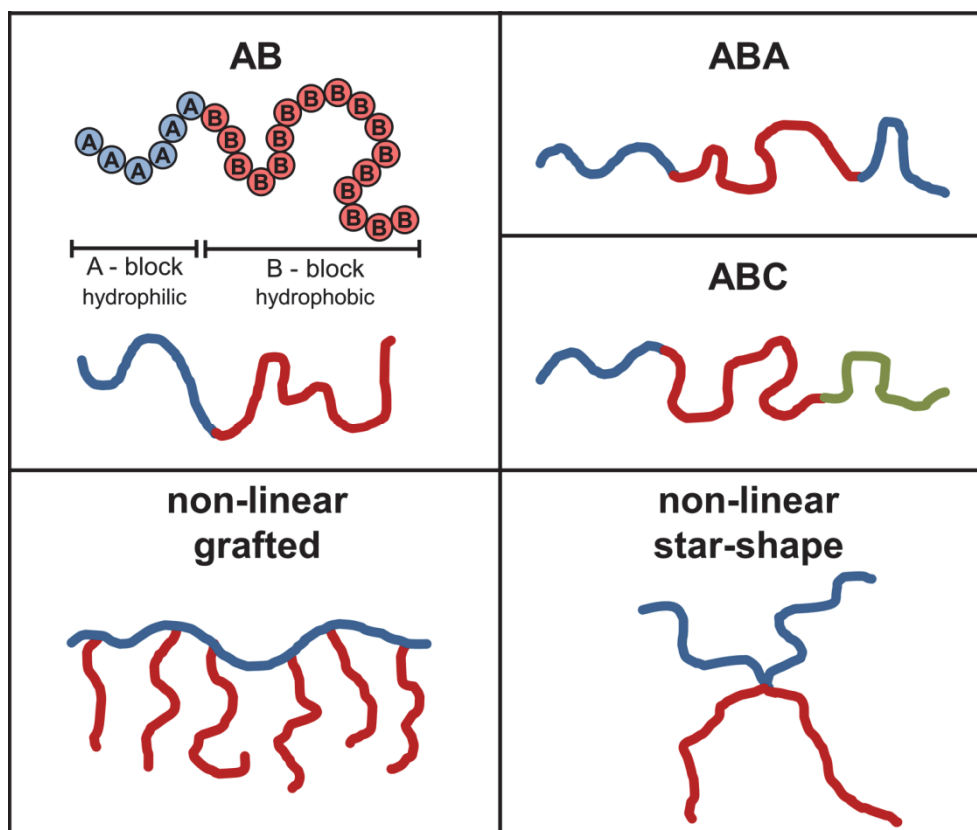


Figure 1.1. Amphiphilic block copolymer arrangements. Top: linear arranged blocks forming linear diblock (AB) or triblock (ABA or ABC) copolymers. Bottom: non-linear block copolymers are grafted or star-shaped block copolymers.

1.4.2 Biological membranes

The basis for the technological advancement for the generation of artificial membrane systems was laid by the analysis of native biological cell membranes. Biological membranes are complex matrices consisting of many different components to fulfil important cellular functions that include maintaining and controlling water and solute exchange, while the membrane itself serves as the protection shell to separate the inner, functional compartment from the harsh outer surrounding [10]. Figure 1.2 shows a schematic illustration of a cell membrane. The membrane is composed of phospholipids that form a thin layer of a protective sheet and usually contains cholesterol to enhance the membrane strength and to maintain cell fluidity at a large temperature range. Membrane proteins are embedded within the lipid matrix and fulfil important cellular functions [17]. The phospholipid bilayer is therefore, a kind of solvent for these integral membrane proteins because the lipid bilayer is considered as a fluid matrix [18].

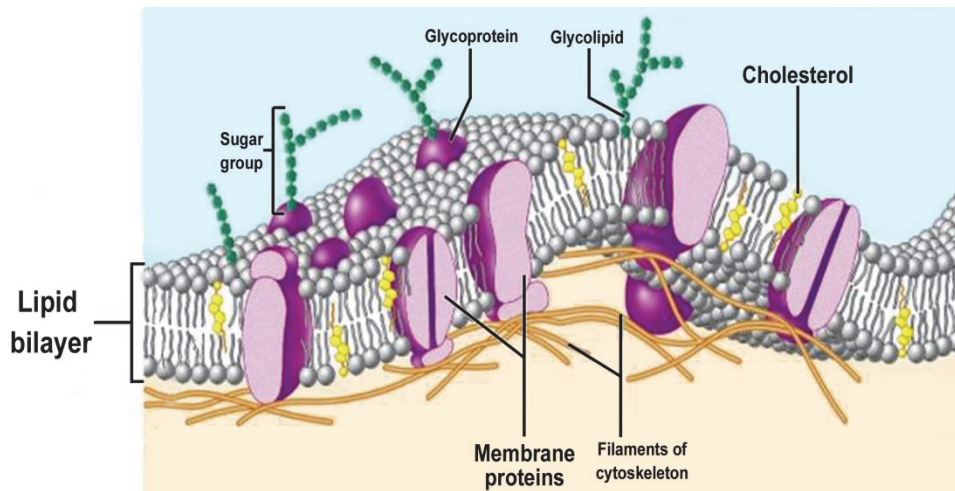


Figure 1.2. Schematic representation of a biological membrane. The membrane constitutes of phospholipids that provide the matrix for membrane proteins. Adapted with permission from [19].

The main components that form the matrix are phospholipids. Lipids consist of a hydrophilic head group (neutral, charged or zwitterionic) and a hydrophobic tail (saturated or unsaturated carbon chain). These amphiphilic molecules form extended two-dimensional structures via self-assembly. The lipid bilayer is capable of holding membrane proteins. Depending on the cell type, between 15 – 80% (by dry weight) of the whole cell membrane are made up of membrane proteins that are designed to fulfil specific and essential functions [10,20]. The importance of membrane proteins is highlighted even more by the fact that around 30% of the cell's genome is coded for them. Besides other functions, membrane proteins evolved as specific and non-specific channels allowing translocation of substrates across the membrane. They conduct substrates or solvents with exceptional selectivity and at high transport rates.

All these components thus build a matrix with essential functions. The first successful report of a stable, artificial lipid bilayer was reported in 1962 [21]. Since then, the structure of membranes has been thoroughly investigated, because it was first described based on theoretical assumptions. After experimental realizations of artificial membranes, the structure of biological membranes had to be revised and Singer and Nicholson suggested a concept describing the biological membrane as a fluid mosaic where membrane proteins can diffuse freely in the two dimensional viscous liquid represented by the lipid bilayer [18]. The initial theory that the membrane components can diffuse relatively freely in the lipid bilayer was revised, at the discovery of compartmentalization of membrane components within the membrane itself. Patterns are formed by non-random co-distribution of specific types of membrane proteins, which create small-scale clusters

at the molecular level and large-scale clusters at the submicrometer level [22]. These so-called rafts, where proteins come together, are important for cellular functions like signal transduction. The forces causing this phenomenon are determined by lipid-lipid, protein-protein and lipid-protein interactions. The highly complex structure, and the many involved components of biological membranes, renders membrane research a great challenge. Therefore, simplifying the membranes by reducing the number of components to obtain an overview of the processes taking place is the basis of studying membrane-associated research.

1.4.3 Biomimetic membranes

The exceptional transport efficiency of membrane proteins, embedded within the membrane, together with the availability of high-resolution analytical techniques, has attracted molecular engineers to design artificial biomimetic membranes for technological applications [9]. These artificial systems were prepared in order to study functions and transport mechanisms of single types of membrane proteins. Thus, many artificial systems start from the simplest models to study specific functions, not only in fundamental research but also for technological applications.

Artificial lipid systems have been widely used to study the functions of single cell components, like transport mechanisms of membrane proteins. On one hand, these simple models are usually composed of only one or a few types of phospholipids and are ideally suited for applications in biomedicine, because the lipids are biocompatible. On the other hand, the low stability of lipid membranes makes them prone to fast degradation and therefore not well suited for technological applications [23]. In contrast, biomimetic membranes made from synthetic amphiphilic block copolymers combine the advantages of specialized biological membrane proteins with the stability of synthetic materials. Figure 1.3 shows a schematic representation of a planar biomimetic membrane on a porous support. Such systems can be engineered either to function as a selective membrane, by insertion of a specific membrane protein to fulfil an enzymatic reaction to a specific molecule, or to immobilize/bind molecules via specific recognition.

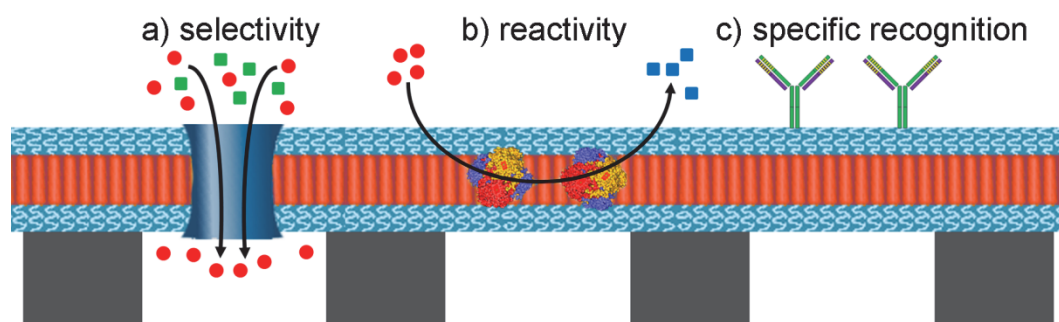


Figure 1.3. Schematic representation of a biomimetic membrane. The function of the generated membrane is designed for a specific need, either for a) selectivity, b) reactivity or c) specific recognition, or a combination thereof.

The development of applied technological biomimetic membranes is currently going towards large scale applications, although major challenges still have to be overcome. These include, on a technological basis, the scalability of these systems and, on an economical basis, the high costs for large scale production. Most importantly, the lack of fundamental understanding of interactions between the functional biological molecules and the synthetic membranes needs to be addressed [9]. Some examples of biomimetic membranes that can be used for technological applications are shown in section 1.6.

1.4.4 Supramolecular assemblies to characterize biomimetic membranes

Membranes are usually considered as large, planar, 2-dimensional sheets, which are very well suited for technological applications due to their large size. However, the nature of self-assembly of amphiphiles allows them to organize into several other morphologies as well. For example, lipids self-assemble in dilute aqueous solutions into micelles and vesicles of different sizes. Like lipids, amphiphilic block copolymers can be designed to self-assemble in aqueous solutions to form micelles, vesicles, cylinders, rod-like- or lamellar structures depending on their concentration, molecular shape, hydrophobic-to-hydrophilic balance and block-length (see section 1.2) [6,24]. A lot of these morphologies are well suited for fundamental research and technological applications.

1.4.5 Membrane-forming amphiphiles used in this thesis

In this thesis, the experimental work has been performed with membranes based on biological phospholipids and synthetic amphiphilic block copolymers (Figure 1.4). Lipid-based membranes were chosen as a reference membrane in order to compare the results to the ones obtained with the artificial biomimetic membranes. The lipid 1-palmitoyl-2-

oleoyl-sn-glycero-3-phosphocholine (POPC) was chosen because POPC is a major lipid component in biological membranes [25,26] and, due to its mono-unsaturated fatty acid chain, it possesses a low glass-transition temperature ($T_g = -2^\circ\text{C}$) [27,28], *i.e.* high fluid membrane character at ambient temperatures.

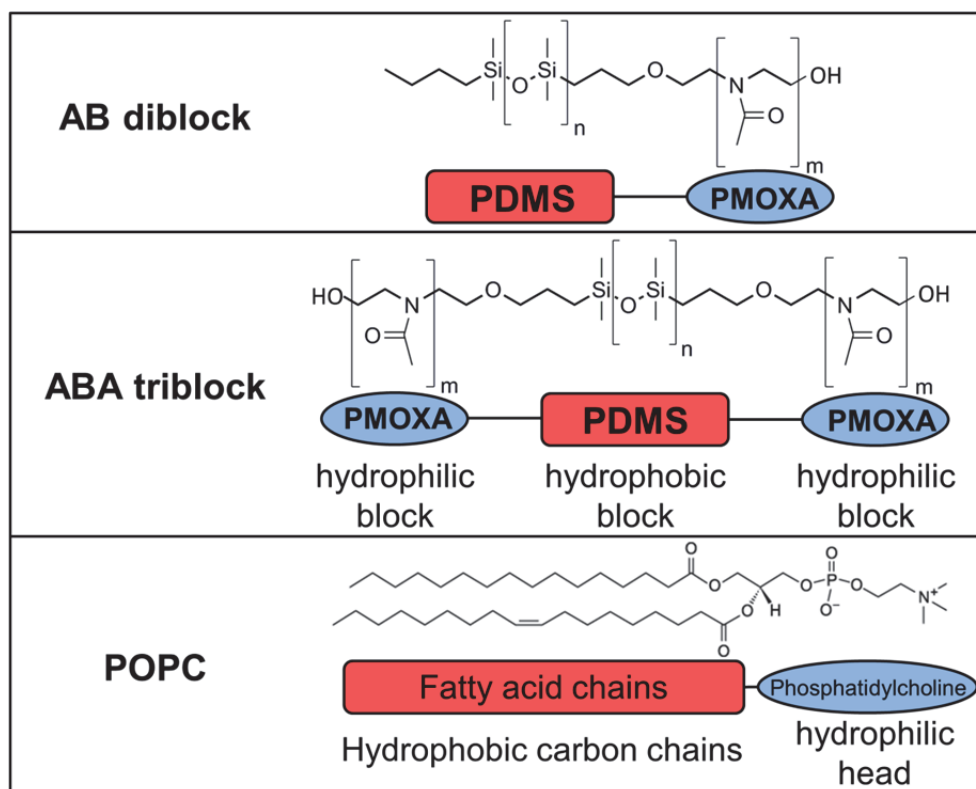


Figure 1.4. Chemical composition of the amphiphilic diblock and triblock copolymers, and the natural phospholipid POPC used in this thesis. Sizes are not representative.

The here generated artificial membranes are based on diblock and triblock copolymers containing poly(2-methyl-2-oxazoline) (PMOXA) and poly(dimethylsiloxane) (PDMS) – abbreviated and further referred to as A_xB_y (diblock) and $A_xB_yA_x$ (triblock), where the subscripts represent the degree of polymerization or the number of repeating units. Biomimetic membranes composed of PMOXA-*b*-PDMS-*b*-PMOXA block copolymers have been widely reviewed [6,29–31].

PMOXA is frequently chosen as the hydrophilic polymer block in different applications because of its biocompatibility and stealth behaviour [32]. These properties make this type of polymer useful for a large field of applications due to its negligible interaction with proteins, cells, and other biological components.

PDMS is primarily used as the hydrophobic block in synthetic biomimetic membranes due to its ability for inserting membrane proteins [33]. PDMS are silicone based polymers

known for its biocompatibility, high flexibility and very low glass-transition temperature ($T_g = -123^\circ\text{C}$) [34], thus having a high fluidity.

1.4.6 Membrane protein insertion into block copolymer membranes

Several studies have shown that membranes self-assembled from PDMS-containing block copolymers are able to functionally embed biological membrane proteins. However, it is a quite surprising phenomenon that biological membrane proteins, which have evolved to be functional solely in a phospholipid bilayer, can be reconstituted into completely synthetic membranes. A summary of all relevant studies of membrane protein insertion into synthetic block copolymer membranes is given in Table 1.1.

In the studies shown in Table 1.1, mainly all block copolymers are triblocks and composed of PDMS as the hydrophobic block. However, there are recent exceptions of lately published examples. In two cases using PEO-*b*-PB diblock [35] and PIB-*b*-PEO-*b*-PIB triblock [36] copolymers, both studies were conducted with polymers composed of a relatively short hydrophobic block with molecular weights very similar to phospholipids (~ 1 kDa), while all the other studies were performed on membranes with large thicknesses (polymer molecular weights of 2 kDa - 10 kDa). In the other two examples [37,38], the membranes were solid supported membranes, *i.e.* immobilized on surfaces, which is different to all other studies, where mainly vesicles (polymersomes) were used. In the case of solid supported membranes, the mechanism of membrane protein incorporation may be different. Overall, the successful incorporation of membrane proteins into synthetic block copolymer membranes is mainly dependent on the molecular weight and the property of the hydrophobic block.

Table 1.1. Summary of published studies of membrane protein insertion into block copolymer membranes.

Block copolymer	Polymer type	Membrane protein	Study	References
PMOXA- <i>b</i> -PDMS- <i>b</i> -PMOXA	Triblock ABA	OmpF	Size-selective permeability	Nardin et al. 2000 [39] Ranquin et al. 2005 [40] Grzelakowski et al. 2009 [41] Dobrunz et al. 2012 [42] Langowska et al. 2013 [43] Langowska et al. 2014 [44] Ihle et al. 2011 [45]
		LamB	Virus assisted DNA loading into polymersomes	Graff et al. 2002 [46]
		AqpZ	Water-selective permeability	Kumar et al. 2007 [8] Wang et al. 2012 [47] Grzelakowski et al. 2015 [48]
		NtAqp1	CO ₂ -selective permeability	Uehlein et al. 2012 [49]
		NADH-ubiquinone reductase (complex 1)	Complex 1 activity – electron transfer	Graff et al. 2010 [50]
		bR	Proton transport	Ho et al. 2004 [51]
		Gramicidin	Monovalent cation-selective permeability	Lomora et al. 2015 [52]
		FhuA	Reduction triggered release	Onaca et al. 2008 [53]
PMOXA- <i>b</i> -PDMS- <i>b</i> -PEO	Triblock ABC	AQP-0	Directed insertion of Aquaporin	Stoenescu et al. 2004 [54]
PEtOz- <i>b</i> -PDMS- <i>b</i> -PEtOz	Triblock ABA	bR and ATPase	ATP production	Choi et al. 2005 [55]
PIB- <i>b</i> -PEO- <i>b</i> -PIB	Triblock BAB	FhuA	Size-selective permeability	Muhammad et al. 2011 [36]
PEO- <i>b</i> -PB	Diblock AB	AQP-0	Water-selective permeability	Kumar et al. 2012 [35]
		α HL	Ion conductivity	Zhang et al. 2013 [38]
PMOXA- <i>b</i> -PDMS	Diblock AB	MloK1	K ⁺ -selective permeability	Kowal et al. 2014 [37]

The main problem for insertion of membrane protein is the large mismatch between the effective hydrophobic length of the membrane proteins (~ 3 nm) and the equilibrium hydrophobic thickness of the polymersome membrane ($\sim 4 - 20$ nm) (Figure 1.5). For a

successful insertion, the requirement is that the membrane has to fit the height of the membrane protein. Pata and Dan [56] and Srinivas et al. [57] have shown in computer simulations that the flexibility and polydispersity of the hydrophobic block of diblock copolymers may lead to a compression or an arrangement of the shorter polymer chains adjacent to the small membrane protein. Thus, the high flexibility of the block copolymer causes the chains to compress, and a high PDI causes a local segregation of the small chains around the protein. The combination of flexibility and polydispersity might lead to “even easier protein incorporation” into block copolymer membranes [56].

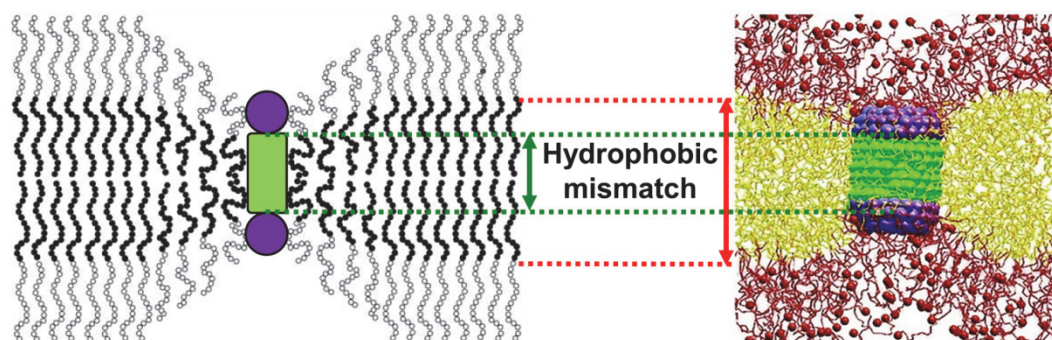


Figure 1.5. Hydrophobic mismatch between membrane proteins and block copolymer membrane. The possible mechanism relies on the compression of the flexible hydrophobic block and the segregation of smaller polymer chains (due to polydispersity) in vicinity to the membrane protein. Left: Model adapted from Pata and Dan 2003 [56]. Right: Coarse-grained molecular dynamics simulation image from Srinivas et al. 2005. With permission from [57].

Polysiloxanes, belonging to the class of organosilicon polymers, possess a very flexible property due to the high torsion and bending flexibility of the Si-O-Si bond [58]. For example, the angle of the Si-O-Si bond can vary between 135° and 180° . This high angular flexibility allows for considerable bending of the whole polymer backbone. Due to the high flexibility of PDMS and the relatively high polydispersity of PDMS-containing triblock copolymers, the above described mechanism of membrane protein insertion is very likely. Despite the possible mechanism, the activity of inserted membrane proteins has been tested thoroughly as shown in Table 1.1. The tested membrane proteins within block copolymer membranes include the bacterial outer membrane proteins OmpF, LamB and FhuA, the aquaporins AqpZ (bacterial), AQP-0 (bovine eye lens) and NtAqp1 (tobacco leaf), the purple membrane H^+ pump bacteriorhodopsin (bR), monovalent-cation selective channel forming peptide gramicidin, the bacterial F_0 - F_1 ATPase, and NADH-ubiquinone reductase (complex 1).

1.5 Self-assembly principle of amphiphilic macromolecules

Supramolecular structures, such as micelles, rods, tubes, vesicles, membranes, *etc.*, play an important role for basic research and possible technological applications in life- and nano-sciences. Therefore, the physico-chemical interactions of molecular aggregates are of high importance for understanding and engineering supramolecular structures self-assembled from amphiphilic block copolymers. The resulting supramolecular structures have no defined size or shape but they are rather distributed within a thermodynamic equilibrium. In this way, they can switch between small aggregates, *e.g.* micelles, and larger aggregates, *e.g.* vesicles. The linking of the two opposing blocks prevents a separation of the blocks and, therefore, forces the amphiphiles to arrange into superstructures in aqueous solutions, because only one block is water soluble [6]. In other words, the different blocks of block copolymers are incompatible with each other, and microphase separation occurs due to the covalent linkage of the blocks, where the size of the domain is given by the chain length.

1.5.1 Thermodynamic forces driving self-assembly

There are 5 major forces that lead to membrane stabilization: the hydrophobic effect, headgroup – water interactions, headgroup – headgroup interactions (ionic), entropy of the hydrophobic chains, and van der Waals forces [10]. The main forces driving the self-assembly process are attributed to the hydrophobic attraction at the hydrophobic-water interface inducing the macromolecules to associate (Figure 1.6). The hydrophobic effect causes the hydrophobic chains to segregate away from water because water prefers to form hydrogen bonds. The hydrophobic effect is the main force involved in membrane stabilization. Since amphiphilic molecules have an amphipathic property, the hydrophilic chains interact with water, which further stabilizes the membrane. Additional ionic interactions between the head groups can even further stabilize the membrane. Self-assembly is also driven by entropy. In water, hydrophobic molecules feel a restricted freedom of motion due to the high surface tension of water and thus, the low entropy of the hydrophobic molecules would be very unfavorable for them. Therefore, reducing the area of interaction with water causes the molecules to aggregate together, where their freedom of motion is increased (increase in entropy). Van der Waals forces also add to stabilization of the hydrophobic part of the membrane, although very weakly.

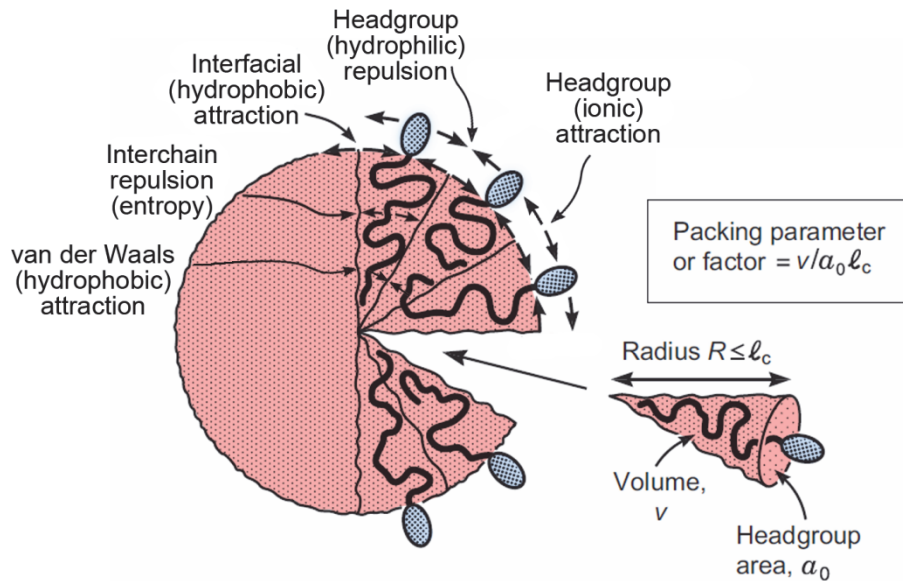


Figure 1.6. Thermodynamic forces driving the self-assembly process of amphiphilic molecules. Adapted with permission from [59].

The hydrophilic, ionic or steric repulsion of the headgroups induces an opposite force so that the headgroup remains in contact with water. Therefore, the interfacial region between the two opposing blocks is an important parameter where one of the forces tends to increase (repulsion), the other one tends to decrease (attraction) the minimal interfacial area per molecule, a_0 [59].

1.5.2 Geometrical considerations driving self-assembly

The geometric parameters of the amphiphiles play a crucial role in determining which type of superstructure the amphiphiles can organize into. In addition to the ideal area per molecule (a_0), a second factor contributes to the geometrical packing, the volume v of the hydrophobic block. In this respect, the packing parameter P provides information about the geometrical shape of the single molecules, and therefore, how the molecules are able to arrange with each other (Figure 1.7). The packing parameter P is described as the volume v divided by the critical length l_c and area a_0 of the molecule [59]:

$$P = \frac{v}{l_c a_0} \quad (1.1)$$

The parameter P essentially describes what kind of conical or cylindrical shape the molecule will have. If P is between 1/2 and 1, the macromolecules tend to arrange as vesicular or planar membranes. In this case, the molecules can pack with their optimal

surface area a_0 and without exceeding the critical length l_c . In case of $P > 1$ inverted structures are generated.

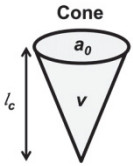
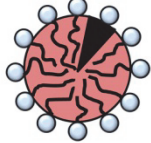
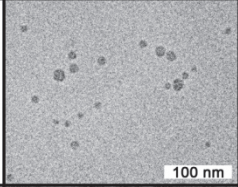

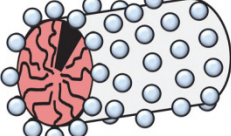
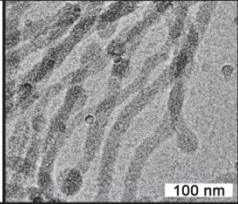

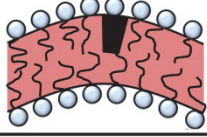
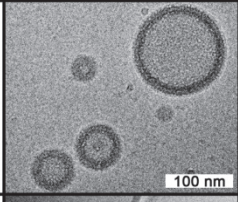

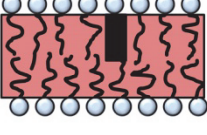
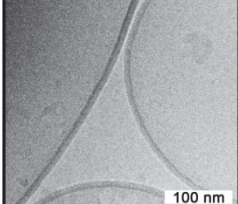
Critical packing shape	Structures formed	Critical packing parameter $v / a_0 l_c$	Examples cryo-TEM
 <p>Cone</p>	 <p>Spherical micelles</p>	$< 1/3$	
 <p>Truncated cone</p>	 <p>Cylindrical micelles</p>	$1/3 - 1/2$	
 <p>Truncated cone</p>	 <p>Flexible bilayers, vesicles</p>	$1/2 - 1$	
 <p>Cylinder</p>	 <p>Planar bilayers</p>	~ 1	

Figure 1.7. Geometrical consideration of the self-assembly process. Depending on what geometrical shape a single amphiphilic molecule has in the specific solvent, the structures formed are different.

The thermodynamic and geometric considerations discussed above also hold true for amphiphilic block copolymers, although many other types of supramolecular structures are accessible in addition to the simple ones in Figure 1.7.

In a more simple and practical case, one unifying rule dictates the geometrical shape of the macromolecules, namely the ratio f of the hydrophilic mass to the total mass [60]. Phospholipids ($f_{lipids} \approx 35\%$) provide an initial hint for the synthesis of membrane-forming block copolymers. When the hydrophilic block is large compared to the hydrophobic block, the overall geometrical shape will be a conical shape inducing the formation of micelles. The correct balance between the hydrophilic and hydrophobic block provides the ability to form membranes. For amphiphilic block copolymers it has been shown that f

has to be between 25 – 35% to form polymer vesicles (polymersomes) [61]. This number can vary for different chemically-composed blocks, for example long side chains within each hydrophobic monomer can induce an overall larger hydrophobic volume. For simple, linear amphiphilic block copolymers, the geometry of a single macromolecules is similar to the structure of a phospholipid, and thus, the self-assembly behaviour is similar as well.

1.6 Block copolymer membrane properties

In general, the properties of block copolymer membranes are determined based on the chemical composition of the blocks, the molecular weight and the block lengths. Due to the long chains of polymers compared to lipids, the molecular arrangements of the chains are more complex than for lipids having a relatively defined structure within membranes. The membrane properties can therefore, be discussed based on their structure, thickness, stability, fluidity and permeability.

1.6.1 Membrane structure

Membranes are usually associated as bilayers due to the nature of biological membranes composed of phospholipids, which arrange as two sheets (two leaflets) of lipid monolayers facing the hydrophilic sides outwards (Figure 1.2). In the case of amphiphilic block copolymers, the membrane can possess more complex structures depending on the type of polymer and block arrangements (Figure 1.8). For the simplest case mimicking a phospholipid molecule very closely, *i.e.* diblock copolymer, the membrane formed does not resemble a bilayer because entanglement and interdigitation can occur between the two hydrophobic blocks [62]. Entanglement occurs due to randomly twisted polymers chains and the effect of entanglement increases with increasing molecular weight and with increasing flexibility of the chains. Interdigitation occurs due to interlinking of the polymer chains of the two opposing leaflets and they can merge together to form a completely interdigitated membrane [63]. The effect of interdigitation is well known in polymer science, since solid polymer matrices develop an elastic property due to interdigitation and entanglement of the polymer chains [64]. While AB diblock copolymers can self-assemble into similar structures as lipid bilayers, ABA triblock copolymers can arrange into two possible chain conformations within the membrane. The polymer chains can form a stretched conformation (I-shape), where the

hydrophobic block spans through the entire membrane resulting in a monolayer-like membrane structure. Alternatively, they can form a hairpin conformation (U-shape), where the hydrophobic block forms a loop resulting in a bilayer-like structure [65,66]. For triblock copolymers, it is assumed that the membrane is composed of a mixture of both chain conformations [65,67]. In addition, asymmetric ABC triblock copolymers can be used to obtain asymmetric membranes that can be used for directed membrane protein insertion, if the membrane protein has to serve for directed transport [54,68].

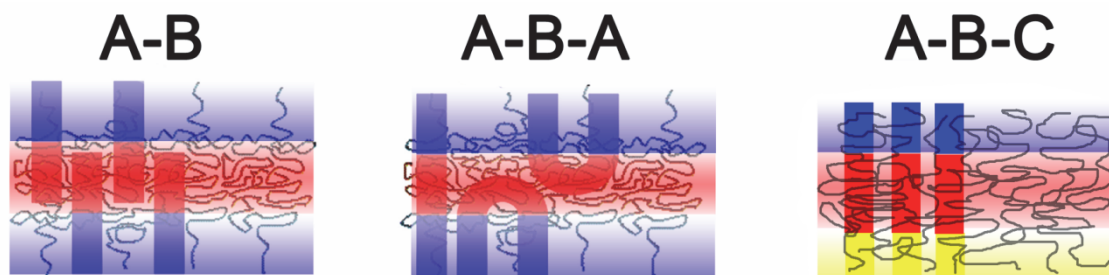


Figure 1.8. Membrane conformation of AB, ABA and ABC block copolymers. For ABA, the U-shape and I-shape conformation is possible, while for the others only one possible conformation exists. Adapted with permission from [66].

1.6.2 Membrane thickness

The increased molecular weight of block copolymers compared to lipids leads to a significantly larger membrane thickness. Lipid bilayers have membrane thicknesses of 3 – 5 nm, which is up to five times thinner than block copolymer membranes. Generally, the membrane thickness for block copolymers increases with increasing molecular weight [69]. This trend is similar to phospholipid bilayers, where the membrane thickness increases with increasing acyl chain length [70]. In a study using a series of poly(ethyl ethylene)-*b*-poly(ethylene oxide) (PEE-PEO) and poly(butadiene)-*b*-poly(ethylene oxide) (PBD-PEO) polymersomes [69], the membrane thicknesses d were analysed in relation to the molecular weight of the hydrophobic block (M_h):

$$d \propto (M_h)^a \quad (1.2)$$

Equation (**Fehler! Verweisquelle konnte nicht gefunden werden.**) shows that the membrane thickness scales with the hydrophobic molecular weight including an exponential factor a . Therefore, this effect does not follow a linear relationship, which is attributed to interdigitation and entanglement of the polymer chains within the self-assembled membrane. In addition, short polymer chains are more stretched when they are

arranged in a membrane, while longer chains tend to form large coils. This stretching behaviour of the chains is reflected by the exponent mentioned in equation 1. Experimentally determined values of a range from 0.5 to 0.66 [63,69,71], and 0.83 for very short polymer chains where the membrane thickness is below 7 nm [72]. A value of 0.66 is attributed to the strong-segregation limit (SSL), where the hydrophilic and the hydrophobic blocks experience a strong repulsion, which results in a reduced interface and the stretching of the chains is increased. A brush conformation, *i.e.* fully stretched chains, corresponds to a value of $a = 1.0$. Non-perturbed chains that are fully coiled would show $a = 0.5$. For example, at low membrane thicknesses (below 7 nm) a higher value of the exponent has been found, and increasing the thickness leads to a gradually decreasing exponent value [62,72,73]. The experimentally obtained values of a can be explained by strong segregation and stretching of the chains which is opposed by interdigitation upon increasing the membrane thickness. Thus, the exponent a is gradually reduced to a value of 0.5 resembling the non-perturbed state.

1.6.3 Membrane stability

The larger membrane thickness of polymersomes leads to an increased mechanical stability. Polymersomes were analysed with respect to bending- and rigidity strength [74] and to maximal areal strain [69]. Improved abilities to withstand lateral strains [61] and increased bending rigidities [74] are consequences of the longer hydrophobic core (6 – 30 vs. 3 – 5 nm for lipid membranes) of block copolymer membranes. On a structural basis, the effect of interdigitation and entanglement of the polymer chains explains the increased membrane stability very well [63]. Besides these experimental studies [5,69,75], a coarse-grain molecular dynamics simulation study [72] revealed that the polymer chains induce an increased interaction, which is increasing with the increase of the hydrophobic block (molecular weight, respectively). Unfortunately, there are only very few computer simulation studies on block copolymer membranes because the increased system size (hundreds to thousands of atoms) and the longer time scales for self-assembly (microseconds) is computationally very intensive.

1.6.4 Membrane fluidity

The fluidity of biological membranes is a crucial property that allows lateral rearrangements of proteins and lipids within membranes [59]. Lipid bilayers possess a highly dynamic character due to the non-covalent interactions between the membrane-

forming amphiphiles. In addition, the membranes are in a non-crystalline state due the low chain-melting temperature of unsaturated phospholipids ($T_c \leq 0$ °C). This fluidity enables biological membranes to deform and bend and to keep the structures stable upon membrane stress. In this way, biological membranes possess an exceptional property to have stability and fluidity at the same time. In contrast to conventional colloidal particles being solid and rigid structures, membranes from self-assembled amphiphilic molecules are considered as soft structures [59]. Therefore, this fluid-like character of membranes is a very important property of biological membranes. Membrane fluidity is described by the two-dimensional lateral diffusion of the membrane components within the membrane, also called diffusivity. The diffusion coefficient is the experimental value given for lateral diffusion and describes the area that the molecule covers per time (SI units: $\text{m}^2 \text{s}^{-1}$). Typical diffusion coefficients of lipids in a phospholipid membrane are $3 - 15 \mu\text{m}^2 \text{s}^{-1}$, depending on the measurement conditions (temperature, viscosity of surrounding medium), measurement technique, membrane composition (saturated- and unsaturated lipids, cholesterol) and model membrane (free-standing- and supported bilayers) [76–79].

In the case of block copolymer membranes, the macromolecules are also able to diffuse within the membrane, because the molecular forces within the self-assembled membrane are the same as in lipid bilayers. However, the lateral mobility of block copolymer macromolecules is expected to be reduced due to the higher molecular weight compared to phospholipids. It was shown that the diffusion coefficients of polymeric membranes are at least one order of magnitude lower than in the case of lipid membranes [80]. The long chains of the hydrophobic blocks are prone to become entangled and interdigitate with other chains, therefore reducing the mobility further. It can be expected that different chemical composition of the hydrophobic block greatly influences the lateral diffusion.

1.6.5 Membrane permeability

In addition to the increased membrane thickness and stability compared to lipid bilayers, the selective permeability to hydrophobic and hydrophilic molecules is a great advantage. Since polar molecules have a low solubility in a hydrophobic environment, for example charged species (ions) encounter a high resistance force from the membranes. As a consequence, the permeability for polar molecules is further reduced with increasing membrane thickness and increasing molecular weight of the hydrophobic block. For example, the permeability to water (P_w) is significantly reduced compared to lipid

membranes. Water permeability through membranes of PEE₃₇-*b*-PEO₄₀ diblock copolymer vesicles was reduced by a factor of 10 ($P_f(\text{polymer}) \sim 2.5 \mu\text{m s}^{-1}$ versus $P_f(\text{lipid}) \sim 25 - 100 \mu\text{m s}^{-1}$) [5]. Water permeability studies on relatively thick PMOXA₁₅-*b*-PDMS₁₁₀-*b*-PMOXA₁₅ triblock copolymer membranes revealed a further decrease ($P_{\text{polymer}} \sim 0.8 \mu\text{m s}^{-1}$) [8]. However, a recent and more detailed water permeability study on lower molecular weight PMOXA-*b*-PDMS-*b*-PMOXA triblock copolymer vesicles revealed much higher water permeabilities of $P_{\text{polymer}} \sim 113 \pm 27 \mu\text{m s}^{-1}$ [48], which is similar to the permeability of lipid bilayers. The current technique to measure water permeability of vesicles (liposomes or polymersome) is dependent on several important factors, such as quality of the sample (resulting signal-to-noise ratio), size of the vesicles and their PDI, and concentration gradient (osmolarity difference) [48]. These factors can alter the final values dramatically and complicate the comparison of the permeability values to other literature values. This shows the difficulties in measuring water permeabilities from block copolymer vesicles.

1.7 Applications of biomimetic membranes

The many published studies on bio-synthetic devices made from biomimetic membranes have shown proof of concepts for future technological applications. The advantages of amphiphilic block copolymers, *i.e.* high mechanical and chemical stability, low permeability, customizable properties by choice of polymer type, endgroup functionalization and insertion of membrane proteins, make them very promising candidates. However, their consideration for direct applications is still at an early stage, and many issues have yet to be overcome for evaluations, such as *in-vivo* studies for biomedical applications or long-term stability for technological applications. In this section, some examples are given of latest research on biomimetic membranes based on PMOXA-*b*-PDMS-*b*-PMOXA block copolymers (Figure 1.9). Examples with different block copolymers are given as references and are also summarized in several review articles [1,7,13,81,81–85].

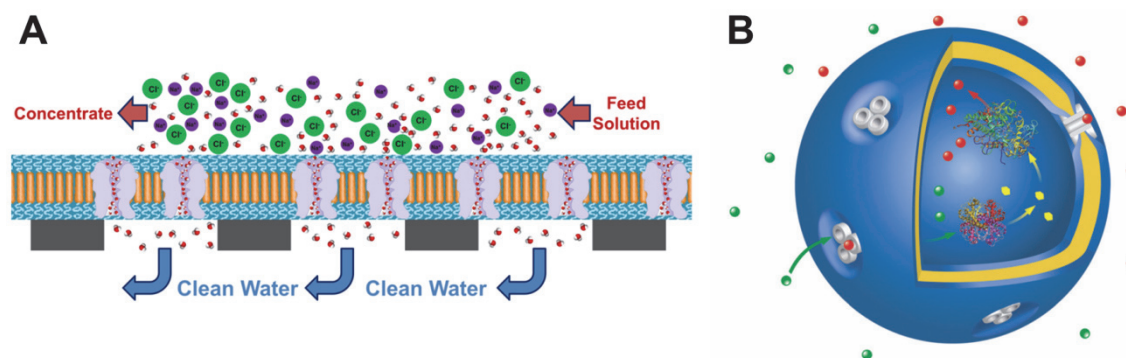


Figure 1.9. Applications of biomimetic membranes. A) Schematic representation of a biomimetic membrane for water purification. Aquaporins are embedded within the membrane, which is supported on a porous substrate. Aquaporins only allow the passage of water molecules, while solutes are rejected. B) Schematic representation of an enzymatic cascade reaction inside a polymeric nanocontainer. A combination of enzymes act inside the nanocontainer in a cascade reaction with substrates (green, yellow) and products (yellow, red). Substrates and products are able to diffuse through the polymeric membrane due to the insertion of the channel protein OmpF. Reproduced with permission from ref [86].

1.7.1 Membranes with selective permeability

- Aquaporin-functionalized membranes for water desalination

Aquaporins are unique membrane proteins that offer high water permeability and high solute rejection. Their great potential for water desalination applications have led to a considerable effort for the development of aquaporin based biomimetic membranes [87] [9]. Today, conventional desalination membranes, such as reverse osmosis (RO), demand relatively high energy and are still limited on their selectivity and permeability. Since biological membranes and thus also synthetic block copolymer membranes offer this great solute rejection property, embedding active aquaporins into planar membranes improves efficiency and energy consumption compared to conventional desalination membranes (Figure 1.9A) [33,47,48]. The proof of concept was presented and patented in the year 2007 [8], and subsequent research and even founded start-up companies are leading this great idea further for future desalination membranes.

- Ion channels for ion-selective membranes

Since membrane proteins are delicate structures prone to degradation, the use of more simple methods to generate selective permeability through synthetic block copolymer membranes led to the study of ion-selective biopores, such as ionophores or helical

peptides. These simple compounds, dissolved at very high concentrations in an organic solvent (*e.g.* EtOH, DMSO) can be added directly to the membranes and will insert immediately due to their hydrophobicity. A very small amount of solvent did not affect membrane stability. Gramicidin (gA), an alpha-helix forming-, 15 amino acid long peptide allows the passage of protons and monovalent cations through the membrane [88]. In a recent study, it was shown that gramicidin successfully inserts into membranes with thicknesses up to 12 nm, while at higher thicknesses the passage of ions was blocked due to incorrect insertion of gA into the membrane [52]. This suggests that a hydrophobic mismatch that is too large causes gA to assemble in an incorrect way. In a second study, by using the simple ionophore, ionomycin, selective permeability for Ca^{2+} ions through these membranes was obtained [89]. In contrast to gramicidin, ionomycin is a carrier molecule and upon a Ca^{2+} gradient, the ions are transported through the membrane. Ion-selective membranes are a further step towards the development of biosensors (*e.g.* detection of pH or ionic strength) or nanoreactors for which ion exchange is required to facilitate *in situ* reactions inside the polymersomes.

1.7.2 Nanoreactors

Nanoreactors are supramolecular structures self-assembled from amphiphilic block copolymers containing a cavity suitable for proteins / enzymes to fulfil their typical function (Figure 1.9B) [13]. The chemical reaction performed by the active entity is confined by a semipermeable shell. Shell permeability has to be guaranteed in order to allow the exchange of substrates and products as such to be counted as nanoreactor [90]. Many examples of nanoreactors were published in recent years differing in the type of polymers used, the number of enzymes involved, type of reaction and location of the reaction [1,13,83,91].

In order to obtain membrane permeability and keep the enzymes entrapped in the interior of the polymersome at the same time, OmpF was inserted allowing an unspecific passage of molecules with molecular weights ≤ 600 Da [92]. In such a way, nanoreactors were obtained and described first by Nardin et al. in the year 2000 [39]. Further improvements and ideas led to several possible applications in life sciences and nanomedicine. Artificial organelles, which mimic cellular organelles, were applied to cells in order to reduce cell stress upon the generation of reactive oxygen species (ROS). ROS are involved in several diseases such as Parkinson's disease, Alzheimer, cancer, *etc.* [87]. These nanoreactors

were taken up by cells and operated *in vivo*, which represents a large step towards nanomedicine (*e.g.* artificial organelles). In another attempt, nanoreactors were used to produce an antibiotic compound (penicillin) from non-active substrates [43,44]. The encapsulated enzyme inside the nanoreactor converted the substrates, upon the addition to the outside environment to penicillin and thereby reducing and/or inhibiting bacterial cell growth.

These examples show a great promise of these synthetic biomimetic membranes for applications in several fields.

Chapter 2

2 Fundamental theories and characterisation methods

In this chapter, the theoretical and technical know-how to describe and detect diffusion in membranes is described. Section 2.1 provides the fundamentals of molecular diffusion based on mathematical descriptions to describe diffusion and diffusion characteristics within membranes. Section 2.2 presents a brief overview of different techniques available to measure lateral diffusion in membranes. In the last two sections of this chapter, the here used method to determine the lateral diffusion coefficients within membranes is introduced, first, on a general basis of fluorescence correlation spectroscopy (FCS) (section 2.3), and, second, on a more specialized type of FCS, the z-scan FCS (section 2.4).

2.1 Fundamentals of molecular diffusion

2.1.1 Brownian motion and diffusion

The diffusion within membranes, of either the membrane-forming amphiphiles (lipids, block copolymers, *etc.*) or small molecules (membrane proteins, cholesterol, *etc.*) diffusing through or within the membrane, can be described by applying the classical analysis of Brownian motion. Brownian motion is an irregular and directionless (random) motion of particles suspended in a gas or fluid phase due to thermal collisions with atoms in the gas or liquid phase [93]. The thermal agitation also induces the movement of the membrane components in the plane of the membrane, which in two dimensions is identical with lateral diffusion [94]. Due to these random collisions, the motion of the particles, on a macroscopic level, does not follow any specific rule and, thus, can be described by mathematical models using the probability theory (stochastics). The Einstein relation describes the free Brownian lateral diffusion in a 2D system (Figure 2.1):

$$MSD = \langle x^2 \rangle = 4Dt \quad (2.1)$$

where $MSD = \langle x^2 \rangle$ is the mean square displacement, D is the diffusion coefficient, and t is the time. The diffusion coefficient is a measure of the area that a particle covers in a certain time (units $\mu\text{m}^2/\text{s}$). Since this process is a random lateral self-diffusion, this definition has to be strictly separated from diffusion by concentration gradients.

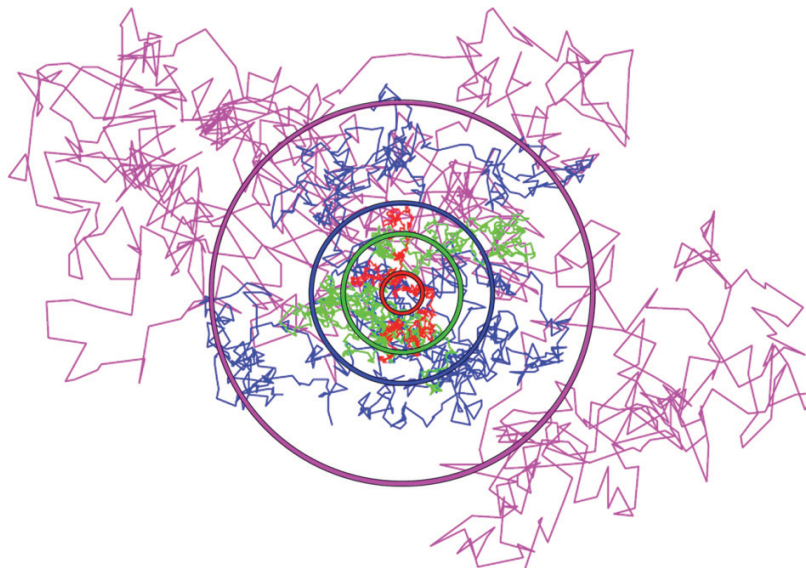


Figure 2.1. Simulated trajectories of random walks in a 2D system. The four different trajectories have different diffusion coefficients symbolized by the different colours. The circles represent the root mean squared displacement $\sqrt{\langle x^2(t) \rangle}$ of the particles from the origin (centre) providing a measure of the area the particles covered during the simulation time.

For example, a lipid molecule with a microscopic lateral diffusion coefficient of $D = 10 \mu\text{m}^2/\text{s}$ covers an area with a radius of $\sim 300 \text{ nm}$ (circle area $\sim 0.28 \mu\text{m}^2$) within the time of 2 ms. These are typical numbers as experimentally obtained by measuring lipid lateral diffusion within a fluid phospholipid bilayer obtained from z-scan FCS (see section 2.4) [95].

The mathematical description of the phenomenon of lipid diffusion in a lipid bilayer membrane has been matter of research for a long time. There are two main models proposed, both of which take into account the size of the diffusing molecules in proportion to the size of the lipids. In case of molecules smaller or similar in size to lipids, the model is based on the free-area (2D) or free-volume (3D) theory [96–98]. In this way, a molecule can only move if the free area is greater than a certain critical size existing next to it [99]. Even though this free area theory is rather simple, experimental

and molecular dynamics simulation studies showed that they are in close agreement to the theoretical model [97,98].

Membrane components that are larger than lipids sense the membrane as viscous continuum and consider the phospholipids as the “solvent” [98]. Since the motion of diffusing molecules is driven by random collisions with solvent molecules (lipids), there are frictional forces occurring, which originate from the viscous solvent [98]. Including the frictional coefficient F , the diffusion coefficient is defined as:

$$D = \frac{k_B T}{F} \quad (2.2)$$

where k_B is the Boltzmann constant. For a spherical particle of radius R in a medium of viscosity η , the frictional coefficient equals to $F = 6\pi\eta R$. Combined with equation 2.2 the Stokes–Einstein equation is obtained:

$$D = \frac{k_B T}{6\pi\eta R} \quad (2.3)$$

The Stokes-Einstein equation shows that the diffusion coefficient is inversely proportional to both the radius R of the diffusing particle, and the medium viscosity, η . This equation is important for the analysis of fluorescence correlation spectroscopy (FCS) data, in order to determine the dimensions of diffusing particles in aqueous solutions, *e.g.* globular proteins (see section 2.3).

2.1.2 Anomalous diffusion

The diffusion within cellular membranes, *i.e.* the lateral diffusion of lipids and membrane proteins, was found to not follow the Einstein relation (equation 2.1), but is successfully described by its slight modified version:

$$\langle x^2 \rangle = 4Dt^\alpha \quad (2.4)$$

where α is the anomalous exponent and is defined as $0 \leq \alpha \leq 1$. If $\alpha = 1$, this is normal or free diffusion. In case of anomalous diffusion ($\alpha < 1$), $\langle x^2 \rangle$ is decreasing with time. This type of diffusion has been observed in many lipid and membrane protein diffusion experiments [77,99–102]. Anomalous diffusion is a result of intermolecular interactions, such as lipid-lipid, protein-protein or lipid-protein interactions. In addition, impermeable obstacles or domains, such as immobile proteins, lipid microdomains and the cytoskeleton lead to multiple diffusion rates and thus an anomalous diffusion

characteristics within the observed area [103–105]. Therefore, the effect of anomalous diffusion is typically observed in membrane systems with more than one component or in other complex systems.

2.1.3 Saffman-Delbrück equation

To describe lateral diffusion of particles in a lipid membrane, the Stokes-Einstein equation (equation 2.3) is only valid for particles/molecules with a certain dimension ($R < 10 \text{ \AA}$) and that are considered as spheres for simplification. However, in case of membrane proteins laterally diffusing in a membrane, the size and geometry is different and the equation becomes invalid. Saffman and Delbrück extended the Stokes-Einstein equation to be applied to membranes [106]. The membrane is considered as a thin sheet of a viscous fluid, while the membrane is surrounded by another fluid (usually water) of much lower viscosity (Figure 2.2). The membrane protein is modelled as a cylindrical particle with radius R [106,107] and the equation becomes:

$$D = \frac{k_B T}{4\pi\eta_m d} \left[\ln \frac{d\eta_m}{R\eta_s} - \gamma \right] \quad (2.5)$$

Here, k_B is the Boltzmann constant, T is the absolute temperature, d is the membrane thickness, η_m is the membrane viscosity, η_s the viscosity of the surrounding medium and γ is the Euler's constant ($\gamma = 0.5772$).

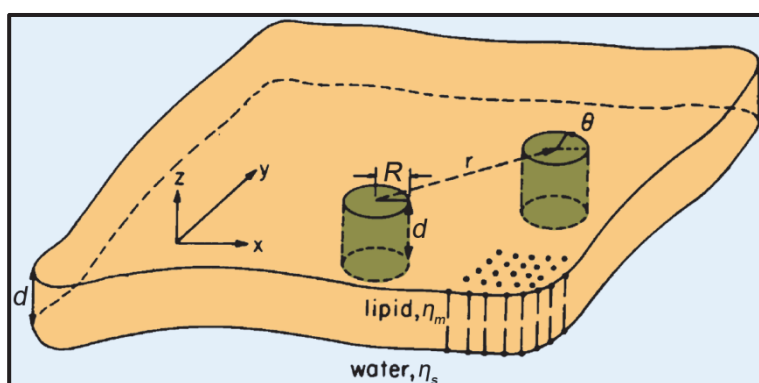


Figure 2.2. The hydrodynamic model proposed by Saffman and Delbrück [106]. The membrane protein is regarded as a cylindrical particle embedded in a lipid bilayer membrane, which is surrounded by water. The cylinder is allowed moving only within the 2D plane of the membrane. Reprinted from [106].

The SD-equation (equation 2.5) predicts that lateral diffusion is relatively insensitive to the size of the diffusing particle. For example, tetramer formation of membrane proteins from their monomers, which roughly corresponds to an increase in radius by a factor of 2,

decreases the diffusion by only a factor of 1.15. Thus, oligomerization or the formation of molecular complexes hardly reduces the diffusion rate.

2.2 Measuring lateral diffusion of macromolecules

2.2.1 Methods of lateral diffusion measurements

There are several standard techniques available to determine lateral diffusion characteristics within artificial or biological membranes. Each of them is suitable for: a specific concentration range of the molecule of interest, concentration of the sample, specific label for detection and each method uses a different time scale of detection and length scale of the detection area. The methods are based on fluorescence detection [108], in particular microscopy-based techniques like single particle tracking (SPT), fluorescence recovery after photobleaching (FRAP) and fluorescence correlation spectroscopy (FCS):

- *Single particle tracking (SPT)*

The position of the particle of interest, *i.e.* a fluorescent dye or nanoparticle, is directly monitored and recorded as a time-directed path using fluorescence microscopy or computer-enhanced video microscopy [109]. Typical spatial resolutions are tens of nanometers (20 – 100 nm) and time resolutions of milliseconds depending on the type of camera (25 μ s – 100 ms) [110,111]. The collected trajectories provide the mean square displacement (equation 2.1) of the particles and the paths can be analysed independent of theoretical fitting models [110]. SPT monitors individual particles, while other methods monitor the motion of a large collection of particles.

- *Fluorescence recovery after photobleaching (FRAP)*

In FRAP, a high intensity laser pulse is directed on a certain area, which irreversibly bleaches the fluorescent particles only in this spot of the membrane. The recovery of the fluorescence intensity due to the diffusion of the non-bleached particles into this illumination spot is then monitored over time, which leads to a recovery fluorescence in the bleached area. The fitting of the recovery curve with an appropriate model allows quantifying the diffusion coefficients and binding kinetics [112]. FRAP needs relatively high concentrations (millimolar range) of fluorescent particles, which might drastically alter the properties of the membrane [112]. In addition, it measures diffusion on length

scales that are restricted by the diffraction limit of the laser beam to ~ 500 nm up to micrometers and timescales of milliseconds to seconds.

- *Fluorescence correlation spectroscopy (FCS)*

FCS measures fluorescence intensity fluctuations in a very small observation volume (~ 1 fL) due to the diffusion of the particles through this observation volume [113]. Autocorrelation analysis reveals diffusion coefficients including information on anomalous diffusion and binding kinetics. FCS measures on a length scale below micrometres and time scales from microseconds up to seconds. For a detailed introduction to FCS, the reader is referred to section 2.3. FCS allows local measurement of diffusion in specific regions of the sample and uses very low concentrations of fluorescent particles. In addition, today's microscopes combine a laser scanning microscope with FCS making the microscope a very versatile tool for other measurements (*e.g.* cell imaging, cell uptake, drug release, *etc.*). In this work, FCS was selected as method of choice because the confocal fluorescence microscopy setup together with the fluorescence correlation spectroscopy detector was available in the research group and is currently one of the most sensitive and precise methods to observe lateral diffusion processes within membranes. Figure 2.3 shows the principle of measurement of lateral diffusion on membranes by FCS.

- Non-fluorescent methods are magnetic resonance techniques, such as nuclear magnetic resonance (NMR) [114,115] or electron spin resonance (ESR) [116,117]. However, they are less sensitive compared to the fluorescence-based techniques and do not permit nano-/micro-scale resolutions. Microscopic techniques allow directly visualizing the samples to distinguish *e.g.* domains within more complex systems.

2.2.2 Fluorescence labelling

In the recent years, the development of microscopy imaging has increased resolution, accuracy and sensitivity for fluorescence detection. The advantage of fluorescence is, that the emitted light can be separated from the excitation light via appropriate filters in the microscope, because the fluorescent compounds are excited with light of a certain wavelength (λ_{exc}) and emit light with a higher wavelength (λ_{em}); this difference between λ_{exc} and λ_{em} is known as Stokes shift. In this way, the detected signal shows a high signal-to-noise ratio. In order to visualize the particles of interest, they have to be modified by fluorescent compounds (Figure 2.3). The labelling of the particle of interest

can be performed by different methods. The most common one is the direct chemical attachment of a fluorophore to the macromolecule. Another one is the use of antibodies carrying a fluorophore. The antibodies specifically bind to the macromolecule of interest (*e.g.* proteins). The third one is the modification by genetic engineering when using proteins. Modification of the genome to the end of the sequence of the protein can co-express for example green fluorescent protein (GFP). In this way, each protein will carry a GFP molecule. It has to be noted, that the introduction of fluorescent labels on a molecule by any of these methods is changing the molecular structure to some extent, which has to be taken into account for data analysis and is the main disadvantage of fluorescence-based methods.

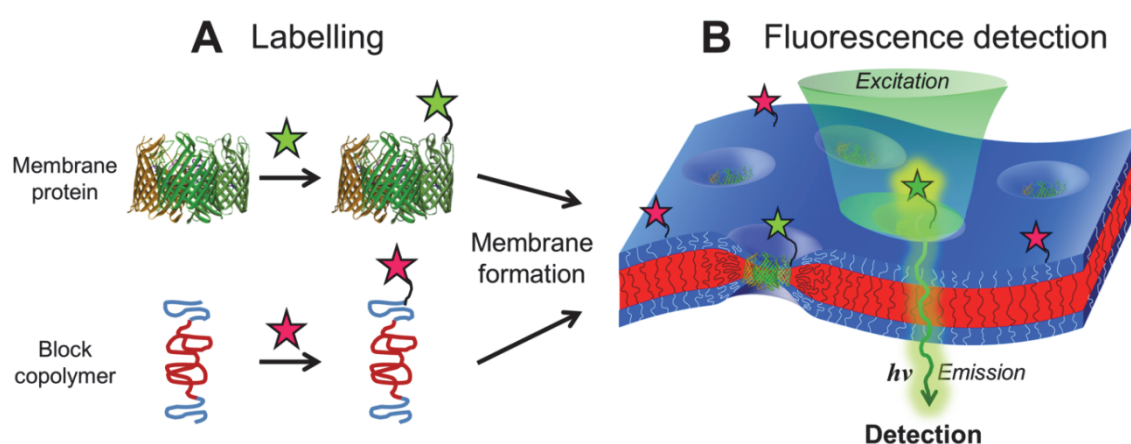


Figure 2.3. Principle of lateral diffusion measurement of diffusing membrane components based on fluorescence correlation spectroscopy (FCS). A) The particle of interest has to be labelled with a fluorescent dye. B) The labelled macromolecules are excited by a laser and the emission is recorded on a detector.

2.3 Fluorescence correlation spectroscopy (FCS)

2.3.1 Basic principle of FCS

Fluorescence correlation spectroscopy is an experimental, fluorescence based, technique and was first described in the early 1970s [118–120]. The technological advancement of the confocal optics, laser lights and photon detection sensors (*e.g.* avalanche photodiodes), increased the sensitivity down to single-molecule levels. FCS uses an extremely small detection volume as the observation cell (femtoliter size, $\sim 10^{-15}$ L = $1 \mu\text{m}^3$) [113]. FCS provides the advantage to detect single molecules at high spatial and temporal resolution at very low concentrations, *i.e.* concentrations down to the nanomolar

range (10^{-9} M), with high signal-to-noise ratio and short measuring times (ms, milliseconds). This largely improves the statistical significance of the measurement. In general, fluorescence intensity and the intensity fluctuation over time – due to the diffusion of the fluorescent molecules – are of interest. This provides information on diffusion and local concentrations, and at the same time information on molecular sizes, molecular weights, aggregation states, association and dissociation constants, chemical rate constants and intermolecular interactions [121–123].

FCS uses a confocal microscope setup (Figure 2.4 A), which, in contrast to conventional fluorescence microscopy, illuminates a single spot (confocal volume) (Figure 2.4 B), therefore providing also resolution in the z-axis. A laser light of specific wavelength is focused onto the specimen by an objective with high numerical aperture (NA). The diffraction causes the laser to be focused not as a single point, but as a focal volume (V_f) element. The width ω_0 of V_f is given by $\omega_0 = \frac{\lambda}{2 \cdot NA}$, where λ is the wavelength of the laser beam. Due to refraction limits, NA has a finite number and, therefore, V_f is only changing with the wavelength λ used in the system. At the same time, the fluorescence signal emitted from the illuminated molecules is collected through a pinhole, which suppresses the out-of-focus light. This increases the axial resolution and scattered light is suppressed (Figure 2.4A) [124].

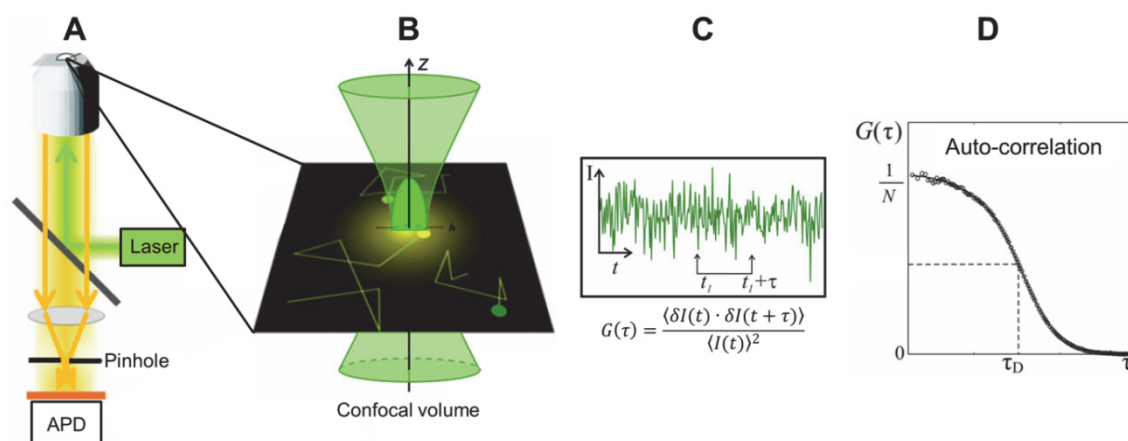


Figure 2.4. Principle of FCS. A) Confocal setup of the microscope. The laser light is focused onto the sample and the fluorescence detected by an avalanche photodiode (APD). B) The laser light is focused onto the sample membrane. Fluorescent molecules diffuse through the confocal volume and the emitted fluorescence is detected. C) The fluorescent molecules give rise to intensity fluctuations, which are subjected to the autocorrelation algorithm. D) The generated autocorrelation function provides the important parameters diffusion time τ_D and number of particles N . Adapted with permission from [125].

2.3.2 Molecule statistics

In FCS, the fluorescence intensity is recorded over time at very high temporal resolution to resolve time steps down to 1 μs and lower. At perfect conditions, *i.e.* single-photon detection, constant excitation intensity, *etc.*, it is possible to record photon by photon emitted by the fluorescent dyes using avalanche photo diodes (APD) (Figure 2.4 A). The fluorescent particles diffuse around and only emit photons while they are in the confocal volume (Figure 2.4 B). Therefore, the fluorescence intensity gives information on the fluorescent particle concentration and the intensity fluctuation around the mean value is used to obtain other parameters such as molecular brightness or hydrodynamic radius [126]. The temporal resolution of the signal provides the basis to generate a correlation (Figure 2.4 C). The intensity fluctuations from the raw data are mathematically quantified by autocorrelating the signal (equation 2.6). The obtained autocorrelation function $G(\tau)$ is a measure of the self-similarity of the signal, *i.e.* the probability to detect the signal at time τ again:

$$G(\tau) = \frac{\langle \delta I(t) \cdot \delta I(t + \tau) \rangle}{\langle I(t) \rangle^2} \quad (2.6)$$

where $\delta I(t) = I(t) - \langle I(t) \rangle$ are the fluctuations around the mean value $I(t)$, $\langle I(t) \rangle$ is the time averaged fluorescence intensity and $\delta I(t + \tau)$ is the intensity at the shifted time $t + \tau$. The calculation of $G(\tau)$ can be performed either using a hardware correlator or a software correlation algorithm [127].

The decay time τ_D (further referred to diffusion time), which is the time at the half intensity of the autocorrelation curve (Figure 2.4D), is then the mean average residence time of the particles in the detection volume. Since the exact volume of the measuring focus (V_f) can be obtained by external calibration, the concentration $\langle C \rangle$ of the analysed particles can be calculated. The zero-time correlation ($G(0)$) yields the average number of particles $\langle N \rangle$:

$$G(0) = \frac{1}{\langle N \rangle} = \frac{1}{V_f \langle C \rangle} \quad (2.7)$$

For a quantitative determination, it is required to fit the experimentally obtained autocorrelation curve by a mathematical model function containing the parameters of interest. Software programs vary these parameters in order to minimize the difference between the experimental correlation curve and the model [125].

For 2D Brownian diffusion within a membrane through a detection area with a Gaussian profile, the model function is described as:

$$G(\tau) = \frac{1}{C\pi\omega_0^2} \cdot \frac{1}{1 + \left(\frac{4D\tau}{\omega_0^2}\right)} = \frac{1}{N} \cdot \frac{1}{1 + \left(\frac{\tau}{\tau_D}\right)} \quad (2.8)$$

Here, $N = C\pi\omega_0^2 = CA_f$ is the average number of particles in the detection area ($A_f = \pi\omega_0^2$) and D is the diffusion coefficient, which is calculated from the diffusion time $\tau_D = \frac{\omega_0^2}{4D}$. In case of anomalous diffusion (see section 2.1.2), the exponent α ($1 \geq \alpha \geq 0$) is added to equation 2.8 and becomes:

$$G(\tau) = \frac{1}{N} \cdot \frac{1}{1 + \left(\frac{\tau}{\tau_D}\right)^\alpha} \quad (2.9)$$

However, it is important to consider that the determination of N and τ_D involves the exact definition of the laser beam area. This parameter is usually obtained by a calibration measurement of a series of known free dye concentrations with a known diffusion coefficient. Other model functions take into account photophysical phenomena generating additional fluctuations (*e.g.* triplet state (Figure 2.5), blinking), the presence of additional fluorescent components (two or more components), free dyes in solution, particle binding

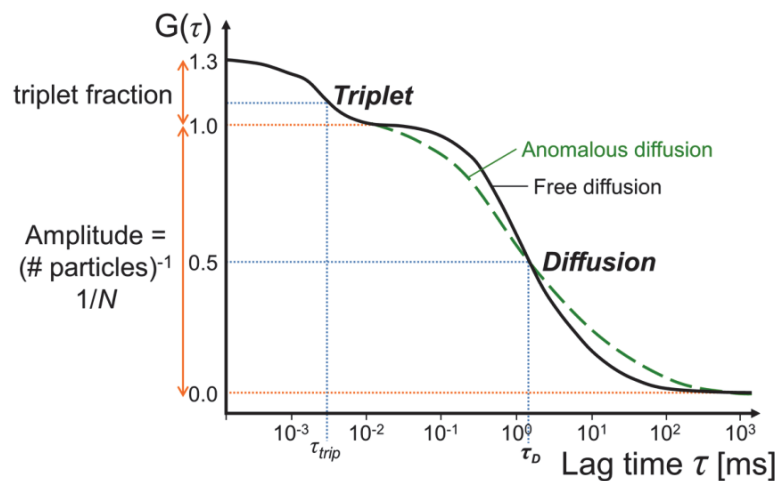


Figure 2.5. Autocorrelation function of diffusing particles analysed by FCS. Triplet dynamics typically appear at $\tau \approx 1\text{-}3 \mu\text{s}$, diffusion dynamics in solution at $\tau > 20 \mu\text{s}$, diffusion in membranes at $\tau > 1000 \mu\text{s}$. Anomalous diffusion flattens the autocorrelation function. The number of particles N is the inverse of the amplitude.

fluorescent components (two or more components), free dyes in solution, particle binding dynamics or a non-Gaussian detection profile [127]. An overview of the different model functions available for FCS is given in the book chapter of Hermann *et al.* (2015) [123].

The following two equations are used to account for 2D diffusion of a single component including the triplet state (equation 2.10) and 2D diffusion of two components including triplet state (equation 2.11):

$$G_{2D-1comp}(\tau) = 1 + \left(1 + \frac{T_{trip}}{1 - T_{trip}} e^{-\frac{\tau}{\tau_{trip}}}\right) \cdot \frac{1}{N} \left[\frac{1}{1 + \left(\frac{\tau}{\tau_D}\right)^\alpha} \right] \quad (2.10)$$

$$G_{2D-2comp}(\tau) = 1 + \left(1 + \frac{T_{trip}}{1 - T_{trip}} e^{-\frac{\tau}{\tau_{trip}}}\right) \cdot \frac{1}{N} \left[\frac{(1-f)}{1 + \left(\frac{\tau}{\tau_{D1}}\right)^\alpha} + \frac{f}{1 + \left(\frac{\tau}{\tau_{D2}}\right)^\alpha} \right] \quad (2.11)$$

The first term in both equations (2.10 and 2.11) represents the correction for intersystem crossing (molecules in triplet state), where T_{trip} is the fraction of fluorophores in the triplet state, τ_{trip} is the corresponding triplet time, and f is the fraction of particle number two ($0 \leq f \leq 1$).

The external calibration is a general drawback of this measurement technique because it is prone to artefacts and all the further FCS measurements rely on this calibration. Optical aberrations are one source of error that can alter the ideal geometry of the confocal volume. This deviation can be caused by incorrect coverslip thicknesses, refractive index mismatch, incorrect pinhole adjustment, or astigmatism, which can lead to high errors in diffusion, and even higher errors in concentration measurements [128]. Other artefacts are related to high excitation intensities, which result in photobleaching of the dyes and depend on the time the dye is residing in the illuminated volume. This is especially important for slow diffusing particles [124,128].

For FCS measurements on planar membranes, the exact positioning of the sample membrane with respect to the focus at the minimum beam waist (ω_0) is crucial because only this size of the measurement area is known. At a small deviation from ω_0 the calculated diffusion coefficient will be wrong. For example, the thickness of a phospholipid membrane is only 5 nm and is therefore several orders of magnitude smaller than the laser beam z-dimensions. These different diameters of the illuminated part of the membrane result in different values of τ_D and N . In order to overcome these problems

discussed above and/or to reduce the measurement errors to significant levels, various extensions to conventional FCS have been developed [127], such as scanning-FCS [129], two-focus FCS [130], TIRF-FCS [131], *etc.* Another extension that is frequently used on membranes and has the advantage that it can be easily performed with a standard FCS setup, is the z-scan FCS method, which allows scanning along the z-axis [105,132]. This method will be discussed in detail in the following sections.

2.4 Z-scan FCS

Z-scan FCS is one out of several existing types of FCS methods that overcomes the calibration problem of the detection volume dimensions and is considered as a calibration-free method of FCS. It was first introduced by Benda *et al.* in 2003 [132]. This technique is well suited for the measurement on supported membranes on surfaces, giant unilamellar vesicles (GUVs) and biological membranes. The most important requirement is that the membrane is stable and non-moving.

2.4.1 Principle of z-scan FCS

Z-scan FCS is used to measure diffusion coefficients and particle number at different beam waists (ω), which is based on recording a consecutive set of FCS autocorrelation curves along the optical axis (z-axis) of the measuring plane (Figure 2.6) [105,122]. Typically, the step-size, *i.e.* the distances between the different measuring planes, is between 100 and 300 nm. In this way, the illuminated area is changed with each position of the step size according to the geometry of the Gaussian beam.

The measured diffusion times and number of particles thus yields an axial dependence of the confocal radius ω . The minimum beam waist ω_0 and thus the diffusion coefficient D and the minimum number of particles N_0 can be determined by fitting the diffusion times and number of particles with respect to the distance Δz from the confocal center [132]:

$$\tau_D(\Delta z) = \frac{\omega_0^2}{4D} \left(1 + \frac{\lambda_0^2 \Delta z^2}{\pi^2 n^2 \omega_0^4} \right) \quad (2.12)$$

$$N(\Delta z) = N_0 \left(1 + \frac{\lambda_0^2 \Delta z^2}{\pi^2 n^2 \omega_0^4} \right) \quad (2.13)$$

Where λ_0 is the excitation wavelength of the laser and n is the refractive index (water: $n = 1.33$). The parameters of interest are τ_D and N , and are calculated from the fit of the

consecutive set of autocorrelation functions obtained for each position along the z -axis. Equations 2.12 and 2.13 show the parabolic dependency of τ_D and N on Δz . The fitting results in statistically precise values of D and N_0 .

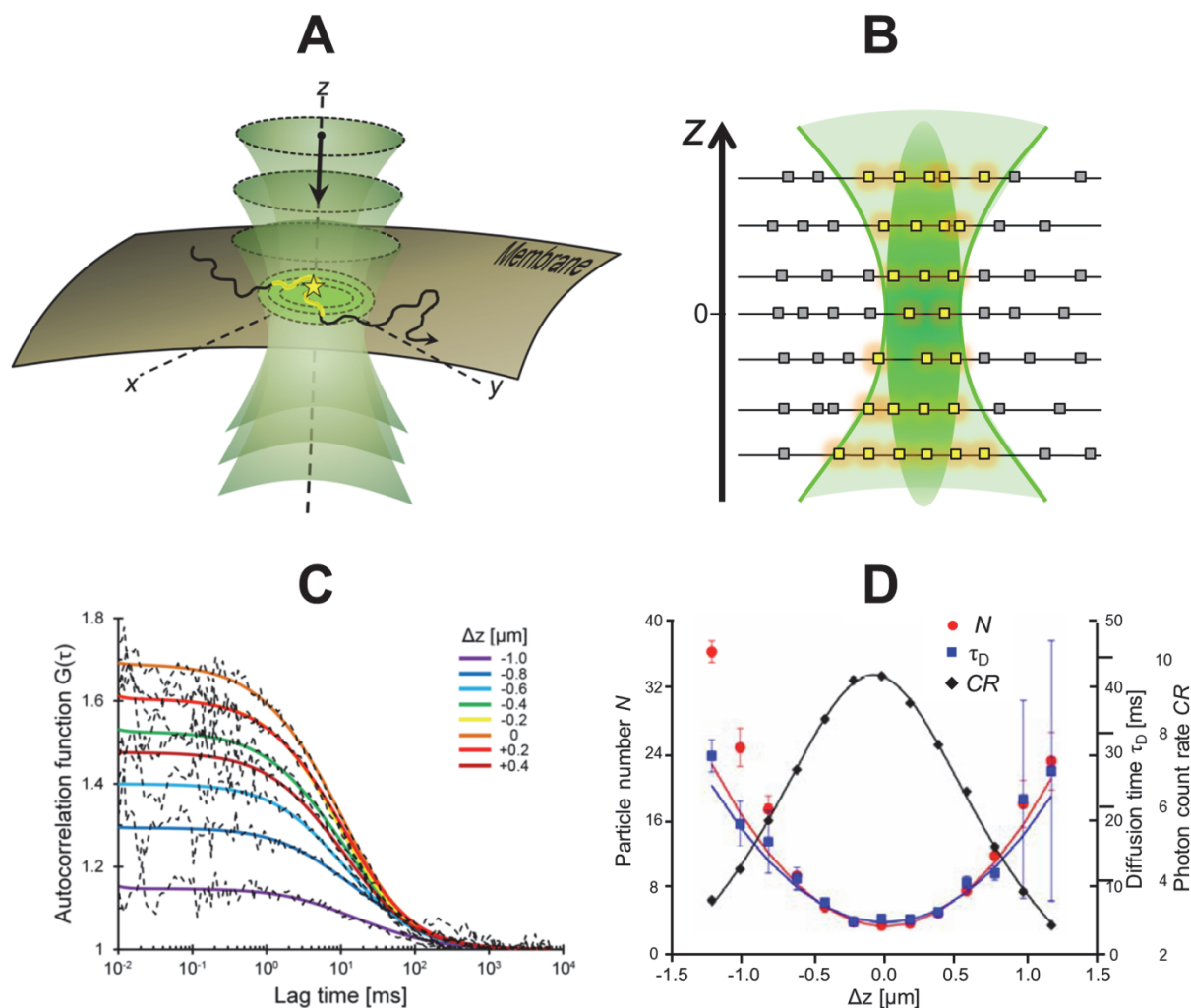


Figure 2.6. Principle of z -scan FCS on a membrane to determine lateral diffusion coefficients. A) The laser beam is shifted in small steps along the z -axis in order to change the observation area on the membrane. Adapted with permission from [133]. B) The number of fluorescent particles is lowest at the centre of the beam waist and increases by increasing the distance from there. C) Obtained autocorrelation functions and corresponding fits. D) Analysed data reveals the parabolic z -dependency of the diffusion time τ_D and number of particles N .

2.4.2 FCS diffusion law

Besides the advantages of z -scan FCS as a calibration-free method, the different illuminated areas provide information on the diffusion characteristics (Figure 2.7) [100]. The combination of the FCS diffusion law and z -scan FCS provides a linear dependence of τ_D on N due to a spot-size variation of the laser beam:

$$\tau_D \left(\frac{N}{N_0} \right) = t_0 + \frac{\omega_0^2}{4 \cdot D_{eff}} \frac{N}{N_0} \quad (2.14)$$

where $\frac{N}{N_0}$ is the relative number of particles in the illuminated area (spot size), ω_0 is the minimum beam waist and D_{eff} is the effective diffusion coefficient calculated from the slope. The interesting parameter here is the intercept t_0 , which provides information on the membrane organization and thus offers an indication on the membrane structure. A value of $t_0 = 0$ is considered as free diffusion as the number of particles is zero at zero beam waist. On the other hand, the diffusion is considered hindered if the value of t_0 becomes nonzero. In this case, the diffusing object can be hindered by traps and domains existing in the membrane, which yields $t_0 > 0$. The decrease in τ_D as a function of the spot size is therefore less steep than in the case of free diffusion. If the diffusing object is guided, for example by a network, $t_0 < 0$, also called hop-diffusion and results in a steeper slope (Figure 2.7). In typical z-scan FCS experiments, the spot size varies from ~ 200 to 500 nm, depending on the laser wavelength [100].

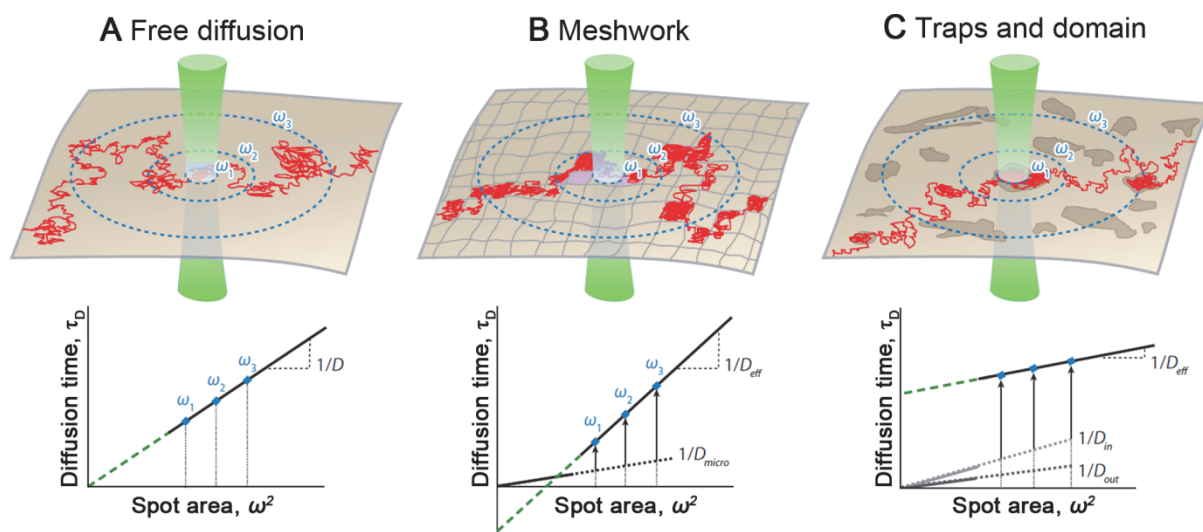


Figure 2.7. Examples of the FCS diffusion law. The diffusion characteristics can be determined by measuring the diffusion time at different spot areas. The y-axis intercept on the plot of the diffusion time versus the spot changes depending on the membrane organizations. A) Free diffusion causes the intercept to be zero. B) In case of a meshwork, the particles experience a guided diffusion and thus, the intercept is negative. C) Hindered diffusion is caused by traps and domains, where the particles reside longer than outside of them, which causes a positive intercept. Adapted with permission from [133].

Chapter 3

3 Molecular organization and dynamics in polymersome membranes: A lateral diffusion study

In this chapter, the results of lateral diffusion measurements on block copolymer membranes are presented. The study provided insight into important membrane properties such as membrane fluidity and membrane thickness of triblock and diblock copolymers. The data was compared to the properties of lipid bilayers.

This study has been published:

F. Itel, M. Chami, A. Najer, S. Lörcher, D. Wu, I. A. Dinu, W. Meier, Molecular Organisation and Dynamics in Polymersome Membranes: A Lateral Diffusion Study, *Macromolecules* (2014), 47, 7588 – 7596.¹

3.1 Problem definition

The increased complexity of functionalized nanoreactors necessitates robust methods to analyse the properties of the created structures. Therefore, the interaction of membranes with their associated molecules and proteins is of fundamental importance and is necessary to deduce information about the activity and function of the artificial system. In order to be fully functional, membrane proteins depend on a flexible and fluid environment as provided by natural lipid bilayers [134]. This can be assured by the fluidity of the membrane, which is an important structural factor deduced from lateral diffusion coefficients of membrane components [100].

¹ Reprinted (adapted) with permission from reference [95]. Copyright (2014) American Chemical Society.

According to the fluid mosaic model proposed by Singer and Nicholson [18], the membrane constituents diffuse freely in a 2D membrane and the molecules are distributed randomly. From high-resolution structures of biological membranes, the definition of “freely” and “randomly-distributed” are imprecise definitions and it is well known today that rather a non-randomness situation within the biological membranes is the case [135]. Lateral diffusion measurements of cell membranes and artificial lipid membranes showed that supramolecular clusters, called rafts, form functional domains, which are important to maintain cellular functions [135]. The experimentally observed fluidity, based on fluorescence measurements, in such membranes is described by different diffusion effects induced by three types of membrane organizations: (i) free diffusion without any hindrance, (ii) hindered-diffusion caused by (micro-) domains and (iii) impeding-diffusion by a meshwork [133]. For this purpose, the lateral mobility and deduced membrane organizations reveal insight into structural aspects at the molecular level.

Lipids, due to their low molecular weight, possess a “soft” property within the separated bilayer [136]. In contrast, amphiphilic block copolymers usually have high molecular weights and thus behave as bulky and coiled macromolecules within the membrane. Regarded from a structural point of view, amphiphilic block copolymers within a self-assembled membrane adopt much more complex structures. This results in slow diffusion properties [23]. Diblock and triblock copolymers are two of the most commonly synthesized block arrangements in the field of self-assembling polymers for the generation of artificial membranes. As described in section 1.5.1, diblock copolymers can form structures similar to lipid bilayers, but due to interdigitation and entanglement of the chains the layers are not fully separated [63]. Triblock copolymer chains having an ABA arrangement (hydrophilic-hydrophobic-hydrophilic) can adopt two possible conformations inside the self-assembled membrane: the I-shape and U-shape [65,66]. It is believed that the membrane is composed of a mixture of both chain conformations [65]. In addition, by increasing the molecular weight of the polymer, the entropic energy contribution increases, leading to an increased number of possible conformations of the polymer chains, *i.e.* stronger interdigitation and entanglement of the chains within the membrane [63,137]. Furthermore, the membrane thickness can be modulated according to the molecular weight of the hydrophobic block [62]. Thicker membranes are more stable due to a larger area of hydrophobic interaction. It was described that the conformation of the polymer molecules changes with the molecular weight due to the strong segregation

limit (SSL) at the block interface. The repulsion between the hydrophilic and the hydrophobic block causes a more stretched chain conformation [62,138]. This results in a lower density of the hydrophobic membrane layer for low molecular weight polymers (similar to lipids, ~ 1000 g/mol). In contrast, higher molecular weight copolymers form larger membrane thicknesses and therefore experience less segregation force due to an increase in chain flexibility. This leads to more coiled and denser structures, which is reflected in interdigitation lower fluidity of the leaflets.

Important membrane properties, such as lateral diffusion coefficients, domain formation, membrane thickness and membrane viscosity provide important information for the generation of biomimetic membranes for certain. The membranes are composed of diblock (A_xB_y) and triblock ($A_xB_yA_x$) copolymers containing poly(2-methyl-2-oxazoline) (PMOXA) and poly(dimethylsiloxane) (PDMS) blocks known to form polymersomes and incorporate membrane proteins in aqueous solution [3,39,139]. In order to determine lateral diffusion coefficients and to investigate the membrane structure, a large library of diblock and triblock copolymers with different molecular weights was synthesized (Table 3.1). Z-scan fluorescence correlation spectroscopy (FCS) was used to determine lateral diffusion coefficients on the membranes of giant unilamellar vesicles (GUVs) and to retrieve information about the existence of rafts and domain structures below the refraction limit of the laser beam [132,140]. Cryogenic transmission electron microscopy (Cryo-TEM) was performed to determine membrane thicknesses of self-assembled polymersomes in order to deduce the chain conformation of the polymer molecules within the membrane [69].

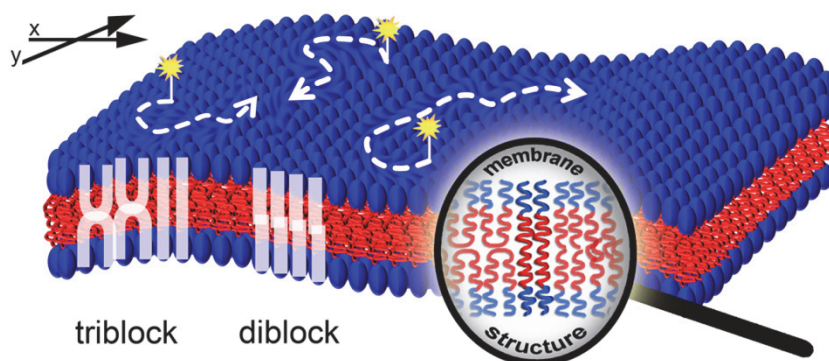


Figure 3.1. Schematic representation of lateral diffusion of amphiphilic block copolymer macromolecules that self-assemble into membranes.

3.2 Results and discussion

3.2.1 Amphiphilic block copolymers and self-assembly

This study on the lateral diffusion within block copolymer membranes is based on a large library of ten different polymers; six were synthesized in triblock- and four in diblock configuration (Table 3.1). The block copolymers are composed of PMOXA_x-*b*-PDMS_y-*b*-PMOXA_x, further referred to as A_xB_yA_x and diblocks as A_xB_y, where the subscripts x and y denote the degree of polymerization as determined by ¹H-NMR. The polymers, known to have high PDIs (Table 3.1), differ only in their block lengths and molecular weights. The calculated hydrophilic weight fractions ($f_{hydrophilic}$) were between 21 - 32%, similar to the hydrophilic weight fraction of lipids ($f_{lipids} \approx 35\% \pm 10\%$), hence these amphiphiles possess the ability to form vesicular structures in aqueous solutions (Figure 3.2) [4]. These block copolymers are able to form GUVs required to measure lateral diffusion by the z-scan FCS method.

Table 3.1. Molecular characteristics of amphiphilic triblock and diblock copolymers (molecular weight M_w , molecular weight of PDMS block $M_{w,PDMS}$, hydrophilic weight fraction $f_{hydrophilic}$, polydispersity index (PDI)).

	molecular composition ^a	M_w [kg/mol]	$M_{w,PDMS}$ [kg/mol]	$f_{hydrophilic}$ [%]	PDI^b
Triblock	A ₃ B ₁₉ A ₃	2.1	1.5	32	2.4
	A ₆ B ₃₄ A ₆	3.8	2.6	32	2.3
	A ₆ B ₄₄ A ₆	4.5	3.3	25	1.8
	A ₇ B ₄₉ A ₇	5.1	3.7	27	2.1
	A ₁₂ B ₆₃ A ₁₂	6.9	4.7	32	2.1
	A ₁₂ B ₈₇ A ₁₂	8.7	6.5	25	1.6
Diblock	A ₆ B ₂₂	2.5	1.7	28	1.8
	A ₉ B ₃₁	3.3	2.4	28	1.4
	A ₈ B ₃₉	3.8	3.0	22	1.5
	A ₁₄ B ₆₅	6.2	4.9	21	1.7
Lipid	POPC	0.77	-	~35	-

^aDetermined by ¹H NMR. ^bDetermined by GPC.

All the block copolymers used in this study form polymersomes in Hepes buffer (20 mM Hepes, 50 mM NaCl, pH 7.4) and their supramolecular assemblies were confirmed by cryo-TEM (Figure 3.2). It is interesting that the self-assembly differs between the block

copolymers, although all feature a similar $f_{hydrophilic}$ value. Some of the polymers generate a lot of polymersomes, while others show a rather low number of polymersomes, although in all the samples the same polymer concentration was used (5 mg/ml). This might be attributed to several factors originating from the block copolymer synthesis [141–144]:

- i) Polydispersity index: The PDI of the block copolymers is very high (1.6 – 2.4) because the synthesis of bifunctional PDMS (for triblock copolymer) was done by polycondensation (step-growth polymerisation). From a general observation in our labs, this technique provides difficulties in controlling the polydispersity of the obtained PDMS. For the synthesis of commercial PDMS, the equilibrium polymerisation is commonly used, which leads to homopolymers with slightly lower PDIs.
- ii) Purification: The purification of block copolymers after the synthesis is an important step to eliminate residual components needed for the chemical reactions (solvents, monomers, initiators, unreacted PDMS, *etc.*). Therefore, it is common to apply ultrafiltration, where the block copolymers are separated from small molecular weight compounds. Due to the amphiphilic nature of the polymers, it is difficult to find a “good” solvent, which is able to extend the polymeric structure of the single macromolecules. For example, PDMS can coil and entrap small hydrophobic molecules, which remain in the final “purified” sample. In addition, minimal amounts of unreacted PDMS (*i.e.* not connected to PMOXA) can remain in the final sample. These residual compounds, even at very small concentrations, can sometimes not be detected by NMR, or the signal from the final sample overlaps the signals from the trace materials. To which extent these compounds influence the self-assembly process is not known and cannot be really controlled.

These issues have always been a problem in PMOXA-*b*-PDMS-*b*-PMOXA block copolymer synthesis and they are especially difficult to control for triblocks. Nevertheless, the here chosen block copolymers self-assemble to polymersomes, and just the efficiency they assemble to polymersomes is differing between each polymer batch.

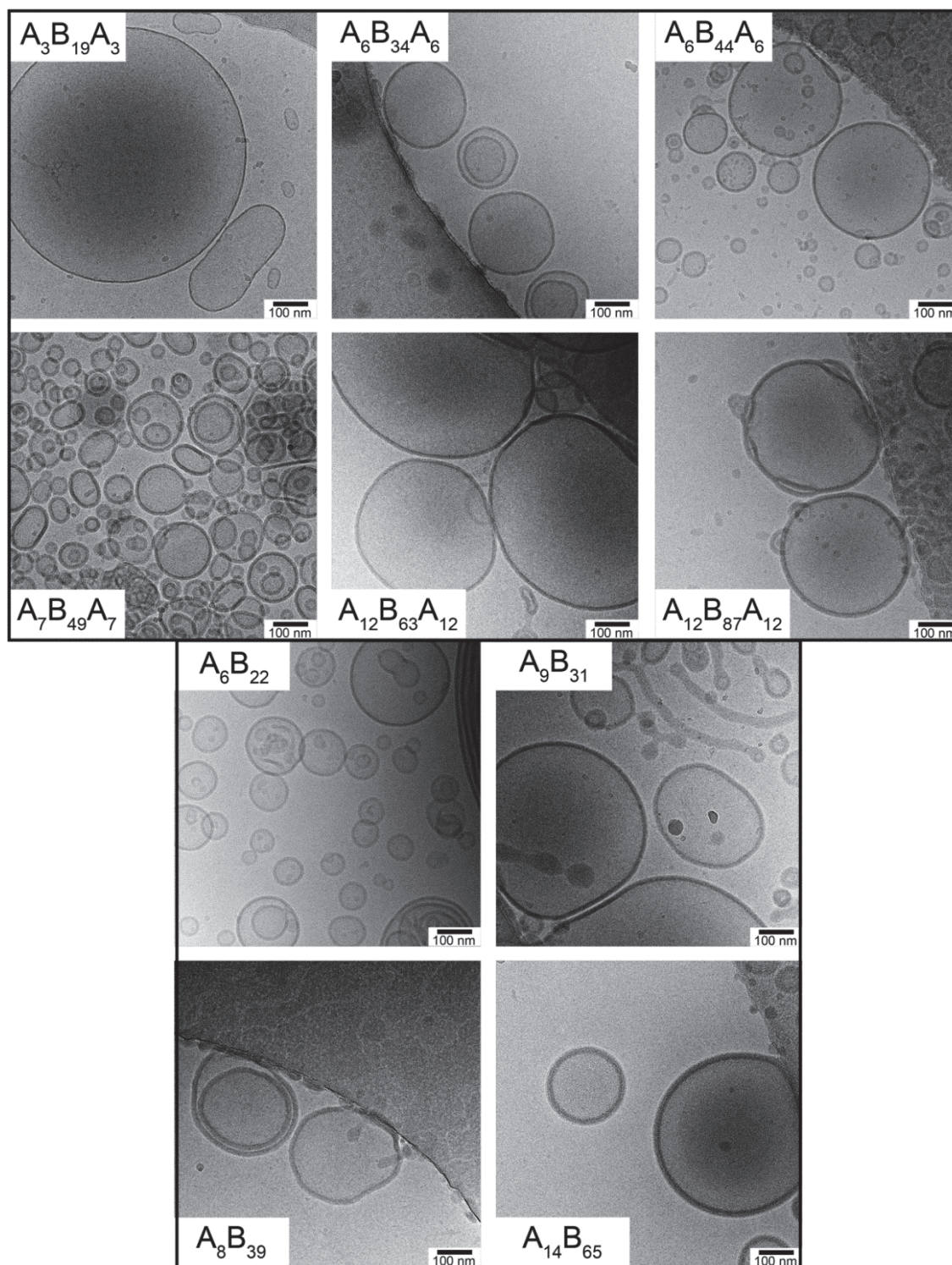


Figure 3.2. Representative cryo-TEM images of all block copolymers. Six different triblock (upper panel, non-extruded) and four different diblock (lower panel) copolymer vesicle dispersions at concentrations of ~ 5 mg/mL in a HEPES buffer (20 mM HEPES, 50 mM NaCl, pH 7.4) were prepared. All images have the same magnification and the scale bar represents 100 nm.

3.2.2 Membrane thickness and molecular weight dependence

Membrane thicknesses of all block copolymers and of the lipid POPC were determined from images obtained by cryogenic transmission electron microscopy (cryo-TEM) (Figure 3.2). The thicknesses were obtained by lineal analysis measuring the distances of the dark part of the membrane using ImageJ software (ImageJ, US National Institutes of Health). Membrane thicknesses were calculated as mean values \pm SD ($n \geq 100$). All samples show a Gaussian distribution of the membrane thickness, while the standard deviation is increasing with increasing membrane thickness (Figure 3.3 and Table 3.2).

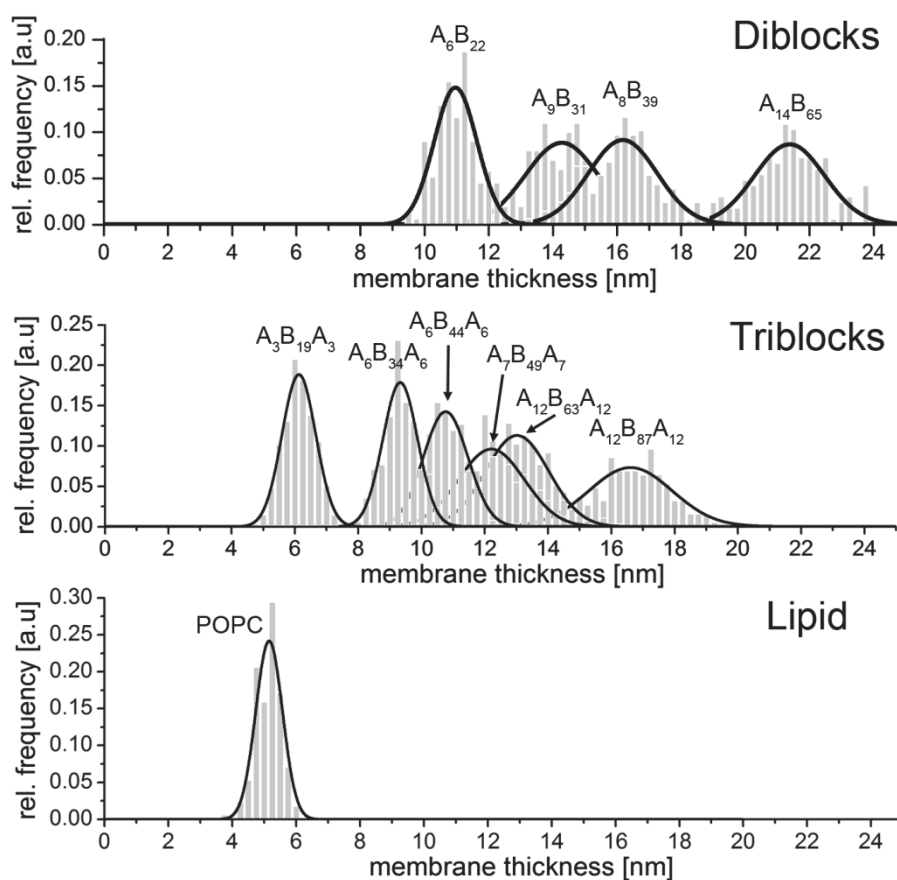


Figure 3.3. Membrane thickness calculation. Gaussian distribution curves of all block copolymer membranes (diblock and triblock copolymers, and the lipid POPC).

The membrane thickness of amphiphilic block copolymer membranes depends on the molecular weight of the hydrophobic block [62,66]. As shown in Table 3.2 and Figure 3.4, the membrane thickness increases with the number of PDMS units (block B).

Table 3.2. Statistical significance of membrane thickness determination for all block copolymer membranes. The results are obtained from Figure 3.3.

	molecular composition	$M_{w,PDMS}$ [kg/mol]	Membrane thickness [nm] Mean value \pm SD	R^2 (Gaussian fit)	n
Triblock	$A_3B_{19}A_3$	1.5	6.0 ± 0.5	0.99	275
	$A_6B_{34}A_6$	2.6	9.2 ± 0.5	0.96	169
	$A_6B_{44}A_6$	3.3	10.7 ± 0.7	0.98	260
	$A_7B_{49}A_7$	3.7	12.1 ± 1.0	0.94	310
	$A_{12}B_{63}A_{12}$	4.7	13.4 ± 0.9	0.96	273
	$A_{12}B_{87}A_{12}$	6.5	16.2 ± 1.4	0.91	187
Diblock	A_6B_{22}	1.7	10.9 ± 0.7	0.91	155
	A_9B_{31}	2.4	14.3 ± 1.1	0.84	100
	A_8B_{39}	3.0	16.0 ± 1.1	0.91	206
	$A_{14}B_{65}$	4.9	21.3 ± 1.2	0.90	165
Lipids	POPC	-	5.0 ± 0.4	0.93	138

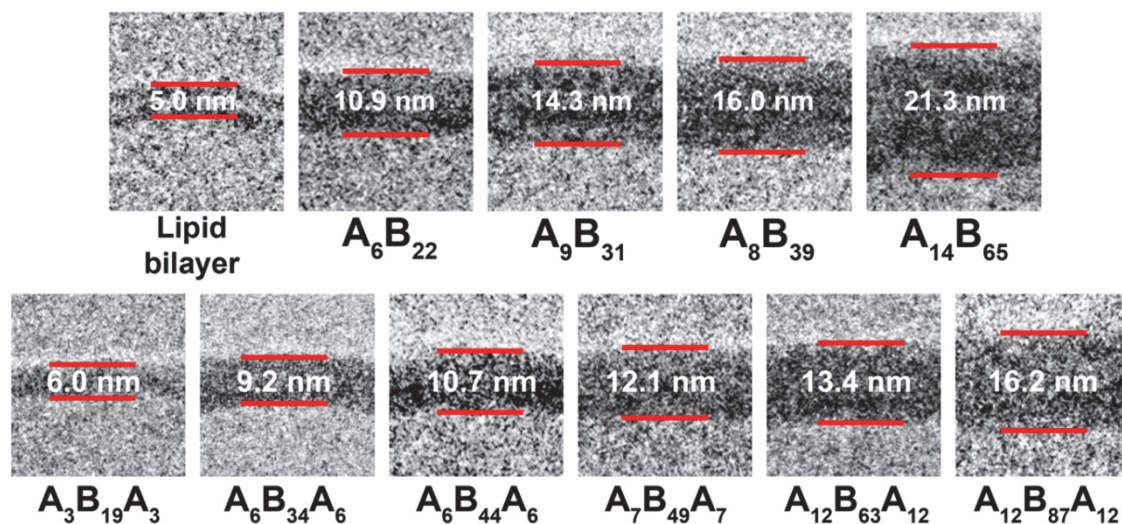


Figure 3.4. Systematic view of membrane thicknesses. Diblock (upper panel) and triblock (lower panel) copolymer membranes are arranged with increasing membrane thickness (from left to right). Images were generated by the cryo-TEM technique.

Systematic studies on the membrane thickness of hydrophobic blocks composed of poly(butadiene) (PBD) [69] and poly(ethylene) (PEE) [72] revealed that the membrane thickness d scales with the molecular weight of the hydrophobic block (M_h) as $d \propto (M_h)^a$ (equation 1.2). The exponent a provides information about the polymer structure [69,145] and was calculated for both diblock and triblock copolymers (Figure 3.5).

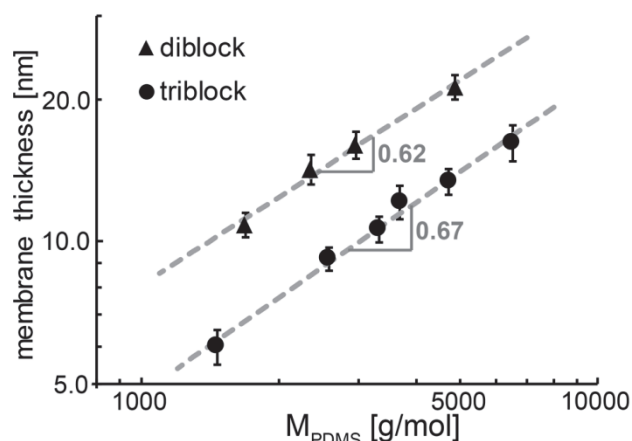


Figure 3.5. Power law dependence of the membrane thickness on the hydrophobic molecular weight of the PDMS block ($M_{w,PDMS}$) with the corresponding calculation of the slope (exponent a). The slope provides information about the chain conformation of the macromolecules. Lines represent linear fits; error bars represent standard deviations (\pm SD).

The analysis of the membrane thickness (Figure 3.5) results in similar values for the exponent a of 0.67 (triblock) and 0.62 (diblock) for both polymer types; values that show a chain conformation according to the strong segregation theory (SSL: $a = 0.66$). Furthermore, the data points do not behave exactly according to equation 1.2; the exponent a is increasing with decreasing $M_{w,PDMS}$ and vice-versa (Figure 3.6) as reported previously [62].

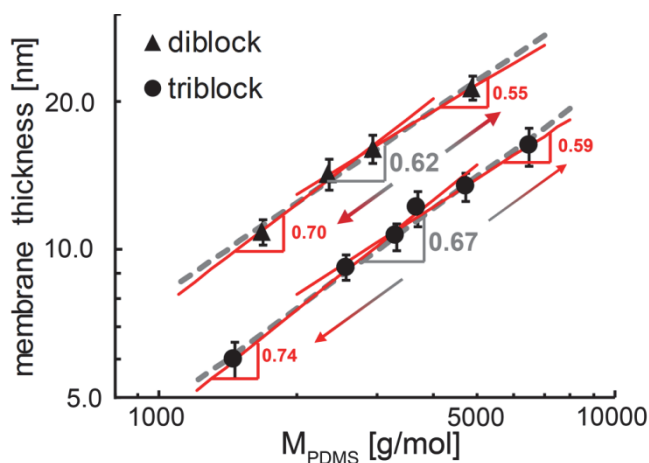


Figure 3.6. Change in power law dependence of the membrane thickness on the hydrophobic molecular weight of the PDMS block ($M_{w,PDMS}$). The slopes are increasing with decreasing molecular weight and vice-versa, indicated by the red numbers.

Figure 3.6 shows the change of the slope when the fit is based on the upper and lower data points. For diblocks, the linear fits in red are based on the upper or lower three data points, while for triblocks, the linear fits are based on the upper or lower four data points.

It has to be noted that this analysis provides just a rough estimation what happens with the polymer structure at higher and lower molecular weights, the effect of which was shown with other polymers [62]. Here, at hydrophobic molecular weights below 2500 g/mol, the chains are more stretched ($a \approx 0.70 - 0.74$) leading to more ordered chain configurations within the membrane. With increasing molecular weight ($M_{w,PDMS} > 4000$ g/mol) the exponent a decreases towards values below 0.6 ($a \approx 0.55 - 0.59$) reflecting more coiled polymer chains leading to more interdigitation [62]. For example, the theoretical maximal PDMS length using the segment length of PDMS (0.311 nm) according to the Si-O bond distance (0.164 nm) and the Si-O-Si angle ($\theta = 143^\circ$) [146] of the smallest triblock copolymer used in this study ($A_3B_{19}A_3$) is equal to the mean value of the membrane thickness determined by cryo-TEM (experimental membrane thickness: 6.0 ± 0.5 nm versus maximal stretched PDMS chain: 5.9 nm). This clearly demonstrates to which extent the macromolecules stretch. However, the smoothness of the membrane (Figure 3.2) decreased, which might lead to a lower membrane stability. On the other hand, the maximal PDMS chain length of the largest triblock copolymer ($A_{12}B_{87}A_{12}$) is 66% longer (+10.7 nm) than the measured membrane thickness. Moreover, the membranes appear more smooth (Figure 3.2).

In case of diblocks, all block copolymers have a smaller membrane thickness than the maximum theoretical PDMS chain lengths, ranging from 25% (A_8B_{22}) to 90% ($A_{14}B_{65}$). They also show the decrease of the exponent a towards smaller values with increasing molecular weight. In the coarse-grain molecular dynamics simulation study of diblock copolymers the same behaviour was observed [72]. Small molecular weight polymers with membrane thicknesses smaller than 7 nm were shown to have exponents of $a \sim 0.8$, while large molecular weight polymers revealed exponents towards values of $a \sim 0.5$ (pure random coil).

Comparing the membrane thicknesses between triblock and diblock copolymers reveals that the thickness of diblocks is roughly twice the thickness of triblocks with same number of PDMS units (Figure 3.7). This suggests a bilayer structure of diblock copolymers, with only slight interdigitation of the two leaflets. A weak interdigitation causes that no clear bilayer structures could be observed in cryo-TEM images as it is always observed for lipid bilayers. However, there was one exception on an image with the A_9B_{31} diblock copolymer, where the membrane stands perpendicular to the projection plane (Figure 3.8). In this image, the membrane reveals a clear bilayer structure.

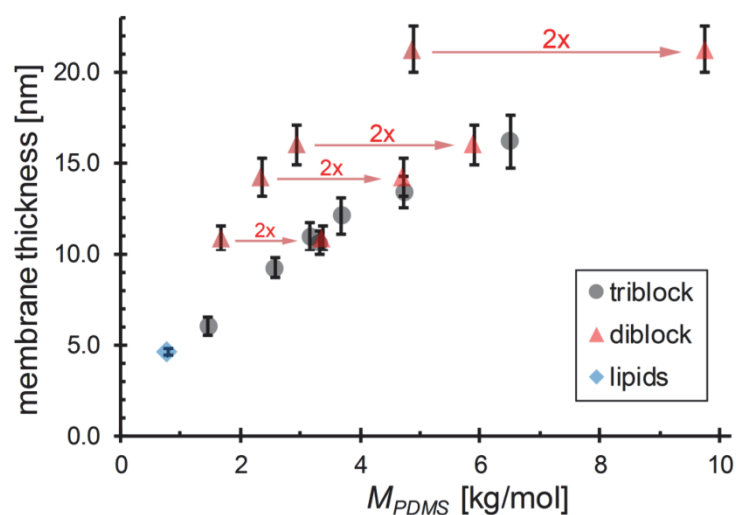


Figure 3.7. Comparison of the membrane thickness of diblocks and triblock copolymer membrane. If $M_{w,PDMS}$ of the diblock copolymers is multiplied by two (assuming a pure bilayer membrane), the membrane thickness is roughly the same as for triblocks.

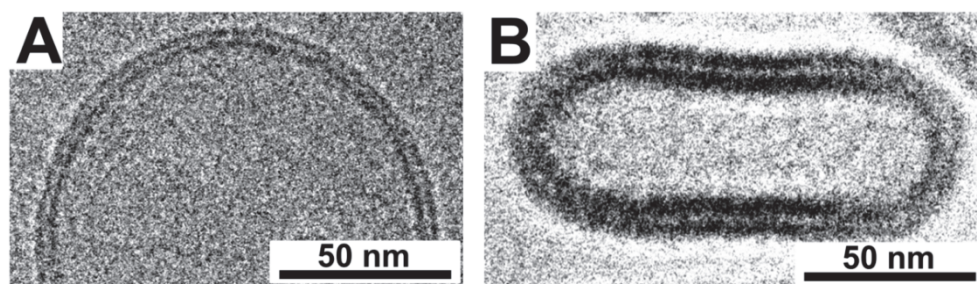


Figure 3.8. Cryo-TEM images of lipid and diblock bilayer structures. A) POPC liposome and B) a deformed A_9B_{31} diblock copolymer vesicle showing a strong bilayer structures. The images were taken with a high defocus ($-4 \mu\text{m}$) to yield a higher image contrast. The special shape of the particular polymer vesicle in (B) improves the contrast on the projection plane. This shows a bilayer structure without interdigitation.

The bilayer-like structure of the here presented membranes is in strong contrast to the previously reported PEO-*b*-PBO block copolymer membranes [63]. Although we used different block copolymers, we question their model of strongly interdigitated polymer membranes. The lateral diffusion measurements and cryo-TEM images of vesicular structures show distinct membranes and provide the basis for this conclusion. We did not determine membrane thicknesses from TEM with negative staining, because the image contrast originates from the stain around the vesicles. In cryo-TEM imaging, it has to be noted that a high defocus increases the effect of the contrast transfer function (CTF) leading to high errors for distance measurements. We corrected images for the CTF,

however, for images with a low defocus we did not observe a significant difference before and after CTF correction. Additionally, thin membranes from self-assembled block copolymers following the strong segregation limit, as stated by the molecular simulation study [72], must have stretched polymer chains. Thicker membranes consequently will reflect coiled chains together with interdigitation. In this respect, fully interdigitated membranes are questioned and were never observed here. Furthermore, the main concern from this simple exponential equation (equation 1.2) is that the exponent a lacks information about the strength of interdigitation and resembles only a mean value of a broad range of different molecular weight polymers. A precise conclusion can only be drawn when at least one structure of the data set is known exactly. Besides cryo-TEM imaging of polymersome membranes, lateral diffusion provides an additional, experimentally obtained hint to conclude more details about the membrane structure, which will be shown in the following sections in this chapter.

3.2.3 Fluorescent labelling of the polymers

In order to measure lateral diffusion of the single macromolecules, four polymers ($A_{12}B_{63}A_{12}$, $A_6B_{44}A_6$, $A_{14}B_{65}$, A_6B_{34}) were labelled with a fluorescent dye, sulforhodamine B (SRB). These four polymers were chosen as intermediate sized polymers to be mixed at a small percentage (0.005 – 0.01% (w/w)) with the other polymers that build up the membrane (Table 3.4). These labelled polymers can be easily mixed with the membrane. The large PDIs of the polymers ensures that the different polymer sizes overlap with each other, which then does not or only minimally influence the membrane structure and property. We do not expect a change in the diffusion property of the mixture due to i) the very small percentage of the mixtures, ii) the large PDIs of the polymers and iii) the high fluidity of the PDMS backbone, which ensures perfect mixing. The polymers were labelled with sulforhodamine B (SRB) acid chloride at the end groups of the hydrophilic PMOXA blocks. The labelling reaction was performed via an esterification reaction on the terminal hydroxyl groups of the block copolymers [147]. The dye-labelled polymers were purified on a LH-20 organic size exclusion column in ethanol to remove free dye from the samples. Fluorescence correlation spectroscopy (FCS) was used to verify the purity of collected fractions after size exclusion because the separation process was not clearly visible by eye. FCS is able to differentiate molecular weights that are factors of 6 – 8 different (SRB: $M_w = 559$ g/mol, polymers: $M_w = 3500 - 6900$ g/mol). The diffusion times were measured in EtOH and compared to the diffusion

of free SRB in EtOH. Only the fractions yielding a single-diffusing species within the sample (100% slow diffusing species) were chosen. The SRB-labelled polymers had diffusion times around $\tau_D \approx 130 \mu\text{s}$ that is significantly higher than free SRB with a diffusion time of $\tau_D \approx 61 \mu\text{s}$. These values are very close to the values published recently [148]. The SRB-containing samples were excited with a He-Ne laser ($\lambda = 543 \text{ nm}$).

Table 3.3. Absorption-, emission-, and diffusion analysis of the SRB-labelled triblock and diblock copolymers, and Rhodamine B labelled lipid (Rhod-PE).

Molecular species	$\lambda_{\text{exc,max}}$ [nm]	$\lambda_{\text{em,max}}$ [nm]	τ_D [μs] ^c
Free SRB ^a	551	571	61
SRB-A ₁₂ B ₆₃ A ₁₂ ^a	554	576	147
SRB-A ₆ B ₄₄ A ₆ ^a	559	578	132
SRB-A ₁₄ B ₆₅ ^a	559	578	145
SRB-A ₆ B ₃₄ ^a	558	578	121
Rhod-PE ^b (lipid)	560	583	-

^aMeasured in EtOH. ^bMeasured in CHCl₃ (data from Avanti Polar Lipids). ^cFCS measurements.

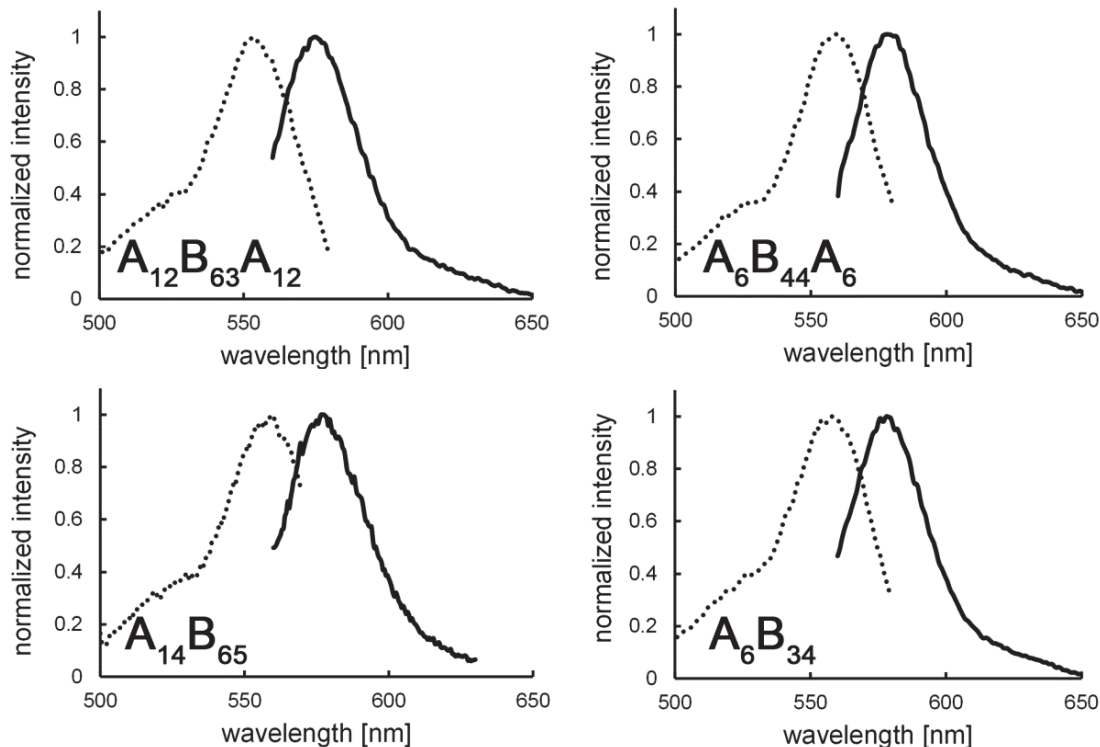


Figure 3.9. Excitation and emission spectra of the SRB-labelled block copolymers. The spectra show that the labelled polymers are fluorescent with a maximum excitation wavelength of $\lambda_{\text{exc}}=555 \text{ nm}$ and a maximum emission wavelength of $\lambda_{\text{em}}=577 \text{ nm}$.

Figure 3.9 shows the excitation and emission spectra of the four labelled block copolymers. The fluorescence spectra show a Stokes shift of around 20 nm between the excitation maximum ($\lambda_{\text{exc}}=555$ nm) and emission maximum ($\lambda_{\text{em}}=577$ nm) (Table 3.3). For excitation measurements, the fluorescence signal was recorded at 575 nm, for emission recordings, the signal was excited at 555 nm.

Table 3.4. Molecular composition of the membranes mixtures used for the lateral diffusion measurements.

	Measured membrane	SRB-polymer mixed	Mixing ratio (labelled vs. non-labelled) [%]
Triblock	$A_3B_{19}A_3$	$A_6B_{44}A_6$	0.005
	$A_6B_{34}A_6$	$A_6B_{44}A_6$	0.005
	$A_6B_{44}A_6$	$A_6B_{44}A_6$	0.005
	$A_7B_{49}A_7$	$A_{12}B_{63}A_{12}$	0.015
	$A_{12}B_{63}A_{12}$	$A_{12}B_{63}A_{12}$	0.01
	$A_{12}B_{87}A_{12}$	$A_{12}B_{63}A_{12}$	0.01
Diblock	A_6B_{22}	A_8B_{34}	0.02
	A_9B_{31}	A_8B_{34}	0.01
	A_8B_{39}	A_8B_{34}	0.01
	$A_{14}B_{65}$	$A_{14}B_{65}$	0.005
Lipid	POPC ^d	POPE-Rhod	0.005

3.2.4 GUV formation and immobilization

Giant unilamellar vesicles (GUVs) were prepared by standard electroformation technique [149]. A dried polymer thin film is formed on an indium tin oxide (ITO)-coated glass plate and is rehydrated within a closed chamber with a second ITO-coated glass plate facing towards the polymer film. By applying a pulsing electrical field, membranes detach from the polymer thin film and steadily grow to form micrometer-sized vesicles with a highly polydisperse size-distribution. A frequency of around 3.0 Hz is applied, while the voltage can be adjusted from 0.5 up to 5.0 V, depending how well the block copolymer forms GUVs. Usually sugar-containing solutions or bidistilled water are used as hydration solutions because salt-containing buffers have to be avoided for electroformation. Here, always a sucrose solution (100 mM) was used. Figure 3.10A shows GUVs observed by light microscopy in the phase contrast mode during the electroformation procedure. After removing the freshly generated GUVs from the

electroformation chamber, the sucrose filled GUVs sink to the surface when transferred to a non-sucrose containing buffer with isosmotic conditions (20 mM Hepes, 50 mM NaCl). The sucrose-filled GUVs are heavier than the surrounding NaCl solution and the GUVs can be easily visualized on the glass surface. In addition, if the glass surface is plasma-treated in order to render it hydrophilic, the GUVs adhere tightly as hemispheres at the bottom without rupturing (Figure 3.10B and C). This effect was observed to be stronger for block copolymers with longer hydrophilic PMOXA chains, *i.e.* the larger molecular weight polymers, while for smaller block copolymer with very few PMOXA units or the lipid vesicles, the adhesion was less strong. These GUVs could move on the glass surface if there was slight flow due to thermal undulation within the observation chamber. Within the observation chamber, isosmotic conditions are required to prevent membrane stress, which can affect the measurements. Z-scan FCS measurements were performed on the top of these stable hemispheres. The stability is an important issue for this method, which requires that the free standing membranes are stable and non-moving [150]. In addition, the fluorescently-labelled polymer fraction was homogenously distributed within the membrane and no domains or separations were observed at the optical resolution.

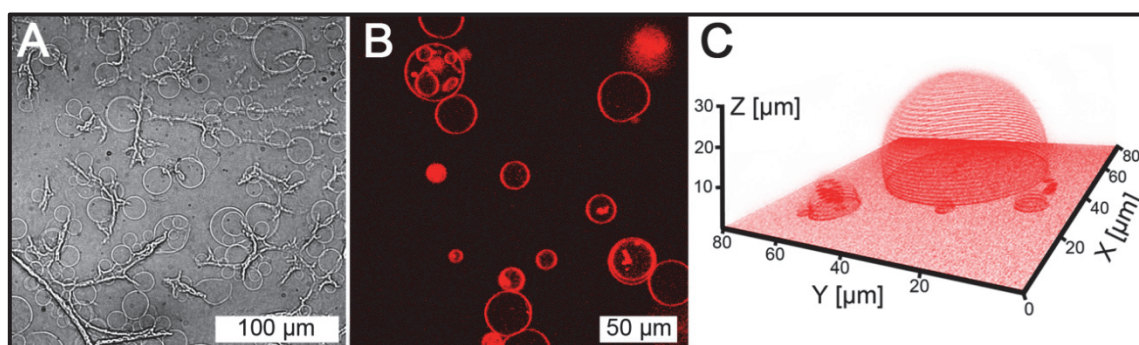


Figure 3.10. Visualization of polymeric GUVs on the example of $A_7B_{49}A_7$ triblock copolymer. A) The formation of $A_7B_{49}A_7$ GUVs can be monitored by simple phase contrast light microscopy. GUVs develop from the surface of a smooth polymer film in a pulsing electrical field (3.0 Hz, 2.0 V) within the electroformation chamber. B) GUVs are observed on the glass surface of the microscopy chamber by LSM. The fluorescent membrane is clearly visible when SRB-labelled polymer was added. C) 3D LSM image of a single polymeric GUV showing the formation of a stable half-sphere on a plasma-treated glass surface.

The visualization of the GUVs (Figure 3.10) is an important step to survey their generation during the electroformation (Figure 3.10), to observe possible defects or multilayer structures within the GUV membranes (Figure 3.10B) and to visualize the 3D structure of the GUVs, which are forming stable half-spheres (Figure 3.10C). Phase

contrast microscopy was used to observe the successful formation of GUVs from dried polymer films within the electroformation chamber. For z-scan FCS measurements, an important requirement is that no artefacts are disturbing the data recording. Therefore, by LSM it is possible to select the suitable GUVs, which are completely empty (no encapsulated smaller GUVs), have a certain size range for stability reasons ($\sim 15 - 25 \mu\text{m}$ in diameter) and are steadily immobile on the surface (non-moving).

3.2.5 Z-scan FCS measurements

For each polymer sample, z-scan autocorrelation curves were recorded in steps of 200 nm (Figure 3.11) on 10 different GUVs from at least two different sample preparations. Autocorrelation curves were fitted with the 2D-anomalous diffusion model (equation 2.10), containing the exponent α , which was always between 0.8 and 1. This parameter flattens the autocorrelation curve. For our system we propose that the parameter α indicates the distribution of the diffusion times around a mean value. There are several reasons for this distribution of the diffusion times in these block copolymer membranes. First, the polydispersity (PDI) in molecular weight is intrinsic to polymer amphiphiles [61] and is especially broad for triblock copolymers [39], but more narrow for diblocks (Table 3.1) [139]. Variation in the molecular weight, represented by the PDI, leads to a slight distribution of diffusion times. Secondly, for triblock copolymers, two different conformations of the ABA copolymer in a membrane have been suggested, influencing the lateral diffusion properties due to the stretched form being represented as I-shape and the curved form as U-shape [65]. In addition, the synthesis of triblock copolymer and the following purification results in a small fraction of diblock polymers. Thus, diblock copolymers may be mixed with triblock polymers, a fact that cannot be proven by standard analytical methods, *i.e.* NMR, GPC. Third, labelling of triblock copolymers with a fluorescent dye is not quantitative and therefore polymer molecules with two SRB (one at each end) or with only one SRB are present in the final assembly. These three factors explain the need for this parameter α explaining anomalous diffusion in a polymeric membrane system.

Diffusion times (τ_D) and number of particles (N) were calculated and plotted against the z-axis (Figure 3.11). The minimum diffusion time was obtained by shifting the z-axis to yield the best fit. The waist ω_0 of the laser beam ($\lambda = 543 \text{ nm}$) was fitted with equations (2.12) and (2.13) and was between 260 and 310 nm ($\omega_0 = 287 \pm 14 \text{ nm}$) for all polymer

samples (Table 3.5), which is in very good agreement to the value obtained from external calibration with free SRB dye in buffer ($\omega_{0,ext} = 285 \pm 23$ nm, $D_{SRB} = 4.14 \cdot 10^{-6}$ cm²/s) [151]. The relative errors obtained from the diffusion coefficients were all between 5 – 15%, which is the error range usually obtained with z-scan FCS [132]. Diffusion coefficients for all polymers listed in Table 3.5 were calculated based on equation (2.12).

Table 3.5. Membrane properties of self-assembled triblock and diblock copolymers, and lipids (membrane thickness d , diffusion coefficient D).

	molecular composition ^a	Membrane thickness ^b d [nm]	Diffusion coefficient ^{b,c} D [$\mu\text{m}^2/\text{s}$]	ω_0 [nm]
Triblock	A ₃ B ₁₉ A ₃	6.0 ± 0.5	4.4 ± 0.7	305
	A ₆ B ₃₄ A ₆	9.2 ± 0.5	2.4 ± 0.2	290
	A ₆ B ₄₄ A ₆	10.7 ± 0.7	1.9 ± 0.2	270
	A ₇ B ₄₉ A ₇	12.1 ± 1.0	1.6 ± 0.2	295
	A ₁₂ B ₆₃ A ₁₂	13.4 ± 0.9	1.0 ± 0.1	270
	A ₁₂ B ₈₇ A ₁₂	16.2 ± 1.4	0.6 ± 0.1	290
Diblock	A ₆ B ₂₂	10.9 ± 0.7	6.0 ± 0.4	270
	A ₉ B ₃₁	14.3 ± 1.1	4.6 ± 0.2	280
	A ₈ B ₃₉	16.0 ± 1.1	3.0 ± 0.3	310
	A ₁₄ B ₆₅	21.3 ± 1.2	1.8 ± 0.2	290
Lipids	POPC ^d	5.0 ± 0.4	12.5 ± 0.5	260

^aDetermined by ¹H NMR. ^bMean value ± SD. ^cZ-scan FCS at 20 ± 0.5 °C. ^dRhod-PE in a POPC bilayer.

3.2.6 Molecular weight dependence of lateral diffusion

The lateral diffusion within the block copolymer membranes decreases with increasing molecular weight for both block copolymer compositions (diblock and triblock). The difference in the diffusion characteristics between diblock and triblock copolymers is represented as a significant shift of the triblocks towards longer diffusion times (τ_d) or higher diffusion coefficients (D) compared to diblocks (Figure 3.12). Triblock copolymers showed lateral mobility values, ranging from 4.4 to 0.6 $\mu\text{m}^2/\text{s}$ for molecular weights from 2100 to 8700 g/mol, almost a 10-fold decrease within the triblock copolymers tested. For diblock copolymers, the trend resembles but the lateral diffusion coefficients shift to higher values, ranging from 6.0 to 1.8 $\mu\text{m}^2/\text{s}$ (2500 - 6200 g/mol).

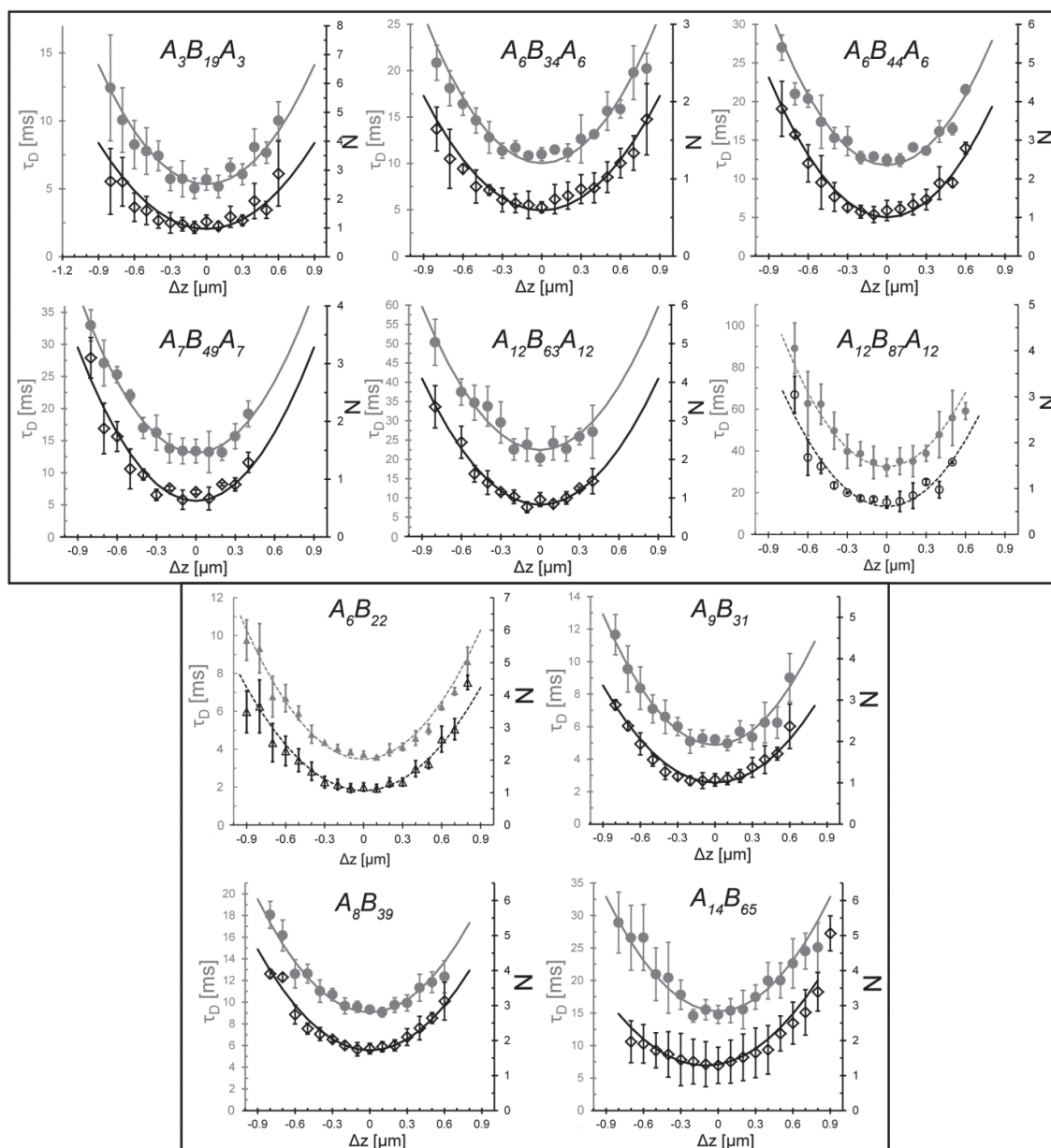


Figure 3.11. Z-scan FCS data plots of all block copolymers. The graphs show the parabolic z-dependency (Δz) of the lateral diffusion τ_D and the number of particles N . Upper panel: z-scans of all triblock copolymers. Lower panel: z-scans of all diblock copolymers. FCS measurements were performed on membranes of giant unilamellar vesicles (GUVs) mixed with a small percentage (0.005–0.01%, w/w) of corresponding SRB-labelled triblock copolymer (Table 3.4).

We also determined the diffusion coefficient of an unsaturated lipid (Rhod-PE) within a POPC bilayer by using the same method applied for block copolymer membranes, revealing a value of $12.5 \pm 0.6 \mu\text{m}^2/\text{s}$ (Figure 3.12). This value is in good agreement with values reported for freestanding lipid bilayers ($10.0 \pm 0.7 \mu\text{m}^2/\text{s}$ by z-scan FCS [152] and $12.9 \pm 1.2 \mu\text{m}^2/\text{s}$ by FRAP [153]) or black lipid membranes ($11.6 \pm 0.6 \mu\text{m}^2/\text{s}$ by 2-focus FCS [77]), which further underlines the accuracy of the z-scan FCS method. The

diffusion coefficients of our block copolymer membranes showed mobilities that were 2-20 times slower than the diffusion coefficients of unsaturated phospholipids. Mobilities reported for other block copolymer membranes, measured by fluorescence recovery after photobleaching (FRAP) experiments, were roughly 10 times slower than in our case for PDMS-containing block copolymers.

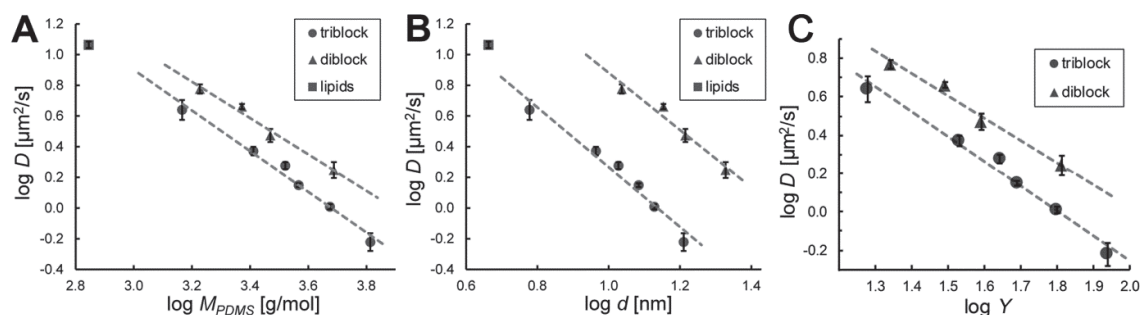


Figure 3.12. Log-log plots of diffusion coefficients D versus molecular weight of PDMS M_{PDMS} (A), membrane thickness d (B) and degree of polymerization Y (C). The polymeric membranes are composed of different molecular weight polymers and different block architecture (triblock and diblock). Membrane thicknesses were determined from cryo-TEM images. In addition, the diffusion coefficient of a fluorescently labelled lipid (Rhod-PE) within a POPC bilayer is shown for comparison (in A and B). Dashed lines represent linear fits; error bars represent standard deviations (\pm SD).

Diblock copolymers with molecular weights in the range of 7000 g/mol diffuse around ten times slower than lipids. This is still faster than values obtained previously by fluorescence recovery after photobleaching (FRAP) experiments for other types of block copolymers. Membranes composed of $\text{EO}_{37}\text{-}b\text{-EE}_{40}$ (poly(ethylene oxide) – poly(ethylethylene)) and $\text{EO}_{80}\text{-}b\text{-BD}_{130}$ (poly(ethylene oxide)-poly(butadiene)) have reported diffusion coefficients of only 0.12 and 0.0024 $\mu\text{m}^2/\text{s}$, respectively [23]. In that study, GUVs were pulled into a glass micropipette, where the membrane can interact with the glass wall and affect the measured diffusion, reflected also by the low diffusion coefficient of pure lipid bilayers. On the other hand, it was stated that the EE polymers diffuse 10 times slower than lipids, while the diffusion coefficient of the lipids was given as 1.0 $\mu\text{m}^2/\text{s}$ [23]. The diffusion was possibly simply underestimated. However, the value had also a ten-fold decrease relatively to the lipid diffusion, as in our study.

Figure 3.12 represents the dependence of the lateral diffusion coefficients on molecular weight, membrane thickness and degree of polymerization of the PDMS block (PDMS_y).

The lateral diffusion scales with the molecular weight in a power law dependency: $D_{ABA} \propto M_{PDMS}^{-1.32 \pm 0.09}$ ($R^2 = 0.98$) and $D_{AB} \propto M_{PDMS}^{-1.19 \pm 0.12}$ ($R^2 = 0.98$) (Figure 3.12A) and the same exponents were calculated with the degree of polymerization (Figure 3.12C). Owing to non-significant linear fits of the log-log plots in Figure 3.12 ($p = 0.40 / p > 0.05$), the scaling of diblock and triblock copolymers, consisting of PMOXA-*b*-PDMS-(*b*-PMOXA), can be generally formulated as: $D \propto M_{PDMS}^{-1.25}$ and $D \propto Y^{-1.25}$.

The difference between diblocks and triblocks mainly results from structural differences in the conformational organization of the polymer chains in the self-assembled membrane. While diblock copolymers introduce stronger in-plane diffusion within the (interdigitated) block copolymer membrane, triblock copolymers form membranes composed of polymer chains in the stretched I-shape and the bent U-shape conformation, which reduces the mobility of the polymer chains. Although the slopes in Figure 3.12A are not significantly different, the more negative slope of triblocks compared to diblock copolymers (-1.32 ± 0.09 vs. -1.19 ± 0.12) underlines the stronger reduction in lateral diffusion of triblock copolymers with respect to the molecular weight. This indicates the influence of I-shaped triblock chains on the lateral mobility within the membrane and represents the strength of entanglement of the polymer chains, which is more pronounced at higher membrane thicknesses and higher molecular weights, respectively. When plotting the lateral diffusion versus the membrane thickness (Figure 3.12B), we observed the same behaviour. The difference is more distinct because the diblock copolymers show almost pure bilayers with only weak interdigitation (Figure 3.8).

For example by comparing the autocorrelation curves at minimum τ_D of the diblock polymer, A₆B₂₂, and the triblock polymer, A₆B₄₄A₆, the diffusion time of the triblock is significantly shifted to higher diffusion times compared to the diblock (Figure 3.13), although both possess the same membrane thickness (Table 3.2). A part of the triblock copolymer macromolecules arranges in the I-shape affecting the membrane structure and therefore reducing the fluidity of the overall membrane. On the other hand, the diffusion coefficients of the smallest diblock copolymer studied is close to the diffusion coefficients of phospholipids in free-standing lipid bilayers. This suggests these polymersomes have a similar structural organization as lipid bilayers, *i.e.* bilayer formation without entanglement and very low interdigitation of the PDMS chains.

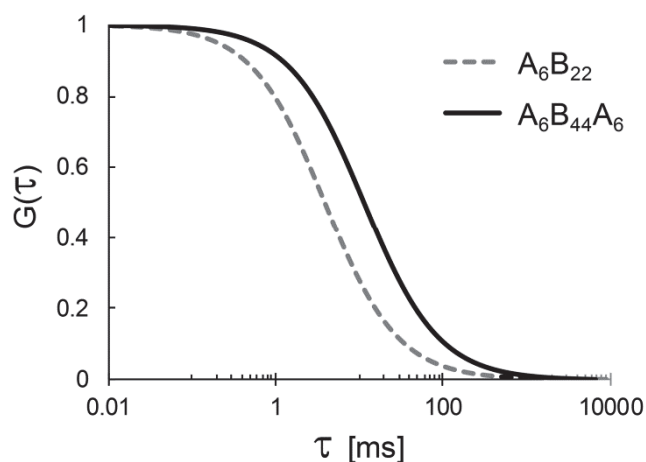


Figure 3.13. Autocorrelation functions of a diblock (A_6B_{22}) and a triblock ($A_6B_{44}A_6$) copolymer. Although the membrane thicknesses of these two block copolymers are identical (10.9 ± 0.7 nm and 10.7 ± 0.7 nm, respectively), the autocorrelation curve of the triblock copolymer is shifted to higher diffusion times compared to the diblock copolymer.

3.2.7 Existence of membrane inhomogeneities

In addition to the obtained diffusion coefficients, z-scan FCS provides information on membrane inhomogeneities by the FCS diffusion law (see section 2.4.2) [100,140]. In the case of hindered diffusion, the diffusion time is not proportional to the illuminated area (represented by the relative number of particles, N/N_0) and extrapolation of the diffusion time to zero beam waist (y-axis intersection) results in a positive value ($t_0 > 0$). This data processing was performed for all block copolymer samples and the lipid control based on the data in Figure 3.11. For clarity reasons, the linear dependencies are given for selected block copolymers shown in Figure 3.14A and B, while the t_0 values for all block copolymers are given in Figure 3.14C. Applying this approach to our different polymer membranes, t_0 was always positive (Figure 3.14C). However, the smallest diblock and triblock copolymers (A_6B_{22} , $A_3B_{19}A_3$) showed free-diffusion ($t_0 \sim 0$) as sole exceptions with membrane thicknesses of 10.9 nm and 6.0 nm, respectively. Negative t_0 values represent a meshwork character with guided-diffusion and were not observed. In general, t_0 steadily increased with the increase of the molecular weight for both block copolymer architectures (triblock and diblock).

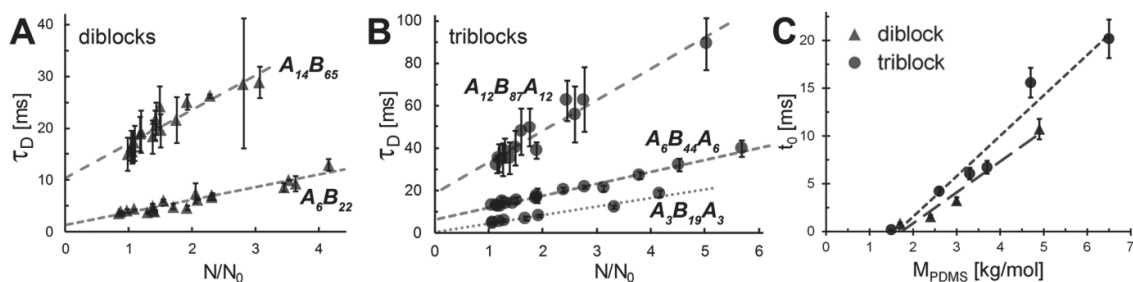


Figure 3.14. Experimental FCS diffusion laws obtained for diblock and triblock copolymers. The data show the trend toward hindered diffusion ($t_0 > 0$) with increasing molecular weight. (A) Diblock copolymers show t_0 values ranging from 1.0 up to 10 ms. (B) Triblock copolymers show t_0 values ranging from 0 to 20 ms. For clarity reasons, only the data of selected block copolymers are presented. (C) t_0 values of all triblock and diblock copolymers plotted against the hydrophobic molecular weight M_{PDMS} . Lines represent linear fits; error bars represent standard deviations (\pm SD).

In case of triblocks, it means that small copolymer chains are assembled in a more stretched conformation (strong segregation limit, SSL). They are organized similar to alkyl chains of lipids in a lipid bilayer. A stretched structure provides a higher freedom of diffusion and the polymer chains are less prone to interlinking / entanglement as observed by the free-diffusion of the smallest triblock copolymer. For long polymer chains, on the other hand, the possibility of entanglement increases and therefore domains can form reducing the overall mobility significantly.

For comparison to the lateral diffusion of phospholipid membranes, the z-scan FCS data of a Rhodamine labelled POPE lipid within a POPC membrane is shown in Figure 3.15. The z-scan FCS law shows that this fluid lipid has a free diffusion character. POPC is known for its fluid property due to the single-double bond on the acyl chains and its low glass transition temperature ($T_g = -2$ °C).

For diblock copolymers, the freedom of diffusion is higher compared to triblocks because of the in-plane diffusion within the bilayer and of a weak interdigitation of the two layers. However, the observation of domains with increasing molecular weight also indicates entanglement of the diblock copolymer chains.

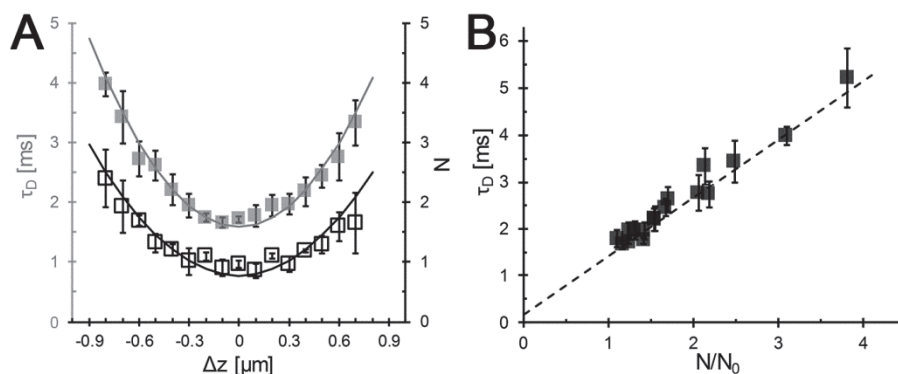


Figure 3.15. Z-scan FCS data of Rhod-PE in a POPC phospholipid bilayer. A) Parabolic z-dependency of the diffusion coefficient and number of particles. B) Z-scan FCS law showing the free-diffusion character within the membrane ($t_0 \sim 0$).

The z-scan FCS law provides a tool to calculate the effective diffusion coefficient D_{eff} of the polymer membrane [100,140]. As the observed lateral diffusion D is reduced because the interaction between the single macromolecules reduces their mobility. As a consequence, the effective diffusion is higher than the observed diffusion ($D_{eff} > D$). This effect is increasing with increasing molecular weight of the polymer molecules as the possibility of entanglements increases, as shown in Figure 3.14C and Table 3.6.

D_{eff} was calculated with equation 2.14 using the minimum beam waist ω_0 , and the fitting quality is represented by R^2 . The numbers in Table 3.6 show the results from the z-scan FCS laws via the linear fit of the diffusion time τ_D versus the change of the beam waist area (N/N_0). As already mentioned and shown in Figure 3.14, the values of t_0 are increasing with increasing the PDMS block length showing a gradually increasing strength of hindered-diffusion. Most probably, this hindered diffusion is caused by domain formation. This linear dependency provides the effective diffusion coefficient calculated from the minimum beam waist ω_0 and the slope. From Table 3.6 it can be seen, that the slope is gradually increasing with increasing PDMS block length, while the beam waist stayed roughly the same ($\omega_0 = 285 \pm 15$), *i.e.* the same wavelength was used for excitation of SRB ($\lambda_{exc} = 543$ nm). The slope provides a hint on the domain concentration and domain size, and, in addition, on the probability that the molecules are trapped within such a domain [100].

Table 3.6. Overview of effective diffusion coefficient calculation.

Membrane	D [$\mu\text{m}^2/\text{s}$]	t_0 [ms]	slope	D_{eff} [$\mu\text{m}^2/\text{s}$]	ω_0 [nm]	R^2	n
POPC	12.5 ± 0.5	0.2 ± 0.1	1.2 ± 0.1	12.9 ± 0.5	260	0.92	18
$A_3B_{19}A_3$	4.4 ± 0.7	0.2 ± 0.6	5.2 ± 0.4	4.3 ± 0.3	305	0.93	18
$A_6B_{34}A_6$	2.4 ± 0.2	4.2 ± 0.4	6.0 ± 0.3	3.5 ± 0.2	290	0.95	11
$A_6B_{44}A_6$	1.9 ± 0.2	6.1 ± 0.6	5.8 ± 0.2	3.3 ± 0.1	270	0.99	17
$A_7B_{49}A_7$	1.5 ± 0.2	6.7 ± 1.1	7.9 ± 0.7	2.8 ± 0.3	295	0.89	17
$A_{12}B_{63}A_{12}$	1.0 ± 0.1	15.6 ± 3.0	8.1 ± 1.8	2.4 ± 0.6	270	0.66	16
$A_{12}B_{87}A_{12}$	0.6 ± 0.1	20.2 ± 2.7	14.3 ± 1.1	1.5 ± 0.1	290	0.93	16
A_6B_{22}	6.0 ± 0.4	0.8 ± 0.3	2.5 ± 0.1	8.3 ± 0.4	270	0.97	11
A_9B_{31}	4.6 ± 0.2	1.6 ± 0.5	3.4 ± 0.3	6.7 ± 0.5	280	0.93	15
A_8B_{39}	3.0 ± 0.3	3.2 ± 0.8	6.0 ± 0.5	3.7 ± 0.3	310	0.91	13
$A_{14}B_{65}$	1.8 ± 0.2	10.7 ± 1.0	6.4 ± 0.5	3.3 ± 0.3	290	0.90	12

3.2.8 Membrane viscosity

The membrane viscosity η_m was determined using the Saffman-Delbrück equation (equation 2.5) [106]. The values were calculated based on the lateral diffusion coefficients D including the membrane thicknesses d for each polymer and the area occupied by a single polymer chain represented as the radius R of a cylinder diffusing in the membrane [77,106]. The radius of each polymer was calculated based on the radius of gyration: $R_g = N^a \frac{b}{6}$, considering N as the number of PDMS units, b the segment length ($b = 0.311$ nm) according to the Si-O bond distance (0.164 nm) and the Si-O-Si angle ($\theta = 143^\circ$) [146] and a as the exponent calculated from Figure 3.5. It has to be noted that this approach gives only a close approximation of R . However, this calculation provides molecular radii that are comparable to Langmuir-monolayer studies, where the mean molecular area is obtained [154].

For triblocks, the membrane viscosity ranges between 80 and 245 mPa·s (19 – 87 PDMS units), which is an approximate three-fold increase of viscosity from the smallest to the largest triblock copolymer (Table 3.7). Besides, the viscosity of diblock copolymers is much lower due to the higher diffusion coefficients and the higher membrane thicknesses

compared to the triblock copolymers. The values for diblocks range between 30 and 59 mPa·s, again a two-fold increase for the four diblock copolymers tested (Table 3.7).

Table 3.7. Calculation of membrane viscosities (η_m) by the Saffman-Delbrück equation.

Membrane	D [$\mu\text{m}^2/\text{s}$]	d [nm]	Molecule radius [nm]	Mean molecular area [nm^2]	η_m [mPa·s]
POPC	12.5 ± 0.5	5.1 ± 0.4	0.44	0.61	39
A ₃ B ₁₉ A ₃	4.4 ± 0.7	6.0 ± 0.5	0.38	0.45	80
A ₆ B ₃₄ A ₆	2.4 ± 0.2	9.2 ± 0.5	0.56	0.98	100
A ₆ B ₄₄ A ₆	1.9 ± 0.2	10.7 ± 0.7	0.66	1.39	111
A ₇ B ₄₉ A ₇	1.5 ± 0.2	12.1 ± 1.0	0.71	1.60	136
A ₁₂ B ₆₃ A ₁₂	1.0 ± 0.1	13.4 ± 0.9	0.85	2.25	174
A ₁₂ B ₈₇ A ₁₂	0.6 ± 0.1	16.2 ± 1.4	1.05	3.58	245
A ₆ B ₂₂	6.0 ± 0.4	10.9 ± 0.7	0.37	0.43	31
A ₉ B ₃₁	4.6 ± 0.2	14.3 ± 1.1	0.46	0.67	31
A ₈ B ₃₉	3.0 ± 0.3	16.0 ± 1.1	0.53	0.90	44
A ₁₄ B ₆₅	1.8 ± 0.2	21.3 ± 1.2	0.74	1.72	59

Compared to lipid bilayers, the viscosity of free-standing lipid membranes is 0.039 Pa·s, which resembles the viscosity values of diblock copolymers (Table 3.7). The calculated membrane viscosity of a free-standing DPPE lipid bilayer [77] is lower than previously reported values for lipid bilayers [98,155] (0.14 Pa·s). This difference can be explained by the lower reported diffusion coefficients, which affects the calculation of the membrane viscosity. Thus, as expected, the viscosity of the triblock copolymer membrane is higher than the viscosity of a lipid membrane by a factor of about three to six depending on the number of PDMS units, while membranes from diblock copolymers have a similar viscosity as lipid bilayers. Compared to other polymeric membranes [80], our values are very close to lipid bilayers and result mainly from the viscosity of pure PDMS, which is about 0.01 – 0.1 Pa·s for molecular weights ranging from 1000 – 6000 g/mol. This highlights the advantage of PDMS containing block copolymers due to its low viscosity and low glass transition temperature ($T_g \approx -123$ °C) [34], mimicking the fluidity of natural membranes.

3.3 Conclusion

Lateral diffusion coefficients were determined based on a large library of different molecular weight amphiphilic block copolymers with triblock and diblock configuration that are able to self-assemble into vesicular structures. Membrane dynamics of PMOXA-*b*-PDMS block copolymers revealed factors of 2 – 20 times lower diffusion coefficients compared to phospholipids within lipid bilayer membranes. We demonstrated that the lateral diffusion D follows a power law dependency according to the molecular weight of the hydrophobic block M_{PDMS} scaling with $D \propto M_{PDMS}^{-1.25}$. Diblock copolymers showed diffusivities higher than triblock copolymers, which can be explained by the different chain conformation within the self-assembled membrane. Triblock copolymers adapt a mixed conformation of the bent U-shape and the stretched I-shape reducing the lateral mobility. On the other hand, diblock copolymers build a bilayer-like structure with only slight interdigitation and entanglement, consequently having more freedom of diffusion than triblock copolymer macromolecules. Interdigitation and entanglement of the polymer chains induces the formation of membrane inhomogeneities and domains. As a consequence, the mobility reveals a hindered diffusion property at molecular weights above 2000 g/mol, while only low molecular weight polymers (< 2000 g/mol) diffuse freely within the membranes. Moreover, the systematic study of the membrane thickness revealed triblock membranes of 6 – 16 nm, diblock membranes of 11 – 21 nm in thickness and the dependence on the molecular weight showed copolymer chains to be in the strong segregation limit (SSL). As expected, small molecular weights the chains are more stretched, while at higher molecular weights the chains tend to adapt random coil structure. Furthermore, we observed only weakly interdigitated bilayer membranes composed of diblock copolymers, forming closely double the membrane thickness compared to triblock copolymers having the same degree of polymerization of the PDMS. This is in strong contradiction to the previously proposed model of strong interdigitation for block copolymer membranes [63]. As expected, the membrane viscosity of these PMOXA-*b*-PDMS block copolymer membranes is just slightly higher as compared to lipids due to the natural low viscosity of pure PDMS.

These artificial membranes can therefore mimic natural lipid bilayers providing a similar fluidity together with improved stability with high membrane thicknesses. The systematic study on the membrane structure taken from a large library of block copolymers can be used to choose suitable block lengths for specific and desired applications. In addition,

this study provides the basis of tracking and visualizing the movement of labelled membrane constituents to prove their successful incorporation into artificial polymeric membranes.

Chapter 4

4 Dynamics of membrane proteins within synthetic polymer membranes with large hydrophobic mismatch

In this chapter, the lateral diffusion of membrane proteins within block copolymer membranes is presented. This study provides a basis for successful incorporation of biological membrane proteins into synthetic membranes consisting of PDMS as the hydrophobic moiety.

This study has been submitted:

F. Itel, A. Najer, T. Einfalt, C.G. Palivan, W. Meier, Dynamics of membrane proteins within synthetic polymer membranes with large hydrophobic mismatch, submitted.

4.1 Problem definition

The study described in chapter 3 has shown that self-assembled membranes composed of PMOXA-*b*-PDMS-(*b*-PMOXA) triblock or diblock copolymers have a fluid property, which is comparable to the fluidity of natural phospholipid bilayers. Therefore, the fluidity within these synthetic membranes offers a similar environment for membrane protein insertion, as it is the case for their original, natural environment, for which they were genetically adapted during evolution. Since the fluidity of membranes is equivalent to lateral diffusion of the membrane components, also membrane proteins diffuse laterally within membranes as they are important membrane constituents for cellular functions. Since it has been shown that membrane proteins are able to insert into mainly PDMS-containing block copolymers, the question arises, how membrane proteins diffuse within a synthetic membrane that is, from a chemical point of view, completely different compared to their natural environment. The diffusion of membrane proteins is analyzed

as a follow up study based on the experiments in chapter 3 for the single polymer macromolecules and phospholipids.

Equally to biological lipid membranes, a key requirement for membrane protein functionality in block copolymer membranes is their ability to move laterally in the membrane. This behaviour strongly depends on the membrane flexibility and membrane fluidity, which are essential properties for the structural integrity of the membrane protein [134]. Consequently, the challenges for membrane protein insertion and their functionality within synthetic block copolymer membranes are high, because of the complex scenario of requirements imposed on a synthetic membrane (hydrophobicity and size, flexibility, elasticity, density, *etc.*).

Lateral diffusion coefficients of membrane proteins in artificial and biological phospholipid membranes has been studied over decades [156,157] because of the importance and crucial role of lateral mobility in cellular functions. The fluidity is a fundamental aspect for biological membranes because many cellular processes, such as energy- and signal transduction, sensing, *etc.* involve several membrane proteins together and rapid, continuous mixing within the membrane is essential [22,135,157–159]. In addition, the functional principle of lateral diffusion has become widespread as the idea of “reduction-of-dimensionality” appeared was postulated by Adam and Delbrück in 1968 [160]. It states that the reaction rates can be enhanced by following a reaction path in 2 dimensions (*e.g.* in the membrane) instead of 3 dimensions (*e.g.* in the cytoplasm). This increases the reaction efficiency where only a low concentration of ligands exists. It was even postulated by Axelrod and Wang (1994) to “speed up reactions of immobilized enzymes” on surfaces [161], who have seen the impact for technological applications. In case of membranes composed of amphiphilic block copolymers, the same issues need to be addressed if more complex scenarios are aimed for advanced systems, such as artificial cells.

The insertion of sensitive, biological membrane proteins or biopores/ionophores into synthetic block copolymer membranes has been thoroughly investigated in the past years and their utility for possible future applications has been thoroughly described (see section 1.6 and Table 1.1) [8,35,39–47,49,50,52,55,89,162–164]. Therefore, synthetic membranes serve as host for biological membrane proteins as the advanced alternative to phospholipid bilayers. It is somewhat surprising that the membrane proteins tested thus far are fully functional and able to specifically and efficiently tune the permeability

properties to a specific need. The function of membrane proteins relies on their molecular stability and structural flexibility, which is determined by the tertiary and quaternary structure of the protein. Therefore, the synthetic membrane, analogous to the lipid bilayer, has to provide a supporting matrix to retain the protein's structure. Equally to natural phospholipid membranes, the insertion process and alignment of the membrane protein within the membrane is based on burying the hydrophobic amino acid residues in the hydrophobic part of the membrane, whilst the hydrophilic residues face to the aqueous side and/or the hydrophilic part of the membrane. As mentioned in section 1.3.6 and shown in the study in chapter 3, the increased thickness of block copolymer membranes, which can be two to ten times more than phospholipid bilayers, which leads to a large mismatch between the membrane thickness and the size of the membrane protein, which is expected to significantly affect the insertion, mobility and functionality of the biomolecules [5,8,57]. Theoretical calculations and molecular dynamics simulations have indicated that block copolymer membranes are capable of adjusting their thickness to the size of the membrane inclusion/membrane protein with a hydrophobic mismatch change of 1.3 nm (22%) [57]. This molecular dynamic simulation explained that the block copolymer chains are able to compress in vicinity of a membrane protein and the effect is greater with increasing flexibility of the polymer type. Recent studies have shown that membrane proteins and biopores remain functional in PMOXA-*b*-PDMS-*b*-PMOXA triblock copolymer membranes that are up to 10 times thicker than the height of the membrane proteins and biopores [8,39–50,52,163,164]. In comparison to hydrophobic mismatches occurring in biological membranes, where the difference is in the angstrom range [136], the ones in block copolymer membranes can be significantly larger lying in the nanometer range. It is remarkable how these synthetic membranes provide an environment, which maintains membrane protein function.

It is still unclear how sensitive biological membrane proteins are able to function in a completely synthetic membrane and it is important to understand, which molecular parameters of the membrane play key roles in providing an appropriate environment for membrane proteins to allow their insertion and functionality. Until now, experimentally determined diffusion properties of membrane-reconstituted biological species within synthetic block copolymer membranes have not been reported. In this chapter, we introduce a detailed view on how differently sized membrane proteins diffuse within self-assembled synthetic block copolymer membranes with thicknesses of 9.2, 12.1 and 13.4

nm. We selected three different PMOXA-*b*-PDMS-*b*-PMOXA triblock copolymers, which distinguish only in their molecular weight, but have same chemical composition (PMOXA and PDMS) and block architecture (triblock) (Table 4.1). Furthermore, we are interested in determining the lateral diffusion coefficients of membrane proteins of different lateral dimensions (radius) in order to establish whether they behave similarly compared to phospholipid bilayers. Figure 4.1 shows the principle of measurement of the lateral diffusion of membrane proteins within GUVs by z-scan FCS, as a follow-up story from chapter 3.

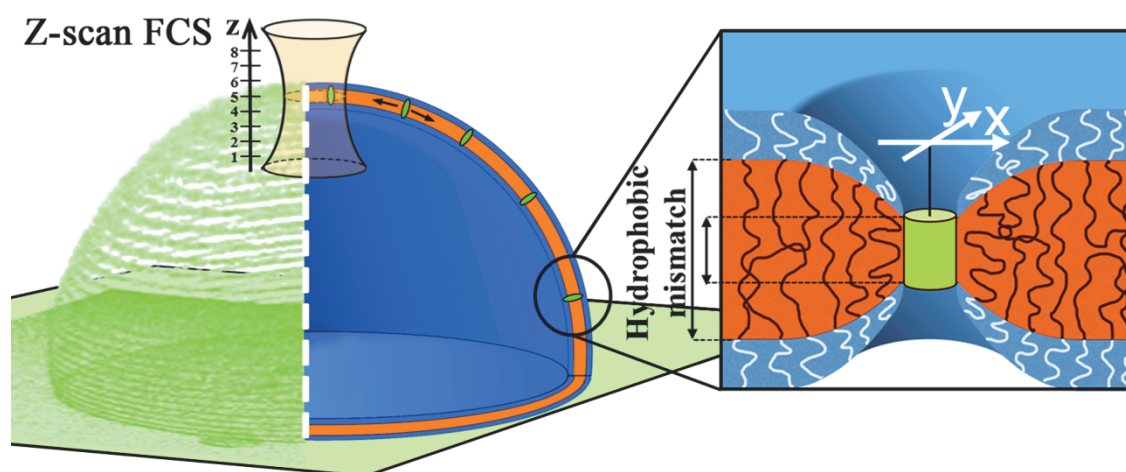


Figure 4.1. Schematic representation of the measurement principle and hydrophobic mismatch. The mismatch is a result of the height difference between the membrane and the membrane protein (represented as the green cylinder). Giant unilamellar vesicles (left) are immobilized as half-spheres on the glass surface to form stable membranes for precise z-scan FCS measurements. The left half of the GUV is a 3D fluorescence microscopy image of the incorporated fluorescent membrane proteins and the right half represents the schematic GUV. Inserted membrane proteins are mobile within the synthetic block copolymer membrane and can diffuse in the 2-dimensional plane of the membrane similar to the situation in a lipid bilayer.

4.2 Results and discussion

4.2.1 Lipids and amphiphilic block copolymers

Three different triblock copolymers and one type of lipid (Table 4.1) were used to form giant unilamellar vesicles with inserted membrane proteins and to determine the protein's lateral diffusion within the membranes. These three specific block copolymers were selected because they form nice polymersomes by the film rehydration method (see Figure 3.2) and they form high number of GUVs from pure dried polymer films. The lipid

POPC was chosen because of its fluid character (unsaturated acyl chains) and high abundance in biological membranes.

Table 4.1. Molecular characteristics of the used triblock copolymers and lipid in this chapter.

	molecular composition	M_w [g/mol]*	membrane thickness d [nm]*
triblock	$A_6B_{34}A_6$	3800	9.2 ± 0.5
	$A_7B_{49}A_7$	5100	12.1 ± 1.0
	$A_{12}B_{63}A_{12}$	6900	13.4 ± 0.9
lipid	POPC	770	5.0 ± 0.4

*Data from reference [95] and chapter 3, respectively.

4.2.2 Expected hydrophobic mismatch

The hydrophobic mismatch plays an important role when reconstituting membrane proteins into block copolymer membranes of large thicknesses. Hydrophobic mismatches also exist in biological membranes, where they can be involved in lipid raft formation and cell sorting. If the membrane protein height and bilayer thickness do not match, the mismatch must be compensated with a structural change either of the lipid bilayer or the protein. Membrane proteins exist with different hydrophobic heights and their interaction with specific types of lipids, for example with specific acyl chain lengths, is of great importance for function [10]. However, hydrophobic mismatches occurring in biological membranes are by far less than the ones that may occur in block copolymer membranes. In biological membranes, the thickness differences are ranging between ± 10 Å. Thus, also negative values exist, where the lipid bilayer has to expand/stretch in vicinity to a large membrane protein, while a positive mismatch results in a membrane thinning.

The hydrophobic mismatch Δd is calculated as: $\Delta d = d_{hydrophobic} - d_{MP}$, where d_{MP} is the hydrophobic height of the membrane proteins taken from the crystal structures and $d_{hydrophobic}$ is the hydrophobic membrane thickness, which has to be calculated from the measured membrane thickness d . Cryo-TEM provides the membrane thickness of the whole polymer and not only the hydrophobic part because the contrast is generated from phase contrast by underfocussing of the objective lens. The phase of the incoming electron beam is shifted at structures with different refractive indices, thus PDMS and PMOXA both provide contrast. As a close approximation, the hydrophobic thickness was

calculated considering the hydrophilic to hydrophobic ratio ($f_{hydrophilic}$) or the hydrophobic to hydrophilic ratio ($f_{hydrophobic}$), respectively (Table 4.2). In this way, the hydrophobic thickness of lipid bilayers can be obtained relatively accurate from cryo-TEM images.

Table 4.2. Theoretical hydrophobic mismatch expected to exist in the different membranes.

Membrane	$f_{hydrophobic}$ [%]	d [nm]*	$d_{hydrophobic}$ [nm]	Membrane protein	d_{MP} [nm]**	Δd [nm]
POPC	0.63	5.0 ± 0.4	3.1 ± 0.3	KcsA	3.5 ± 0.1	-0.4 ± 0.4
				AqpZ	3.0 ± 0.1	0.1 ± 0.4
$A_6B_{34}A_6$	0.68	9.2 ± 0.5	6.3 ± 0.3	AqpZ	3.0 ± 0.1	3.3 ± 0.4
$A_7B_{49}A_7$	0.73	12.1 ± 1.0	8.8 ± 0.7	KcsA	3.5 ± 0.1	5.3 ± 0.8
				AqpZ	3.0 ± 0.1	5.8 ± 0.8
				OmpF	2.4 ± 0.1	6.4 ± 0.8
$A_{12}B_{63}A_{12}$	0.75	13.4 ± 0.9	10.1 ± 0.7	AqpZ	3.0 ± 0.1	7.1 ± 0.8

* from reference [95] and chapter 3. ** Crystallographic data from PDB database.

A POPC lipid bilayer has a membrane thickness of $d = 5.0 \pm 0.4$ nm determined from cryo-TEM, whereas a hydrophobic membrane thickness results when multiplied with the hydrophobic to hydrophilic weight ratio of POPC of 0.63. The hydrophobic thickness of 3.1 nm for a POPC bilayer is in good agreement to values reported in literature [70]. By using the $f_{hydrophobic}$ of the here used triblock copolymer membranes, the hydrophobic mismatch eventually ranges from 3.3 to 7.1 nm (Figure 4.2). As one can see, the hydrophobic membrane thickness is not that large anymore, whereas the difference to the lipid bilayer thickness is ranging by factors of 2 – 3. However, the resulting hydrophobic mismatch in case of block copolymer membranes is significantly larger than the ones occurring in biological membranes.

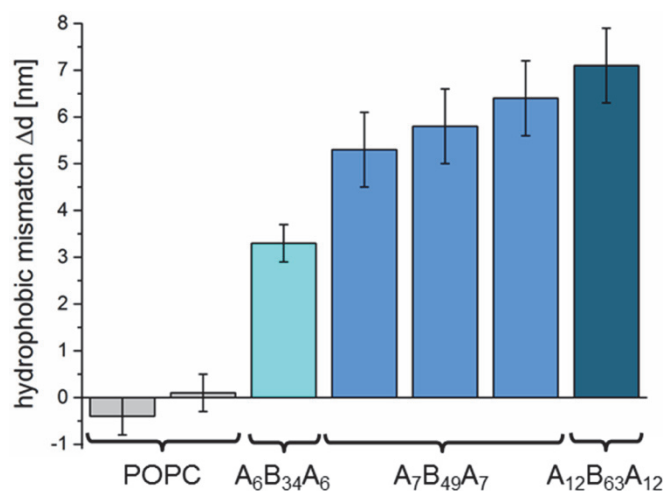


Figure 4.2. Theoretical hydrophobic mismatch existing in the different membrane systems.

4.2.3 Membrane proteins and labelling

The following, integral membrane proteins were selected as models (Figure 4.3): the potassium crystallographically-sited activation channel (KcsA), the bacterial water-selective channel protein AquaporinZ (AqpZ), and the outer membrane protein F (OmpF). All three membrane proteins differ in their structure, such as tertiary structure (alpha helical vs. beta-barrel) and quaternary structure (trimer and tetramer) as well as their dimensions (radii and hydrophobic heights). KcsA and AqpZ are both alpha-helical transmembrane proteins, both of which form tetramers as their functional quaternary structure. OmpF is a beta-barrel membrane protein, which forms trimers. In addition, they also possess different hydrophobic thicknesses, *i.e.* their activity can depend on their membrane environment such as the length of the phospholipid carbon chains and thus the membrane thickness [136].

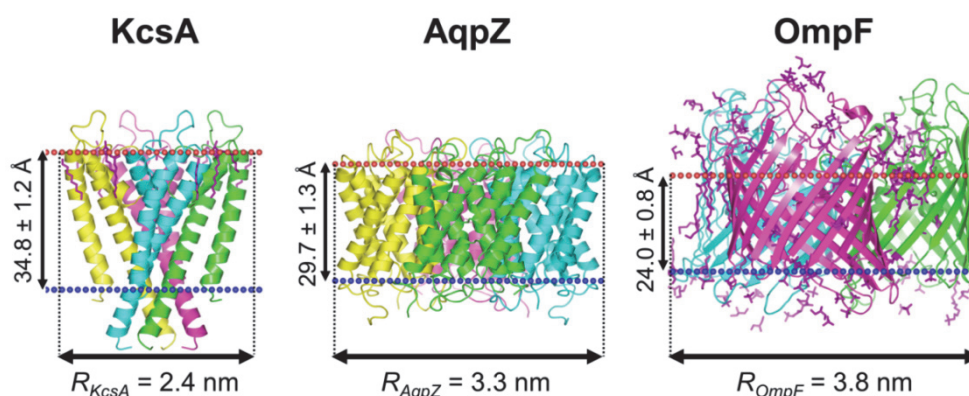


Figure 4.3. Crystal-structures of the membrane proteins used in this study. Shown are the respective multimers (KcsA: tetramer, AqpZ: tetramer, OmpF: trimer) and their dimensions (hydrophobic height and radius). Dimensions were obtained from the proteins crystal structures from orientations of proteins in membranes database (OPM, <http://opm.phar.umich.edu/>).

The selected membrane proteins form trimers and tetramers, thus their quaternary structure of the proteins finally determines the size (lateral dimension) of the diffusing species. They possess different sizes with radii of 2.4 nm (KcsA tetramer), 3.3 nm (AqpZ tetramer) and 3.8 nm (OmpF trimer). The quaternary structure was also preserved in detergent solutions as shown in SDS-PAGE gels (Figure 4.4A). The typical bands on coomassie stained SDS-PAGE gels shows the purity and stability of the KcsA tetramer at around $\sim 55 \text{ kDa}$ (lane A, Figure 4.4A) [165] and $\sim 65 \text{ kDa}$ for the AqpZ tetramer (lane B, Figure 4.4A) [166]. Both proteins show only weak monomer bands ($\sim 17 \text{ kDa}$ for KcsA, $\sim 20 \text{ kDa}$ for AqpZ). For the purity analysis of OmpF, the protein solution was boiled at

95 °C for 10 min, therefore, the protein band is seen only in its typical monomeric form at ~39 kDa (lane C, Figure 4.4A) [167]. Therefore, we assume that these multimers are present not only within the POPC phospholipid membranes [77], but also within the block copolymer membranes because they are resistant to SDS detergent solution, and do not disassemble into the monomers. In addition, the block copolymer membrane provides a soft environment where the membrane proteins can keep their structure.

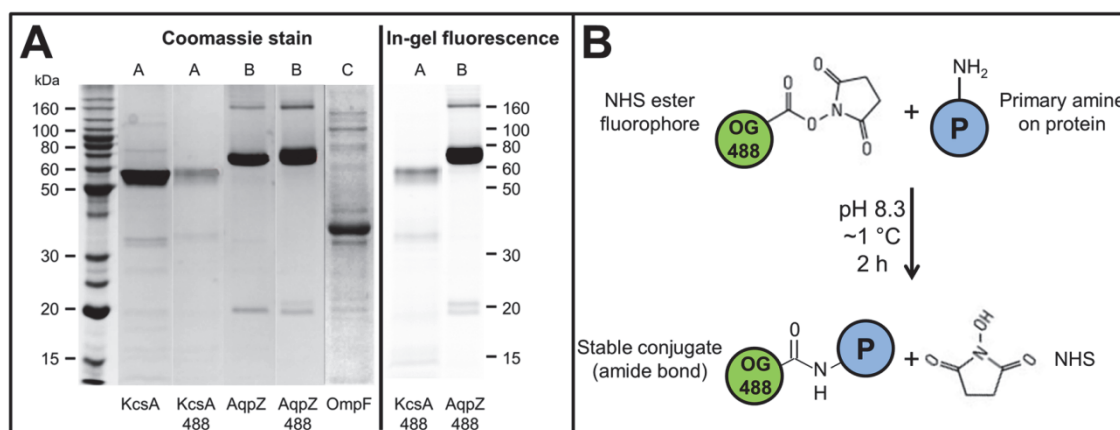


Figure 4.4. Membrane protein purification and labelling. A) Protein purity and fluorescent labelling was confirmed on 12% SDS-PAGE gels by coomassie staining. In-gel fluorescence shows the labelling with the fluorescent dye (labelled with 488). B) Reaction scheme of protein labelling via NHS-ester activated fluorescent dyes.

The fluorescent labelling of the membrane proteins KcsA and AqpZ was performed by NHS-ester coupling reaction to primary amines on the proteins (Figure 4.4B). The N-terminus of these two proteins contains only hydrophilic amino acid residues. Therefore, it is available for the labelling reaction in the aqueous phase and is not buried in the hydrophobic part of the membrane protein. In this case, the fluorescent dye Oregon Green 488 (OG488) was used to track the diffusion of the membrane proteins by z-scan FCS. However, OmpF, which does not have a His-tag for purification and whose N-terminus is buried in the interior of the protein, was labelled with Atto-488-maleimide (ATTO-TEC, Siegen, Germany) via maleimide crosslinking to cysteine. The fluorescent labelling of KcsA and AqpZ was confirmed by in-gel fluorescence on SDS-PAGE gels, which clearly shows the bands are specifically labelled (Figure 4.4A). Unfortunately, the labelling of membrane proteins involves some issues to be addressed in comparison to the labelling of water soluble proteins. Since membrane proteins involve concentrations of detergents above the critical micellar concentration (cmc), there are also detergent micelles present in the solution, which can entrap the fluorescent dyes. In addition, these detergent

micelles have similar molecular weights (sizes) as the membrane protein / detergent complex, which make the separation of unreacted free dye from the labelled membrane proteins difficult to achieve. Thus, this purification cannot be achieved by standard size exclusion chromatography, which was sometimes performed in literature [77]. In addition, performing the labelling reaction on Ni-NTA beads, results in adsorption of unreacted dye into the Ni-NTA agarose beads and thus even after thorough washing of the column, there will still be free dye when eluting the protein from the beads. Thus, in order to improve these problems of labelling and purification, we performed the labelling on Ni-NTA beads with subsequent elution of the labelled protein, and as an additional step, a second immobilization of the proteins on “fresh” Ni-NTA beads, in order to reduce the amount of free dye in the protein solution further more. However, we still observed free dye within SDS-PAGE gels and also in lateral diffusion measurements, which can complicate the analysis of membrane protein diffusion, because it creates an additional species that diffuses within the membrane (see section 4.2.5).

4.2.4 GUV formation and immobilization

As model membranes, we generated giant unilamellar vesicles (GUVs, 5 – 50 μm in diameter) with inserted membrane proteins. GUVs were prepared by the electroformation technique [149] with modifications in order to obtain membrane proteins embedded in the GUV membrane. In detail, the standard vesicle formation method via the film rehydration technique, followed by dialysis and extrusion was used to obtain small polymersomes with inserted membrane proteins [8,35,48,168]. We observed strong interaction of detergent molecules with the block copolymer membranes, thus purification by long-time dialysis is an important step as reported previously [35,48,168]. In addition, we used a buffer system with low salt concentration (1 mM Hepes, 2 mM NaCl, pH 7.4) in order to be able to apply an electrical field for the electroformation technique. Second, small droplets from the polymersome solution were distributed on ITO-coated (indium tin oxide) glass plates and partially dried in order to form a smooth membrane for subsequent electroformation. The polymersome deposition results in several spots of a visually observable thin films when hold under light.

For the purpose of obtaining a high signal-to-noise ratio in FCS measurements, fluorescence-labelled and unlabelled membrane proteins were mixed at a molar ratio of 1:10 in order to avoid too many fluorescent membrane proteins in the confocal volume

[169]. Membrane proteins were incorporated into block copolymer membranes at a targeted polymer-to-protein ratio (PoPR) of 50 (w/w) (see Table 4.5, section 4.2.8). This procedure for the generation of membrane protein containing GUVs leads to a relatively small number of GUVs (Figure 4.5) compared to GUVs generated from pure ABA films (see chapter 3, Figure 3.5). In addition, these GUVs are much smaller, which is even more problematic to find suitable GUVs for z-scan FCS measurements. These generated membrane protein-containing GUVs were immobilized on plasma-treated glass surfaces resulting in stable half-spheres as performed in chapter 3 [95].

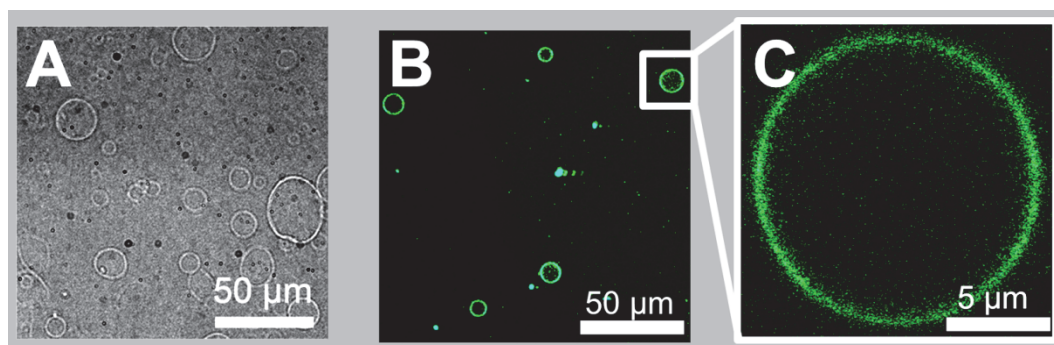


Figure 4.5. Imaging of block copolymers GUVs with inserted membrane proteins. A) The reduced number of GUVs formed during electroformation shows the difficulty to prepare GUVs with inserted membrane proteins. B) LSM image of a low number of appropriate GUVs to perform z-scan FCS. C) GUV showing the labelled membrane proteins homogeneously distributed within the polymer membrane.

By using LSM, suitable GUVs (*i.e.* non-moving, stable half-spheres, 15 – 25 µm diameter) [95] were selected for z-scan FCS measurements. As shown in Figure 4.5B and C, the fluorescence-labelled fraction of membrane proteins is homogeneously distributed within the polymer membrane. However, in some cases we observed GUVs with inhomogeneously distributed fluorescence indicating membrane protein aggregation (Figure 4.6A). These GUVs were avoided for FCS measurements because the intense peaks (count rate) in the FCS raw data (Figure 4.6B) superimpose on the signal of the non-aggregated membrane proteins, and thus produce an additional shoulder in the FCS autocorrelation function (Figure 4.6C).

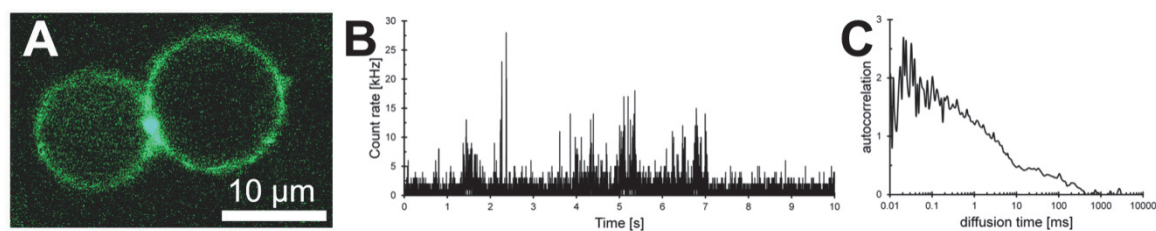


Figure 4.6. Protein aggregation in block copolymer membrane. A) Membrane proteins seem to aggregate especially when two GUVs come into contact. B) The fluorescence intensity fluctuations over time show high peaks considerably differing from the free protein intensity. Due to the large aggregates which contain also many fluorescent dyes cause the high peaks. C) The autocorrelation analysis of the aggregates proteins reveals an additional shoulder with a high diffusion time, which strongly affects the final calculations.

4.2.5 Membrane protein diffusion in lipid bilayers

Lateral mobility of membrane proteins diffusing within model phospholipid membranes have been determined by several research groups [77,158,170,171]. Several theoretical models have been proposed to describe the diffusion of membrane proteins in a 2D membrane, the most famous being the Saffman-Delbrück (SD) model [77,106,158,171–174]. The radius of the membrane proteins is an important factor, which together with membrane-related properties influences the lateral mobility within the membranes as observed within phospholipid bilayers and described by the Saffman-Delbrück equation (equation 2.5, section 2.1.3) [77,106,158,171,174]. The SD-model treats the membrane inclusions as cylinders with a radius R diffusing freely in a 2D membrane described by a thickness d and a membrane viscosity η_m [106]. In the most recent study on membrane protein diffusion in free-standing phospholipid bilayers, the Saffman-Delbrück model was well-suited to describe diffusion for differently sized proteins, which allowed calculating a membrane viscosity of 40 mPa·s [77].

Here, we were able to incorporate membrane proteins into GUVs composed of a POPC bilayer. The diffusion coefficients of the membrane proteins within GUVs determined by z-scan FCS (Figure 4.7, Table 4.3). The analysis of the FCS law showed, that the membrane proteins are diffusing freely within the fluid POPC membrane, represented by the t_0 value, which was always close to zero.

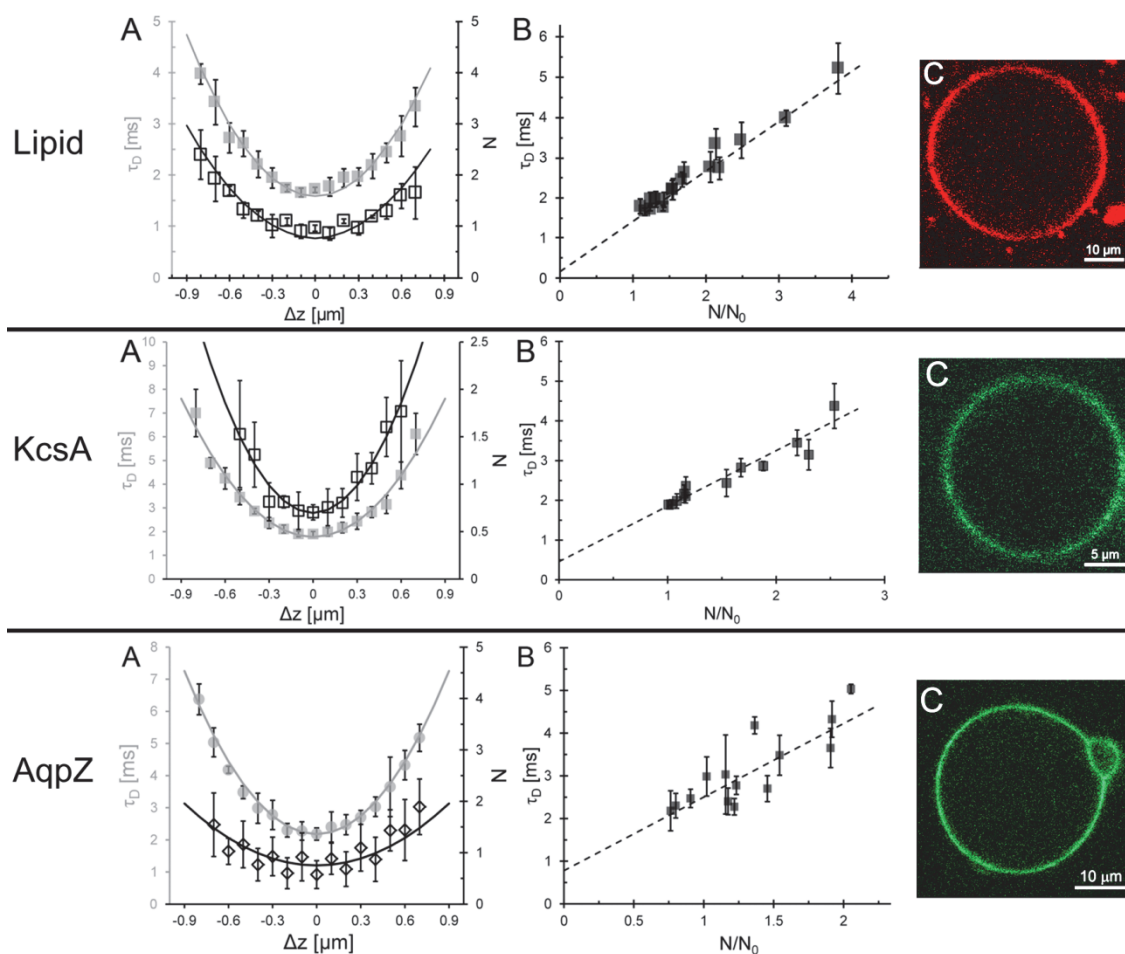


Figure 4.7. Membrane protein diffusion within lipid GUVs determined by z-scan FCS. Diffusion coefficients were calculated for POPE-Rhod- (top line), KcsA- (middle) and AqpZ- (bottom) diffusion within POPC GUVs. A) Parabolic z-dependency. B) z-scan FCS law. C) Examples of LSM images of selected GUVs.

Table 4.3. Diffusion coefficients of membrane proteins within POPC GUVs.

Membrane	Measured species	Radius R [nm]	Diffusion coefficient D [$\mu\text{m}^2/\text{s}$] (20 °C)
	POPE-Rhod	0.44	$12.6 \pm 0.6^*$
POPC	KcsA-OG488 (tetramer)	2.4	8.5 ± 0.8
	AqpZ-OG488 (tetramer)	3.3	7.9 ± 0.5

*from ref [95], and chapter 3.

In order to estimate the preciseness of our measurement technique, we compare our obtained diffusion coefficients of KcsA and AqpZ diffusion in POPC GUVs to the data presented by Weiss et al. (2013) (Figure 4.8) [77]. The membrane viscosity of the POPC membrane was calculated by using the SD-equation and is 32.7 ± 1.2 mPa·s, which is in good agreement with the value reported for POPE:POPC phospholipid membrane viscosity (39.5 mPa·s). The slightly higher diffusion coefficients might be attributed to the different measurement technique (dual-focus FCS) and the different lipid composition (POPE:POPC mixture (3:2 molar ratio) of the membrane).

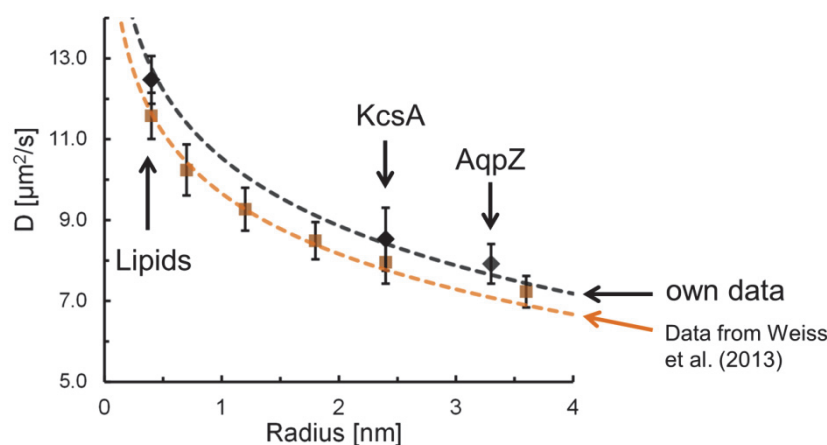


Figure 4.8. Saffman-Delbrück model (dashed line) of membrane protein diffusion within POPC GUVs. The data obtained by z-scan FCS is compared to the data from Weiss et al. (2013).

4.2.6 Interaction of dye with polymer membrane

During the analysis of the FCS autocorrelation functions, we detected traces of free-dye in the GUV membranes originating from membrane protein labelling (see section 4.2.3). This minimal amount of free dye (10 – 20%) present in the membrane is a result of the slightly hydrophobic character of OG488 and is known for many other fluorescent dyes [89,175]. The two different components (free dye and membrane proteins) within the membrane influence the lateral diffusion measurement and we therefore used a two-component fitting model (equation 2.11). In order to evaluate if small molecular mass fluorescent dyes diffuse similarly to the labelled membrane proteins within the membranes, we first verified the diffusion of a selected dye as model. Bodipy-630/650 (Bodipy) was chosen based on its small molecular weight (~ 550 g/mol) and its hydrophobic character supporting a direct insertion into the membrane (Figure 4.9). Bodipy is often used to stain membranes. The diffusion coefficient of Bodipy within the $A_7B_{49}A_7$ membrane was 3 times higher than the $A_7B_{49}A_7$ macromolecules themselves (4.6

± 0.5 and $1.6 \pm 0.2 \mu\text{m}^2/\text{s}$, respectively). In addition, small molecular weight hydrophobic molecules diffuse freely ($t_0 \approx 0$) within the membrane (Figure 4.9B), contrary to pure macromolecules, which show a hindered-diffusion character [95]. In the case of the more hydrophilic dye OG488, which was used for labelling the membrane proteins, the diffusion coefficient of $7.4 \pm 0.9 \mu\text{m}^2/\text{s}$ was higher than the diffusion of the hydrophobic dye Bodipy (Figure 4.9C), as expected due to their difference in their molecular weight. As already mentioned in section 4.2.3 (membrane proteins and labelling), the remaining free dye in the stock solution of the membrane proteins results in an accumulation of free dye in the block copolymer membrane.

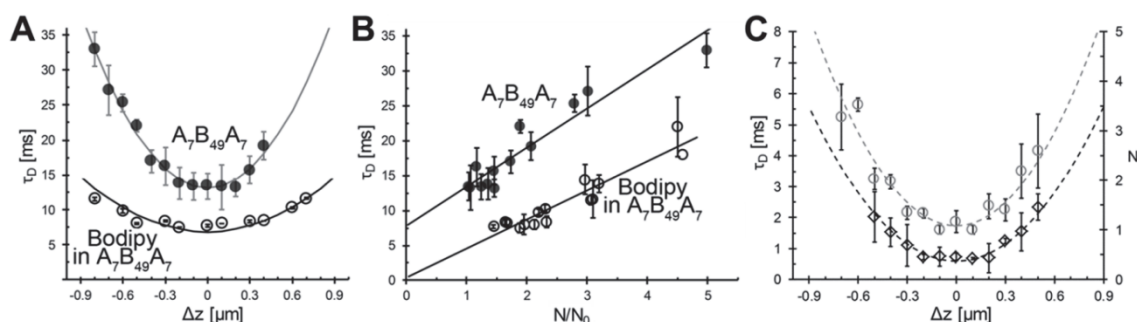


Figure 4.9. Z-scan FCS data and FCS law of $A_7B_{49}A_7$ membrane. A) Z-scan FCS plots of the SRB-labelled block copolymer fraction (SRB- $A_7B_{49}A_7$ -SRB, filled circles) and of Bodipy 630/650 diffusing in the membrane (open circles). B) Z-scan FCS law showing hindered diffusion of the polymer macromolecules ($t_0 = 6.8$ ms, $R^2 = 0.89$) and free-diffusion of Bodipy ($t_0 = -0.1$ ms, $R^2 = 0.76$). C) Z-scan FCS plot of OG488 diffusion in $A_7B_{49}A_7$ membrane. The minimum diffusion time of OG488 was $\tau_D = 1.7$ ms ($\lambda = 488$ nm, pinhole diameter = $70 \mu\text{m}$). Open circles: τ_D ; open squares: N .

4.2.7 Membrane protein diffusion in block copolymer membranes

The lateral diffusion of membrane proteins within synthetic membranes composed of amphiphilic block copolymers has not been reported yet. We could already show in chapter 3, that the lateral mobility of the polymer macromolecules of the different membranes (triblock and diblock) is similar to those of phospholipids. Therefore, we can expect to see a similar behaviour for membrane protein diffusion. In order to obtain insight into the mechanisms and behaviour of membrane protein diffusion within synthetic membranes, we varied the membrane thicknesses of the block copolymer membranes and the size of the membrane proteins. Both features, membrane thickness

and radius of the diffusing object, are factors in the Saffman-Delbrück equation and potentially influence the diffusion coefficient. In this respect, we chose three different triblock copolymers, $A_6B_{34}A_6$, $A_7B_{49}A_7$ and $A_{12}B_{63}A_{12}$ with membrane thicknesses of 9.2, 12.1 and 13.4 nm, respectively. As shown in chapter 3, the polymer diffusion within the self-assembled membrane decreases with increasing molecular weight [95].

We could successfully insert the membrane proteins into the three different triblock copolymer membranes and were able to measure their mobility by z-scan FCS within membranes of GUVs (Figure 4.10). The measurements clearly indicate that the membrane proteins are mobile in these membranes.

Table 4.4. Diffusion coefficients of membrane proteins within triblock copolymer GUVs.

Membrane	Diffusing species	Measured species	Radius R [nm]	Diffusion coefficient D [$\mu\text{m}^2/\text{s}$] (20 °C)
$A_6B_{34}A_6$	Polymer	$A_6B_{34}A_6$ -SRB*	0.56*	$2.4 \pm 0.2^{**}$
	Membrane protein	AqpZ-OG488 (tetramer)	3.3	1.7 ± 0.1
$A_7B_{49}A_7$	Polymer	$A_7B_{49}A_7$ -SRB*	0.68*	$1.6 \pm 0.2^{**}$
	Membrane protein	KcsA-OG488 (tetramer)	2.4	1.3 ± 0.1
	Membrane protein	AqpZ-OG488 (tetramer)	3.3	1.1 ± 0.1
	Membrane protein	OmpF-Atto488 (trimer)	3.8	1.1 ± 0.1
$A_{12}B_{63}A_{12}$	Polymer	$A_{12}B_{63}A_{12}$ -SRB*	0.85*	$1.0 \pm 0.1^{**}$
	Membrane protein	AqpZ-OG488 (tetramer)	3.3	0.8 ± 0.1

*radius of gyration. ** from chapter 3 and reference [95].

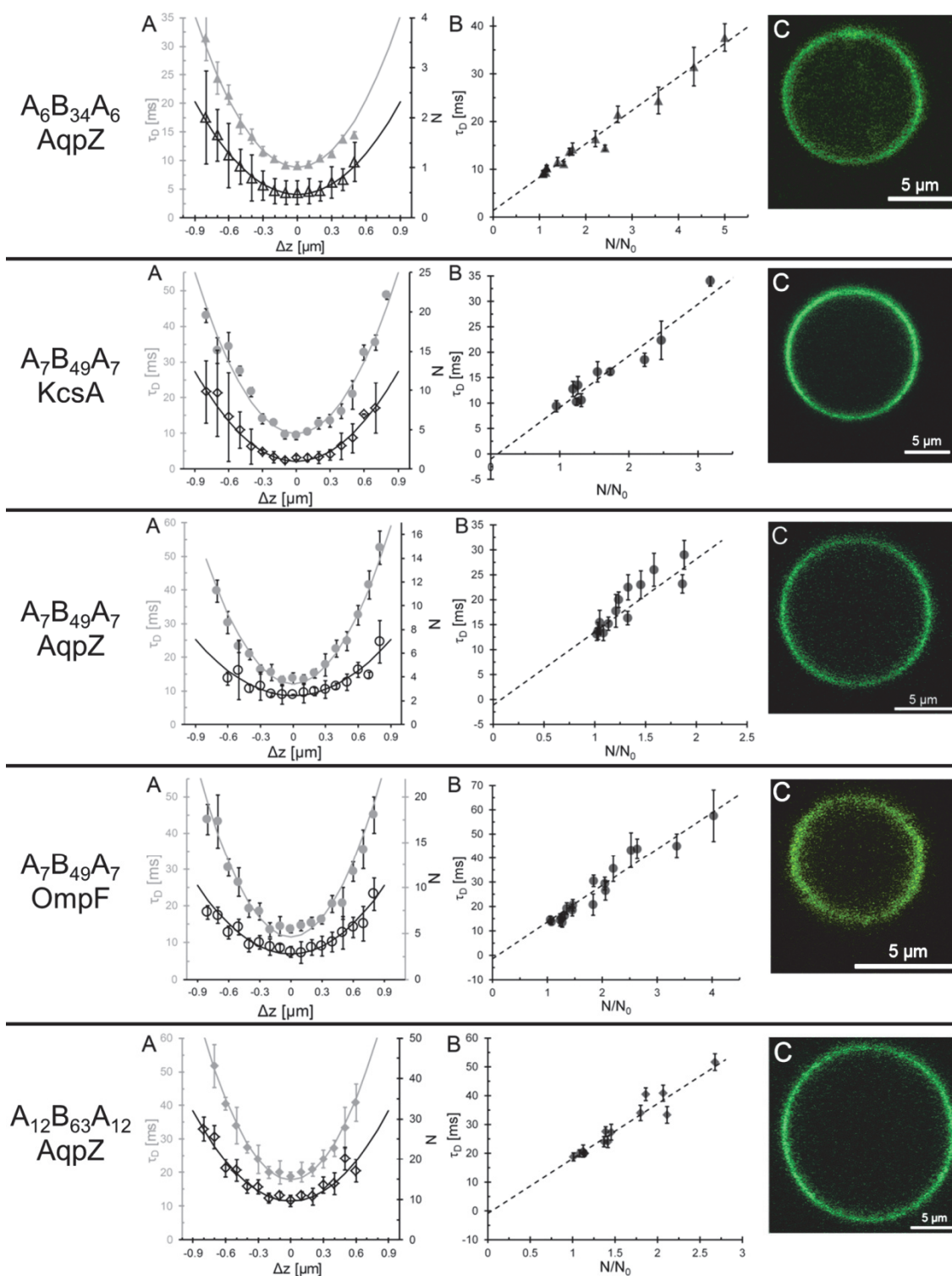


Figure 4.10. Z-scan FCS data of KcsA-, AqpZ- and OmpF-diffusion within polymeric GUVs. A) Parabolic z-dependency of diffusion time and number of particles. B) FCS diffusion laws. C) LSM images of GUVs of the mentioned membrane protein and triblock polymer.

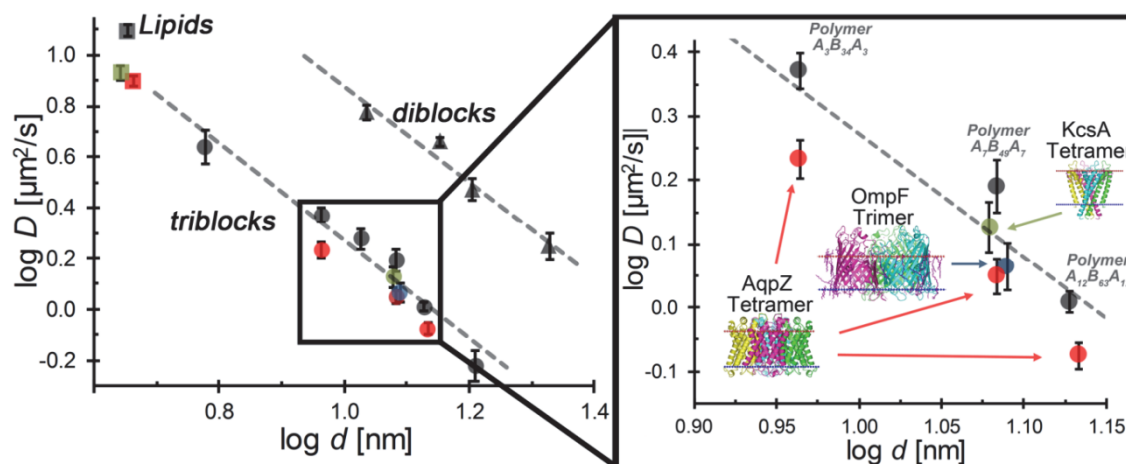


Figure 4.11. Log-log plots of the diffusion coefficient D in relation to the membrane thickness d . Lipids (squares) and triblock copolymers (circles) are taken as reference membrane systems from ref [95]. The dashed line represents the power law dependence of the diffusion coefficient in relation to the membrane thickness as $D \sim d^{-1.25}$. The zoom into the area of interest shows the diffusion coefficients of KcsA (green), AqpZ (red) and OmpF (blue) within the three different triblock copolymer membranes ($A_6B_{34}A_6$, $A_7B_{49}A_7$, $A_{12}B_{63}A_{12}$) tested in this study.

Interestingly, despite the large difference in thickness between the triblock copolymer membranes (9.2 – 13.4 nm) and the height of the membrane proteins ($\sim 3 - 4$ nm), the mobility of the membrane proteins within the membrane is close to the diffusion of the single polymer macromolecules within the membrane itself (Table 4.4). The diffusion coefficients of the three different membrane proteins (KcsA, AqpZ, OmpF) within the three different triblock copolymer membranes are only around 20-30% lower than the pure polymer diffusion (Figure 4.10). In comparison to membrane protein diffusion in a natural POPC phospholipid bilayer, the difference of the diffusion coefficients between the membrane and the membrane proteins are similar when plotted on a logarithmic scale (Figure 4.11).

We applied the Saffman-Delbrück model to assess its applicability to triblock copolymer membranes. The diffusion coefficients of membrane proteins within the $A_7B_{49}A_7$ membrane could be fitted to the SD-equation (Figure 4.12). In order to see the diffusion coefficients of the membrane proteins within both lipid and synthetic triblock copolymer membranes, the results were plotted in terms of relative diffusion, which is defined as the ratio of the membrane protein diffusion (D_{MP}) to the diffusion of the corresponding membrane (D_0) where the membrane protein is inserted. The resulting membrane viscosity (η_m) for the $A_7B_{49}A_7$ membrane yields a value of 126.6 ± 2.5 mPa·s ($R^2 = 0.94$),

which is four times higher than the membrane viscosity determined for a POPC phospholipid membrane ($32.7 \pm 1.2 \text{ mPa}\cdot\text{s}$, $R^2 = 0.97$).

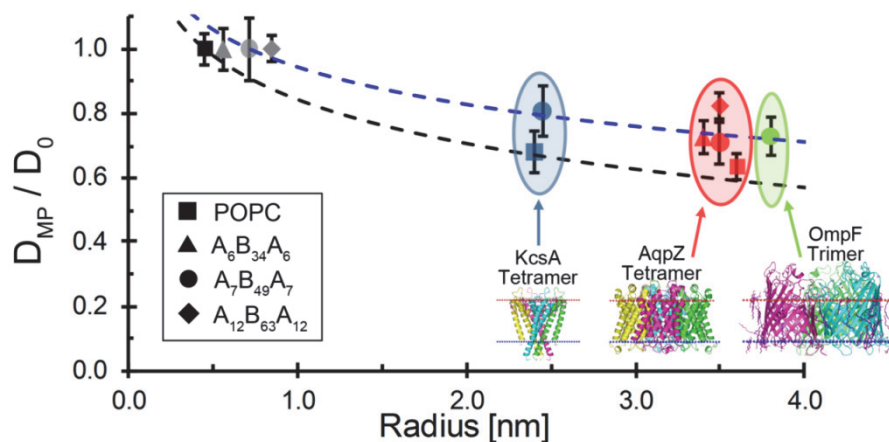


Figure 4.12. Size-dependent (radius) lateral diffusion of KcsA, AqpZ and OmpF within different membrane systems (natural phospholipids vs. triblock copolymer membranes). The relative diffusion (D_{MP}/D_0) of the membrane proteins in comparison to the membrane diffusion shows the similarity between two completely different membrane types. On a relative scale, the diffusion of membrane proteins in the $A_7B_{49}A_7$ membrane (blue dashed line, $\eta_m = 126.6 \pm 2.5 \text{ mPa}\cdot\text{s}$, $R^2 = 0.94$) is only 3-fold lower than in a biological phospholipid bilayer (POPC: black dashed line, $\eta_m = 32.7 \pm 1.2 \text{ mPa}\cdot\text{s}$, $R^2 = 0.97$).

4.2.8 Membrane protein insertion efficiency

FCS allows determination of concentrations in the nanomolar range. Therefore, it is possible to calculate the number of membrane proteins diffusing in the GUVs. The membrane protein incorporation efficiency into the block copolymer membranes can be estimated when the number of particles in the illuminated area on the polymer membrane is known. Table 4.5 shows the calculation of the incorporation efficiency of the here used proteins and the different membrane systems. The number of membrane proteins N per μm^2 is calculated based on the obtained beam waist ω_0 . With the labelling efficiency, which was determined based on SDS-PAGE gel electrophoresis, the total number of membrane proteins N_{MP} is calculated. The number of lipids or polymers per μm^2 is calculated based on the radii of the molecules occupying in the membrane (Table, which then provides the theoretical mean area per molecule values. For POPC, the radius is around 0.44 nm [176]. For the dimensions of the polymers occupying in the membrane, the radius of gyration was used as shown in section 3.2.8 in chapter 3. In this way, the

LPR or PoPR can be calculated and compared to the theoretical value, which was used for the preparation of the samples.

Table 4.5. Calculation of membrane protein incorporation efficiencies into GUVs.

Membrane	MP	N [1/ μm^2]	Labelling efficiency	Total N_{MP} (10 x) [1/ μm^2]	# lipids / polymers [1/ μm^2]	Exp. LPR /PoPR (molar)	Theo. LPR / PoPR (molar)	Theo. LPR / PoPR (w/w)	Incorp. efficiency [%]	n
POPC	KcsA	3.9	~0.8	49	1.64E+06	40773	1500	60	4.5	16
	AqpZ	3.8	~0.8	48	1.64E+06	41806	1700	50	4.9	9
$A_6B_{34}A_6$	AqpZ	2.5	~0.8	32	1.02E+06	32153	75	10	0.2	9
	KcsA	8.1	~0.8	101	6.23E+06	6150	200	50	3.3	9
$A_7B_{49}A_7$	AqpZ	12.7	~0.8	15	6.20E+06	3905	250	50	6.4	10
	OmpF	16.7	n.a. ~ 0.5	33	6.23E+06	18648	650	85	3.5	10
$A_{12}B_{63}A_{12}$	AqpZ	48.5	~0.8	606	4.36E+05	32192	200	50	27.9	12

MP: membrane protein. N : number of diffusing particles detected by FCS. Labelling efficiency: number of fluorescent dyes per MP monomer determined by SDS-PAGE analysis of the membrane protein bands according to Coomassie stained and in-gel fluorescence bands. Total N_{MP} (10 x): the unlabelled-MP fraction was 10 times of the labelled-MP fraction and inversely multiplied with the labelling efficiency. #lipid/polymer: number of lipids or polymers per μm^2 (theoretical estimation from mean area per molecule, with radius of gyration). LPR: lipid to protein ratio. PoPR: polymer to protein ratio. n: number of measurements.

The incorporation efficiencies are in the order of a few percent for GUVs, which is comparatively low. Although the calculation is not very precise, it provides a rough estimate. The low insertion efficiency may be mainly caused by the drying process of the vesicle suspensions before the formation of the GUVs (electroformation) because membrane proteins are very sensitive upon drying. It has to be noted that a too long drying process was avoided as good as possible. Other studies reported drying of proteoliposomes under vacuum for 12 hours, but the activity of reconstituted membrane proteins within lipid bilayers could be preserved only by the addition of minimal amounts of sucrose [170] or ethylene-glycol [158]. The preparation method is therefore a crucial step and needs to be adjusted to each type of polymer. Here, we generated GUVs without drying the polymersomes under vacuum. In addition, the number of GUVs formed was relatively small (Figure 4.4) compared to GUVs generated from pure ABA films (Figure 3.4, chapter 3), which makes the selection of suitable GUVs for z-scan FCS more difficult. Non-perfect incorporation of membrane proteins is also reported for the preparation of proteoliposomes and 100% incorporation efficiencies are usually very unlikely [177].

4.2.9 Structural meaning of membrane protein diffusion

In order to assess the effect of the membrane thickness on the mobility of the membrane proteins, we plotted the relative membrane protein diffusion (D_{MP}/D_0) with respect to the hydrophobic thickness mismatch (Figure 4.13). Interestingly, D_{MP}/D_0 increases slightly with increasing hydrophobic mismatch. Due to the formation of domains within the block copolymer membranes caused by entanglement and interdigitation of the macromolecules, the measured/observed diffusion D of the polymer macromolecules is in fact a reduced diffusion. This effect is caused by anomalous diffusion also observed in biological membranes (see section 2.1.2) and described in section 3.2.6 [77,99–102]. For example, the presence of domains due to lateral phase separation can lead to multiple diffusion rates in the observation area decreasing the mean value of the measured/observed diffusion coefficient [103–105]. For block copolymer membranes, the possibility and strength of interaction of the macromolecules with each other is molecular weight dependent, and thus membrane thickness dependent [95]. Thus, the slight increase in the relative diffusion of the membrane proteins indicates the effect of these domains on their diffusion. The larger these domains, the slower the measured/observed diffusion, and as a result, the relative diffusion of the membrane proteins increases slightly as shown in Figure 4.13A.

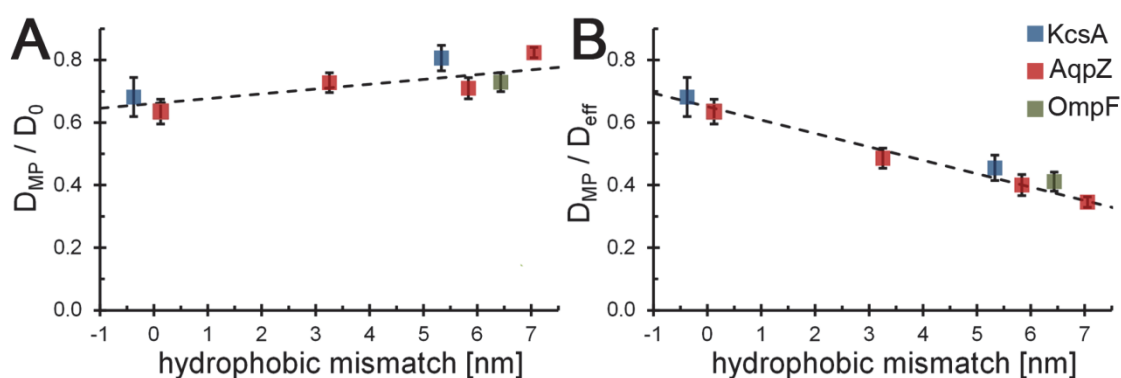


Figure 4.13. Dependence of the relative diffusion coefficients on the hydrophobic mismatch of membrane proteins diffusing within lipid and triblock copolymer membranes. A) The observed relative diffusion coefficient (D_{MP}/D_0) of the membrane proteins increases slightly with increasing mismatch. B) The relative, effective diffusion coefficient (D_{MP}/D_{eff}) decreases with increasing mismatch.

Contrary to the diffusion of the single macromolecules within the block copolymer membranes, all membrane proteins followed a free-diffusion character ($t_0 \approx 0$), or even a

slightly guided-diffusion ($t_0 \leq 0$) (Table 4.6), based on the analysis of the lateral diffusion coefficients according to the FCS diffusion law (see section 2.4.2) [100,178].

Table 4.6. Effective diffusion coefficient (D_{eff}) calculation using FCS diffusion law.

Membrane	Measured species	Diffusion coefficient D [$\mu\text{m}^2/\text{s}$]	t_0 [ms]	slope	ω_0	R^2 (t_0 -fit)	D_{eff} [$\mu\text{m}^2/\text{s}$]	n
POPC	POPE-Rhod	12.5 ± 0.6	0.2 ± 0.1	1.2 ± 0.1	260	0.92	13.6 ± 1.0	18
	KcsA-488	8.5 ± 0.8	0.5 ± 0.3	1.4 ± 0.2	240	0.88	11.8 ± 1.1	16
	AqpZ-488	7.9 ± 0.5	0.8 ± 0.3	1.7 ± 0.3	260	0.72	9.8 ± 1.7	9
	Bodipy 630/650	12.4 ± 1.1	-0.1 ± 0.6	2.6 ± 0.3	336	0.83	11.1 ± 1.3	7
$A_6B_{34}A_6$	$A_6B_{34}A_6$ -SRB	2.4 ± 0.2	4.2 ± 0.4	6.0 ± 0.3	290	0.95	3.5 ± 0.2	11
	AqpZ-488	1.7 ± 0.1	1.4 ± 0.8	7.0 ± 0.3	230	0.98	1.9 ± 0.1	9
$A_7B_{49}A_7$	$A_7B_{49}A_7$ -SRB	1.6 ± 0.2	6.7 ± 1.1	7.9 ± 0.7	294	0.89	2.8 ± 0.3	17
	KcsA-488	1.3 ± 0.1	-1.3 ± 1.8	10.2 ± 1.0	230	0.92	1.3 ± 0.1	9
	AqpZ-488	1.1 ± 0.1	-1.1 ± 3.0	14.6 ± 2.4	240	0.75	1.0 ± 0.2	10
	OmpF-488	1.1 ± 0.1	-1.4 ± 2.6	15.0 ± 1.0	230	0.93	0.9 ± 0.1	10
	Bodipy 630/650	4.4 ± 0.4	3.8 ± 1.1	5.0 ± 0.6	355	0.77	6.3 ± 0.8	16
$A_{12}B_{63}A_{12}$	$A_{12}B_{63}A_{12}$ -SRB	1.0 ± 0.1	15.6 ± 3.0	8.1 ± 1.8	280	0.66	2.4 ± 0.6	16
	AqpZ-488	0.8 ± 0.1	-0.9 ± 3.0	19.1 ± 1.7	245	0.91	0.8 ± 0.1	12
	Bodipy 630/650	4.0 ± 0.5	2.8 ± 0.5	5.6 ± 0.2	335	0.98	5.0 ± 0.2	8

Based on equation 2.14 (section 2.4.2), the calculation of D_{eff} depends on the slope of this linear equation. The slope depends on ω_0 , which again is dependent on the wavelength of the laser. This makes the comparison of the data in Table 4.6 difficult. However, the comparison between the data that were generated using the same laser wavelength (*i.e.* all proteins: $\lambda = 488$ nm, all polymers: $\lambda = 543$ nm and Bodipy: $\lambda = 633$ nm) is feasible.

The data presented in Table 4.6 can be summarized as follows: i) A slower diffusion results in a steeper slope (increasing the area of detection (ω_0) causes longer diffusion times τ_D). This can be seen for the different polymers and the lipid, all of which have the same excitation wavelength ($\lambda = 543$ nm). ii) A hindered diffusion results in a less steep slope, while guided diffusion results in a steeper slope. In this case, the less steep slope caused by the hindered diffusion of the polymers cannot be observed because the effect of the slower diffusion in (i) causes the slope to be steeper than the reduction of the slope

caused by hindered diffusion effect. On the other hand, the effect of guided diffusion can be observed as seen from the increasing slope between the membrane protein diffusion within its respective membrane. The difference becomes larger (steeper) with increasing the membrane thickness, which is largest in the case of $A_{12}B_{63}A_{12}$ membrane.

For the final calculation of the effective diffusion coefficient D_{eff} it is reasonable to state, that in case for free diffusion ($t_0 \approx 0$), $D_{eff} \approx D$, while in case of hindered diffusion ($t_0 \approx 0$), $D_{eff} > D$. Therefore, the value and quality of D_{eff} for the three triblock copolymer membranes, $A_6B_{34}A_6$, $A_7B_{49}A_7$ and $A_{12}B_{63}A_{12}$ are realistic. D_{eff} represents the diffusion of non-entangled polymer chains. For the three different triblock copolymer membranes, the slope increases with increasing molecular weight and thus, the decrease in the observed/measured diffusion to D_{eff} increases with increasing molecular weight as well.

In case of the membrane proteins, they are not expected to be entrapped in the domains of entangled block copolymer chains, but rather embedded between them where they are guided through. D_{eff} provides a value for the fluidity of the membrane that the membrane proteins sense. Due to the presence of these small entangled polymer “balls”, each membrane protein has to move between them. Taking D_{eff} as the standard diffusion coefficient of the corresponding membrane, the relative diffusion of the membrane proteins decreases with increasing hydrophobic mismatch (Figure 4.13B). Interestingly, the data suggest that we can observe the effect of the hydrophobic mismatch between the membrane proteins and the large membrane thickness of block copolymer membranes experimentally. The effect of adjusting the membrane thickness to the height of the membrane proteins was explained by the chain flexibility of the block copolymer macromolecules [57]. However, as only two block copolymer sizes were tested in that molecular dynamics simulation study, there is no information on the maximum possible compressibility. As a consequence, the block copolymer molecules have to adjust their thickness in close vicinity to the membrane proteins. This is more pronounced with larger membrane thickness, and thus the local viscosity increases, and the lateral mobility of the proteins is reduced with increasing membrane thickness. PDMS is well known for its flexibility and low viscosity ($T_g = -123 \text{ }^\circ\text{C}$) [34], which explains the significant compressibility of the hydrophobic domain around the inserted membrane proteins.

4.3 Conclusion

An insight into the local factors characterizing a successful membrane protein insertion process into synthetic block copolymer membranes requires various essential considerations: i) from fundamental point of view, an understanding of how biomolecules behave in a synthetic environment, and ii) the practical development of new hybrid materials with improved properties and functionality. Biomimetic membranes self-assembled from amphiphilic triblock copolymers composed of PMOXA-*b*-PDMS-*b*-PMOXA offer great potential for use in technological applications, due to their ability to incorporate sensitive biological membrane proteins and their high chemical and mechanical stability. In this study we showed that membrane proteins inserted into synthetic block copolymer membranes that are much thicker than the protein diffuse within the membrane only an order of magnitude slower than within natural phospholipid membranes. The hydrophobic size mismatch between the membrane thickness and the membrane protein could be observed experimentally by z-scan FCS measurements. This is formed either i) by a contraction of the block copolymer macromolecules in vicinity of the membrane protein, ii) by the arrangement of smaller block copolymer chains around the protein whilst the longer chains build up the stable membrane, or iii) by a combination thereof. A thicker membrane induces a stronger compression or a larger domain around the membrane protein. Both processes are thickness-dependent, which reduces the lateral mobility of the membrane proteins within the membrane. Further, the high polydispersity index (PDI) of these block copolymers might therefore be an essential requirement as well for successful membrane protein insertion. Therefore, this type of block copolymer combines these essential properties. PDMS offers the great advantage of having flexibility and fluidity to entangle and interdigitate to provide stability, while at the same time stretching and compressing in the vicinity of a small biomolecule to preserve its active conformation. This study provides both a fundamental basis for the choice of block copolymers to engineer synthetic biomimetic membranes, and support their implementation into future applications in technology (*e.g.* membranes for water filtration) and the biomedical field (*e.g.* nanoreactors, artificial organelles).

Chapter 5

5 General conclusion and outlook

In this work, the molecular structure and dynamics within synthetic biomimetic membranes self-assembled from amphiphilic block copolymers was described in detail. The study involved several steps to elucidate the complex structure of these membranes to be compared to phospholipid bilayers. A large library of eleven different triblock and diblock copolymers was used to investigate the differences in membrane structure and diffusion properties. This involved a detailed analysis of i) their membrane thickness and ii) diffusion properties with respect to their molecular weight, and iii) the diffusion of membrane reconstituted membrane proteins. Membrane thicknesses were determined by cryo-TEM imaging and diffusion related properties by z-scan FCS on giant unilamellar vesicles.

The central findings of this work are the following:

- i) The membrane thicknesses of the block copolymers used in this thesis are increasing with increasing molecular weight, while interdigitation and entanglement of the polymer macromolecules increases as well. Diblock copolymers form almost pure bilayer structures with only weak interdigitation, contrary to the general assumptions of fully interdigitated membranes as stated in literature. In addition, the membrane thickness of diblocks is almost twice compared to triblocks with same number of PDMS units.
- ii) PDMS-containing block copolymers possess fluidity properties that are comparable to the fluidity of phospholipid bilayers. As expected, the fluidity decreases with increasing molecular weight and membrane thickness. This decline was explained by the increased strength of interdigitation and entanglement, which is an important effect known to enhance membrane stability. Entanglement also causes the polymer

chains to form small domains, which results in a hindered diffusion character of the membranes. However, the smallest polymers used showed free-diffusion as it is the case for fluid lipids (unsaturated phospholipids). Such low molecular weight block copolymers form membranes with reduced stability, which would not have a beneficial effect for applications.

- iii) Membrane proteins were inserted into triblock copolymer membranes with thicknesses ranging from 9 to 13 nm and their diffusion within giant unilamellar vesicles was measured. The membrane proteins were mobile within the synthetic membranes and showed a free-diffusion character, contrary to the hindered-diffusion of the polymer macromolecules within the membrane. Interestingly, a decrease in the normalized diffusion was observed with increasing membrane thickness, thus providing an experimental observation of the large hydrophobic thickness mismatches existing within synthetic biomimetic membranes.

The data presented here allows concluding that membranes self-assembled from amphiphilic block copolymers that are based on PDMS as their hydrophobic moiety, are able to embed biological membrane proteins due to their high flexibility and fluidity. The block copolymer macromolecules can compress in close vicinity to the smaller membrane proteins, while the relaxed polymer chains build up a stable membrane. These results will help provide choosing the type of block copolymers to engineer biomimetic polymer membranes, and support their implementation into future applications in technology.

Further investigations are needed to gain more insight into membrane protein insertion efficiencies into these synthetic block copolymer membranes. We showed that membrane proteins were inserted into membranes with a hydrophobic mismatch up to 7 nm, but the limit of membrane thicknesses at which successful insertion is still possible has to be further investigated. This would be important for the creating more stable membranes with increased membrane thickness. Thicker membranes would involve the synthesis of larger triblock copolymers, which are able to self-assemble into polymersomes. The increased hydrophobic block will further improve the stability of the generated biomimetic membranes. In order to improve membrane protein insertion efficiencies and their functionality, essential information on the optimization of membrane preparation methods is needed and at the same time to understand the mechanism of membrane protein insertion more detailed. Standard preparation techniques are important for scale-

up for large production quantities. Another option is to consolidate the results by computer simulations. Modelling the amphiphilic block copolymer membranes, calculating their fluidity and computing the membrane proteins in these systems would greatly add value to the story. However, due to the complex structure of block copolymers, this is very computationally intensive.

Chapter 6

6 Experimental section

Materials

Reagents and materials were of the highest commercially available grade and used without further purification, unless indicated. Monofunctional carbinol-terminated polydimethylsiloxane (PDMS-OH) was purchased from ABCR GmbH (AB146681, degree of polymerization DP = 65 from NMR). Bifunctional carbinol-terminated polydimethylsiloxane (HO-PDMS-OH) were purchased from Dow Corning® (5562 carbinol fluid, DP = 22 from NMR), Shin-Etsu (KF-6002, DP = 40 from NMR) and ABCR GmbH (AB 116675, DP = 61 from NMR). 1,3-bis(hydroxybutyl) tetramethyldisiloxane and dimethyldimethoxysilane were purchased from ABCR GmbH, Germany. 2-methyl-2-oxazoline, triethylamine, trifluoromethanesulfonic anhydride, sulforhodamine B acid chloride, and all solvents were purchased from Sigma Aldrich. Oregon Green 488 carboxylic acid succinimidyl ester and Bodipy® 630/650 NHS ester were from Thermo Fisher Scientific Inc. (Waltham, MA, USA). Atto 488 maleimide was from ATTO-TEC GmbH (Siegen, Germany). *n*-octyl- β -d-glucopyranoside (β -OG) was purchased from Anatrace (Maumee, OH, USA). Ni-NTA agarose beads were from Qiagen (Valencia, CA, USA). POPC (Egg PC; L- α -phosphatidylcholine (Egg, Chicken)) and Rhod-PE (16:0 Liss Rhod PE; 1,2-dipalmitoyl-*sn*-glycero-3-phosphoethanolamine-N-(lissamine rhodamine B sulfonyl) (ammonium salt)) were from Avanti Polar Lipids (Alabaster, AL, USA). All solvents at highest purity were purchased from Sigma Aldrich without further purification.

Polymers and lipids used in this thesis

All polymers and lipids used in this thesis are listed in Table 6.1 and 6.2. Diblock copolymers were synthesized according to a previously reported procedure [139,147].

PDMS-OH with molecular weight of 5 kDa (DP=65) was purchased from ABCR. PDMS-OH with molecular weights of 3.0 kDa (DP = 39), 2.4 kDa (DP = 31), and 1.7 kDa (DP = 22) were synthesized by anionic ring-opening polymerization [139]. The polydispersity indices (PDI) of PDMS-OH were determined in THF on a Viscotek GPC max system (RI detector calibrated against polystyrene standards, Agilent PL gel columns) and were all around 1.10.

Triblock copolymers were synthesized and purified according to the method described previously [8,39,95]. Bifunctional hydroxybutyl-terminated poly(dimethylsiloxane)s (HO-PDMS-OH) with a molecular weight of 4.5 kDa (PDI = 1.8) and 2.5 kDa (PDI = 1.9) were synthesized by acid-catalyzed polycondensation of dimethyldimethoxysilane in the presence of water and end-capper. Hydroxyl-terminated bifunctional PDMS was reacted (below -10 °C) with trifluoromethanesulfonic anhydride in dry hexane, resulting in bitriflate-activated PDMS macroinitiator. The reaction mixture was filtered under argon through a G4 frit. The hexane was evaporated and dry ethyl acetate was added, in which the macroinitiator was reacted with dry 2-methyl-2-oxazoline (MOXA) in a symmetric cationic ring-opening polymerization. The polymerization reaction was quenched using triethylamine : water (1:4 v/v). The crude product was purified by ultrafiltration (MWCO 5000 g/mol, 3000 g/mol, or 1000 g/mol based on polymer weight) in water : ethanol (1:1 v/v) to remove low molecular weight impurities, yielding bi-hydroxyl-terminated triblock copolymer.

Table 6.1. List of amphiphilic block copolymers and lipids used in this thesis.

	molecular composition	M_w [g/mol]	M_{PDMS} [g/mol]	PDI	Membrane thickness [nm]
Triblock	$A_3B_{19}A_3$	2150	1470	2.4	6.0 ± 0.5
	$A_6B_{34}A_6$	3770	2580	2.3	9.2 ± 0.5
	$A_6B_{44}A_6$	4450	3320	1.8	10.7 ± 0.7
	$A_7B_{49}A_7$	5050	3690	2.1	12.1 ± 1.0
	$A_{12}B_{63}A_{12}$	6940	4730	2.1	13.4 ± 0.9
	$A_{12}B_{87}A_{12}$	5660	6500	1.6	16.2 ± 1.4
Diblock	A_6B_{22}	2340	1690	1.8	10.9 ± 0.7
	A_9B_{31}	3260	2360	1.4	14.3 ± 1.1
	A_8B_{39}	6770	2950	1.5	16.0 ± 1.1
	$A_{14}B_{65}$	6210	4870	1.7	21.3 ± 1.2
Lipid	POPC	770 ^a	-	-	5.0 ± 0.4

^a data from Avanti Polar lipids

Fluorescence labelling of polymers

Four polymers ($A_{12}B_{63}A_{12}$, $A_6B_{44}A_6$, $A_{14}B_{65}$, A_6B_{34}) were labelled with sulforhodamine B (Table 7.2) acid chloride (Sigma-Aldrich) (SRB) by esterification according to a previously published method [148]. The reaction mixture as first purified by ultrafiltration (MWCO 3000 g/mol) or dialysis and residual, non-reacted free dye was further removed on an organic size exclusion column (Sephadex LH-20, GE Healthcare) in ethanol.

Table 6.2. List of labelled polymers and lipids used in this thesis.

	molecular composition	M_w [g/mol]
SRB-triblocks	SRB- $A_6B_{44}A_6$ -SRB	~ 5600
	SRB- $A_{12}B_{63}A_{12}$ -SRB	~ 8090
SRB-diblocks	SRB- A_6B_{34}	~ 3810
	SRB- $A_{14}B_{65}$	~ 6790
Rhod-Lipid	Rhod-PE	1250 ^a

^a data from Avanti Polar lipids

Membrane protein purification and labelling

Expression and purification of the membrane proteins KcsA, OmpF and AqpZ was performed by standard molecular biology methods. KcsA and AqpZ were purified based on His-tag chromatography.

Briefly, the plasmid, expressing KcsA with a hexahistidine tag, was transformed into E.coli BL21(DE3) cells. KcsA and AqpZ were purified according to previously described method with slight modifications [8,166,179,180]. E.coli were grown in terrific broth (TB) media containing 25 µg/mL kanamycin (KcsA) or 100 µg/mL ampicillin (AqpZ) at 37 °C. At OD₆₀₀ = 0.8, the cells were induced with 1.0 mM isopropyl-β-D-thiogalactoside (IPTG) for 3 h. Cells were harvested by centrifugation and stored at -80 °C. Cells were resuspended in lysis buffer (50 mM Na₂HPO₄, pH 8.0, 50 mM KCl, 50 mM NaCl, 1mM MgSO₄, 10 mM imidazole, 1 mM phenylmethylsulfonylfluoride (PMSF), 0.1 mg/ml DNase I) and lysed using a French Press with 3 cycles. Unbroken cells were separated by centrifugation (10'000 g, 4 °C, 20 min). Membrane fractions were pelleted by ultracentrifugation (120'000 g, 4 °C, 1 h) and solubilized in solubilisation buffer (50 mM Na₂HPO₄, pH 8.0, 5% *n*-octyl-β-d-glucopyranoside (β-OG) 50 mM KCl, 50 mM NaCl, 15 mM imidazole) with agitation on ice (overnight). The suspension was centrifuged again (10'000 g, 4 °C, 15 min). To the supernatant, 1 mL of freshly washed Ni-NTA agarose beads (Qiagen, Valencia, CA, USA) were added and incubated on ice for 2 h. The Ni-NTA beads were loaded on a column and washed with 10 mL of wash buffer (50 mM Na₂HPO₄, pH 8.0, 1% β-OG, 50 mM KCl, 50 mM NaCl, 50 mM imidazole). The beads were then incubated with elution buffer (50 mM Na₂HPO₄, pH 7.4, 1% β-OG, 50 mM KCl, 50 mM NaCl) supplemented with 500 mM imidazole for KcsA, or 750 mM imidazole for AqpZ for 30 min at RT and collected.

For labeling, a fraction of the membrane protein stock solution (in elution buffer) was mixed with Oregon Green 488 succinimidyl ester (OG488, 10 mg/ml in DMSO) at a 10-fold molar excess and incubated on ice with agitation for 3 hours in dark. Primary amines were targeted for the labelling reaction to covalently couple the N-terminus of the MP's amino acid sequence. The labelling reaction was performed on ice at pH 8.3 in order to increase the labelling efficiency and to reduce the self-hydrolysis of the succinimidyl ester. For purification, the membrane protein-dye solution was first diluted with the same buffer, but without imidazole, to a final imidazole concentration of 10 - 15 mM. Then freshly washed Ni-NTA beads were added and incubated for 2 hours on ice with

agitation. The beads were then loaded on a column, thoroughly washed to elute free dye, and the labelled membrane protein was eluted as described above. Labelling efficiency and purity was verified by SDS-PAGE gel electrophoresis via Coomassie staining and in-gel fluorescence.

OmpF was purified according to a previously described method [41,181], except that OmpF was solubilized using 3% β -OG detergent. OmpF was labelled after incorporation into block copolymer membranes with subsequent dialysis against pure buffer. OmpF was labelled with Atto-488-maleimide (ATTO-TEC, Siegen, Germany) via maleimide crosslinking to cysteines. The dye (0.1 mg/mL in DMSO) was added to the polymersome-OmpF solution at a ~1:5 molar ratio of OmpF:Atto488. The labelling reaction was stirred for 3 hours at 4 °C. Unreacted free dye was removed by dialysis using dialysis buttons at 4 °C in dark for 48 hours.

OmpF was labelled when inserted into the polymersomes, because the lack of His-tag makes it impossible to remove unreacted free-dye. Within membrane protein stock solutions, the free-dye is partially dissolved within the detergent micelles. Since detergent micelles have similar sizes (molecular weight and hydrodynamic diameter) as the membrane protein-detergent complex, size-exclusion chromatography (SEC) was not an option for separation of free dye and labelled-membrane protein.

Vesicle preparation

Liposomes and proteoliposomes were prepared by standard preparation techniques using dialysis method [168,180]. Briefly, 3.5 mg of L- α -phosphatidylcholine (PC) (Egg, Chicken, from Avanti Polar Lipids, dissolved in chloroform) were dried inside of a glass vial using a gentle nitrogen stream vial to form a smooth lipid film. The lipid film was further dried at high vacuum for 1 h. The lipid film was rehydrated in Hepes buffer including 1% beta-OG (5 mM Hepes, pH 7.4, 5 mM NaCl) at a final lipid concentration of 5 mg/mL. Membrane proteins were added to yield the desired lipid-to-protein-ratio (LPR) of 50 (w/w). The mixture was stirred for 1 h and then transferred to dialysis buttons (350 μ L volume, Hampton Research, Aliso Viejo, CA, USA) using dialysis membranes with a molecular cut-off of 12 kDa (Spectra/Por; Spectrum Labs, Rancho Dominguez, CA, USA) and dialyzed for at least 48 hours at 4 °C exchanging the buffer 4 times (2 x 500 mL, 1 mM Hepes, pH 7.4, 1 mM NaCl). The lipid-MP vesicles were then extruded through 200 nm pore-size polycarbonate membranes (Nuclepore; Whatman,

Maidstone, UK) using an Avanti mini-extruder (Avanti Polar Lipids, Alabama, USA). Standard lipid vesicles were rehydrated with a Hepes buffer (1 mM Hepes, pH 7.4, 1 mM NaCl) without detergent overnight at RT and immediately extruded.

Polymersomes with inserted membrane proteins were prepared from PMOXA_x-*b*-PDMS_y-*b*-PMOXA_x triblock copolymers (A₆B₃₄A₆, A₇B₄₉A₇, A₁₂B₆₃A₁₂) at room temperature according to a previously described method with slight modifications [8,168]. Briefly, a smooth polymer film was formed on the inside of a glass flask by slowly evaporating the solvent (10 mg/mL polymer in ethanol) using a rotary vacuum evaporator and further drying for 1 h at high vacuum. The film was rehydrated with a Hepes buffer containing 1% beta-OG (2 mM Hepes, pH 7.4, 5 mM NaCl) to yield a final polymer concentration of ~5 mg/mL. Membrane proteins were added at the desired polymer-to-protein ratio (PoPR) of around 50 (w/w). The suspension was rehydrated at RT by slow rotation in a rotary vacuum evaporator without applying vacuum for 4 hours. A stir bar was added to the flask and the mixture was stirred overnight and finally transferred to dialysis buttons (350 µL volume, molecular cut-off of 12 kDa). The samples were dialyzed at 4 °C for at least 48 hours with exchanging the buffer 4 times with slightly reduced salt concentrations (4 x 500 mL, 1 mM Hepes, pH 7.4, 2 mM NaCl). The polymersome suspension was extruded, first through 400 nm, then 11 times through 200 nm pore-size polycarbonate membranes.

Electroformation

Giant unilamellar vesicles (GUVs) were prepared according to the standard electroformation method [149], using a Nanion Vesicle Prep Pro setup (Nanion Technologies, Munich, Germany). In short, 50 µl of 4 mg/ml (w/v) polymer solution in ethanol was spread on an ITO-coated glass slide and the solvent was evaporated in a vacuum chamber for at least one hour. For FCS studies, the polymer solution was mixed at 0.005 - 0.02% (w/w) of SRB-labelled polymer in order to yield the best signal-to-noise ratio [169]. A chamber was formed by using an O-ring, filled with 100 mM sucrose solution and closed with a second glass plate with the ITO-coated side facing down. The chamber was exposed to a 2.5 V AC current at a frequency of 3.0 Hz for three hours at RT. The GUV-solution was then transferred to an Eppendorf tube and stored at 4 °C before use for FCS experiments. Usually, GUV samples stored in the fridge were stable for several months without any effect on the FCS measurements.

Electron microscopy imaging: cryo-TEM

Polymer suspensions in buffer (20 mM Hepes, pH 7.4, 50 mM NaCl) at high concentrations (5 mg/ml) were deposited on glow-discharged holey carbon grids (Quantifoil, Germany) and blotted before quick-freezing in liquid ethane using a Vitrobot plunge-freezing device (FEI company, USA). The grids were stored in liquid nitrogen before transferring them into a cryo-holder (Gatan, USA). Imaging was performed on a Philips CM200 FEG TEM at 200 kV accelerating voltage in low-dose mode with a defocus value of about $-4\ \mu\text{m}$, and a defocus of $-2\ \mu\text{m}$ for membrane thickness measurements. Membrane thicknesses were calculated as mean values $\pm SD$ from at least 100 different places on membranes of each polymer type [182]. In addition, images were corrected for the contrast transfer function (CTF) and no significant difference of the membrane thickness before and after CFT correction was observed. Furthermore, membranes of liposomes were used as control with known membrane thickness.

Confocal laser scanning microscopy (CLSM)

LSM and FCS measurements were performed on a confocal laser scanning microscope (Zeiss LSM 510-META/Confocor2, Carl Zeiss, Jena, Germany). For Atto-488 and OG488 dyes, an Argon-2 laser with $\lambda = 488\ \text{nm}$ (15 mW output), for sulforhodamine B (SRB) dyes, a He-Ne laser ($\lambda = 543\ \text{nm}$), and for Bodipy 630/650 dyes, a He-Ne laser with $\lambda = 633\ \text{nm}$ (15 mW output) were used. The laser output intensity was adjusted for each sample depending on the dye concentration by changing the transmission in order to keep the laser intensity at a minimum. For 488 nm laser, a main dichromatic beam splitter (HFT 488/543/633), a secondary dichroic beam splitter (NFT 545) and a low pass filter (LP 505) were used. For 543 nm laser, a dichroic beam splitter (DBS HFT 543), a secondary dichroic beam splitter (NFT 545) and a band pass BP 560 - 615 nm filter were used. For 633 nm laser, a main dichromatic beam splitter (HFT 488/543/633), a secondary dichroic beam splitter (NFT 545) and a low pass filter (LP 650) were used. The light was focused on the sample using a C-Apochromat 40x water immersion objective (NA=1.2).

Calibration of LSM-FCS offset

The z-scan FCS method involves a switching between the LSM- and FCS-modes. In addition, the measuring spot for FCS has to be set manually by choosing the spot from the LSM images. As a consequence, the offset between LSM images and the measuring focus

in the FCS mode has to be determined. This was assessed by a standard protocol described by the microscope manufacturer. Briefly, a dried film of the fluorescent dye sulforhodamine B was prepared on standard microscopy coverslips. First, a LSM picture was taken. Secondly, on this LSM picture spots were selected and each point was bleached with a high intensity laser pulse for 10s at maximum transmission. Thirdly, a next LSM picture was recorded and the offset was measured and changed in the software settings. This procedure was repeated until the bleached spots in the LSM image exactly overlap with the marked positions in the FCS mode (Figure 6.1).

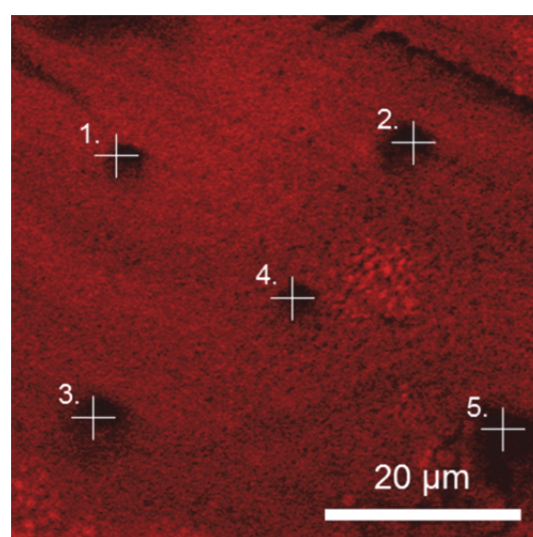


Figure 6.1. Determination of the LSM-FCS offset. For exact positioning of the laser focus on GUV membranes, the offset between LSM images and the real measuring spot in the FCS mode has to be determined and specified in the software settings. After the calibration, the best position was exactly in the middle of the LSM image.

Fluorescence correlation spectroscopy (FCS) and z-scan FCS

FCS experiments were performed according to the protocol described previously [95]. The laser beam and the fluorescent signal were guided through appropriate beam splitters, band pass filters and pinhole diameters. The pinhole was calibrated before each experiment using a buffered solution (20 mM Hepes, 50 mM NaCl) containing the dye at a concentration of ~ 10 nM (pinhole diameter = 70 μm for $\lambda = 488$ nm (OG488 / Atto488), pinhole diameter = 78 μm for $\lambda = 543$ nm (SRB), pinhole diameter = 90 μm for $\lambda = 633$ nm (Bodipy 630/650)). For z-scan FCS experiments on GUVs, the laser power was kept at a minimum in order to reduce photobleaching (488 nm: $\sim 1\%$ transmission at 15 mW output intensity; 543 nm: 10% transmission at 1 mW; 633 nm: 0.5% transmission at 15

mW). The pinhole was also calibrated at the same laser intensity/transmission that was used for z-scan FCS on the membranes.

For z-scan FCS, SRB-labelled GUVs have to be immobilized on the glass surface of the microscopy chamber (Nunc™ Lab-Tek™ Chamber Slide System, Thermo Fisher Scientific). The glass surface was O₂-plasma cleaned in order to render it hydrophilic. Then, a microscopy chamber was filled with 300 μL of buffer (20 mM Hepes, 50 mM NaCl, pH 7.4) and around 20 – 75 μL of the GUV solution (depending on the amount of GUVs) was added. In this way, the sucrose-filled GUVs sink to the bottom and adhere tightly at the glass surface. The surface was first scanned by LSM to find suitable GUVs to perform z-scan FCS measurements. The area of one single GUV is zoomed exactly in the middle of the LSM image and the focus is then changed to the top of the GUV membrane. There, a series of LSM images is taken (z-scan) in steps of 100 nm (for 488 and 543 nm lasers) or 300 nm (for 633 nm laser). After switching to the FCS mode, the height (z-position) with maximum count rate is first determined by doing a single FCS measurement on the membrane by moving up and down with the focus. The position is noted and from there, a series of FCS measurements are recorded by starting the measurement from around $\Delta z = -1.0 \mu\text{m}$ to $+1.0 \mu\text{m}$ in steps of 200 nm (for 488 and 543 nm lasers) or 300 nm (for 633 nm laser). The data can already be verified during the measurement by checking the Δz -dependency on the count rate, diffusion time and number of particles, *i.e.* maximum count rate at $\Delta z = 0$, minimum diffusion time and number of particles N at $\Delta z = 0$. For each sample, the diffusion time was determined for at least 5 different GUVs from two independently, freshly prepared GUV samples. The mean value of all diffusion coefficients and number of particles for each sample was calculated and error bars represent the corresponding standard deviation. All measurements were performed at $20.0 \pm 0.5 \text{ }^\circ\text{C}$.

Autocorrelation curves were fitted with FFS Data Processor 2.3 (SSTC, Minsk, Belarus) by either using the single-component (equation 2.10) or the two-component (equation 2.11) anomalous 2-D diffusion fitting model. Diffusion coefficients (D), number of particles (N) and beam waist (ω_0) obtained from z-scan FCS recordings are presented as mean values of at least six independent measurements, *i.e.* six different GUVs, whereas each single GUV could be measured up to 3 times. The triplet time (τ_{trip}) was always fixed at 3.0 μs.

The fitting procedure of z-scan FCS data sets using the two-component 2-D diffusion model involves some issues to be considered. As the number of particles N is given as the total number of fluorescent particles observed in the observation area of the laser beam, the number of particles of the two components have to be calculated separately using the fraction f obtained from equation 2.11. The diffusion times of both components (τ_{D_1} and τ_{D_2}) and the total number of particles N are increasing with increasing beam waist (according to equation 2.12). The fraction f remains constant as the concentration of both components stays the same. According to these considerations, both components were fitted according to the z-scan model. The fraction of the fast diffusing component (free dye) was around 10 – 20 % for all sample preparations. Therefore, the parabolic z-dependency data sets were obtained in all cases for both components and both components could be fitted to equations 2.12 and 2.13.

The FCS diffusion law (equation 2.14), derived from z-scan FCS, provides additional information about structurally related diffusion properties [100,140,183]. The diffusion times were plotted against $\frac{N}{N_0}$, and is fitted to a linear equation to yield t_0 (y-intercept) and the slope. The effective diffusion coefficient D_{eff} can then be calculated by using the beam waist ω_0 (equation 2.14). The linear regression was obtained by fitting the data with weighted y-errors as stated in reference [183] using OriginPro 9 (OriginLab Corp., Northampton, MA, USA).

Bibliography

7 References

- [1] F. Iteț, I.A. Dinu, P. Tanner, O. Fischer, C.G. Palivan, Nanoreactors for Biomedical Applications, in: V. Torchilin (Ed.), *Handbook of Nanobiomedical Research*, WORLD SCIENTIFIC, 2014, pp. 457–508.
- [2] S.M. Borisov, O.S. Wolfbeis, Optical biosensors, *Chemical reviews*, 108 (2008) 423–461.
- [3] P. Tanner, P. Baumann, R. Enea, O. Onaca, C. Palivan, W. Meier, Polymeric vesicles: from drug carriers to nanoreactors and artificial organelles, *Accounts of Chemical Research*, 44 (2011) 1039–1049.
- [4] D.E. Discher, F. Ahmed, POLYMERSOMES, *Annual Review of Biomedical Engineering*, 8 (2006) 323–341.
- [5] B.M. Discher, Polymersomes: Tough Vesicles Made from Diblock Copolymers, *Science*, 284 (1999) 1143–1146.
- [6] K. Kita-Tokarczyk, J. Grumelard, T. Haefele, W. Meier, Block copolymer vesicles—using concepts from polymer chemistry to mimic biomembranes, *Polymer*, 46 (2005) 3540–3563.
- [7] C.G. Palivan, X. Zhang, W. Meier, Protein-polymer supramolecular assemblies: a key combination for multifunctionality, *Chimia*, 67 (2013) 791–795.
- [8] M. Kumar, M. Grzelakowski, J. Zilles, M. Clark, W. Meier, Highly permeable polymeric membranes based on the incorporation of the functional water channel protein Aquaporin Z, *Proc. Natl. Acad. Sci. U.S.A.*, 104 (2007) 20719–20724.
- [9] Y.-x. Shen, P.O. Saboe, I.T. Sines, M. Erbakan, M. Kumar, Biomimetic membranes: A review, *Journal of Membrane Science*, 454 (2014) 359–381.
- [10] W. Stillwell, *An introduction to biological membranes: From bilayers to rafts*, Elsevier/Academic Press, Amsterdam, Boston, 2013.

- [11] P.C. Painter, M.M. Coleman, Fundamentals of polymer science: An introductory text, 2nd ed., Technomic Pub. Co., Lancaster, Pa., 1997.
- [12] A.N. Singh, S. Singh, N. Suthar, V.K. Dubey, Glutaraldehyde-activated chitosan matrix for immobilization of a novel cysteine protease, procerain B, *Journal of agricultural and food chemistry*, 59 (2011) 6256–6262.
- [13] C.G. Palivan, O. Fischer-Onaca, M. Delcea, F. Itel, W. Meier, Protein-polymer nanoreactors for medical applications, *Chemical Society Reviews*, 41 (2012) 2800–2823.
- [14] M. Karlsson, M. Davidson, R. Karlsson, A. Karlsson, J. Bergenholtz, Z. Konkoli, A. Jesorka, T. Lobovkina, J. Hurtig, M. Voinova, O. Orwar, Biomimetic nanoscale reactors and networks, *Annual review of physical chemistry*, 55 (2004) 613–649.
- [15] D.M. Vriezema, M. Comellas Aragonès, Elemans, Johannes A A W, Cornelissen, Jeroen J L M, A.E. Rowan, Nolte, Roeland J M, Self-assembled nanoreactors, *Chemical reviews*, 105 (2005) 1445–1489.
- [16] A. Graff, M. Winterhalter, W. Meier, Nanoreactors from Polymer-Stabilized Liposomes, *Langmuir*, 17 (2001) 919–923.
- [17] A.A. Spector, M.A. Yorek, Membrane lipid composition and cellular function, *Journal of Lipid Research*, 26 (1985) 1015–1035.
- [18] S.J. Singer, G.L. Nicolson, The Fluid Mosaic Model of the Structure of Cell Membranes, *Science*, 175 (1972) 720–731.
- [19] W.M. Becker, L.J. Kleinsmith, J. Hardin, J. Raasch, The world of the cell, Benjamin Cummings San Francisco, 2003.
- [20] M. Luckey, Membrane structural biology: With biochemical and biophysical foundations, 2nd ed., Cambridge University Press, Cambridge, 2014.
- [21] P. Mueller, D.O. Rudin, H. Ti Tien, W.C. Wescott, Reconstitution of Cell Membrane Structure in vitro and its Transformation into an Excitable System, *Nature*, 194 (1962) 979–980.
- [22] G. Vereb, J. Szöllosi, J. Matkó, P. Nagy, T. Farkas, L. Vigh, L. Mátyus, T.A. Waldmann, S. Damjanovich, Dynamic, yet structured: The cell membrane three decades after the Singer-Nicolson model, *Proc. Natl. Acad. Sci. U.S.A.*, 100 (2003) 8053–8058.

- [23] J.C. Lee, H. Bermudez, B.M. Discher, M.A. Sheehan, Y.Y. Won, F.S. Bates, D.E. Discher, Preparation, stability, and in vitro performance of vesicles made with diblock copolymers, *Biotechnology and Bioengineering*, 73 (2001) 135–145.
- [24] P. Broz, H. Kroto, P. O'Brien, Polymer-based nanostructures: Medical applications.
- [25] G.C. Hansson, K. Simons, G. van Meer, Two strains of the Madin-Darby canine kidney (MDCK) cell line have distinct glycosphingolipid compositions, *The EMBO Journal*, 5 (1986) 483–489.
- [26] L.L. Hsiao, R.J. Howard, M. Aikawa, T.F. Taraschi, Modification of host cell membrane lipid composition by the intra-erythrocytic human malaria parasite *Plasmodium falciparum*, *Biochemical Journal*, 274 (1991) 121–132.
- [27] R. Koynova, M. Caffrey, Phases and phase transitions of the phosphatidylcholines, *Biochimica et Biophysica Acta (BBA) - Reviews on Biomembranes*, 1376 (1998) 91–145.
- [28] R.F. de Almeida, A. Fedorov, M. Prieto, Sphingomyelin/Phosphatidylcholine/Cholesterol Phase Diagram: Boundaries and Composition of Lipid Rafts, *Biophysical Journal*, 85 (2003) 2406–2416.
- [29] A. Taubert, A. Napoli, W. Meier, Self-assembly of reactive amphiphilic block copolymers as mimetics for biological membranes, *Current Opinion in Chemical Biology*, 8 (2004) 598–603.
- [30] A. Mecke, C. Dittrich, W. Meier, Biomimetic membranes designed from amphiphilic block copolymers, *Soft Matter*, 2 (2006) 751.
- [31] X. Zhang, P. Tanner, A. Graff, C.G. Palivan, W. Meier, Mimicking the cell membrane with block copolymer membranes, *Journal of Polymer Science Part A: Polymer Chemistry*, 50 (2012) 2293–2318.
- [32] K. Knop, R. Hoogenboom, D. Fischer, U.S. Schubert, Poly(ethylene glycol) in drug delivery: pros and cons as well as potential alternatives, *Angewandte Chemie (Int. ed.)*, 49 (2010) 6288–6308.
- [33] M. Kumar, M. Payne, S. Poust, J. Zilles, Polymer-Based Biomimetic Membranes for Desalination, in: C. Hélix-Nielsen (Ed.), *Biomimetic Membranes for Sensor and Separation Applications*, Springer Netherlands, 2012, pp. 43–62.
- [34] I. Yilgor, E. Yilgor, Thermal stabilities of end groups in hydroxyalkyl terminated polydimethylsiloxane oligomers, *Polymer Bulletin*, 40 (1998) 525–532.

- [35] M. Kumar, Habel, Joachim E O, Y.-x. Shen, W.P. Meier, T. Walz, High-density reconstitution of functional water channels into vesicular and planar block copolymer membranes, *Journal of the American Chemical Society*, 134 (2012) 18631–18637.
- [36] N. Muhammad, T. Dworeck, M. Fioroni, U. Schwaneberg, Engineering of the E. coli outer membrane protein FhuA to overcome the hydrophobic mismatch in thick polymeric membranes, *Journal of Nanobiotechnology*, 9 (2011) 8.
- [37] J.L. Kowal, J.K. Kowal, D. Wu, H. Stahlberg, C.G. Palivan, W.P. Meier, Functional surface engineering by nucleotide-modulated potassium channel insertion into polymer membranes attached to solid supports, *Biomaterials*, 35 (2014) 7286–7294.
- [38] X. Zhang, W. Fu, C.G. Palivan, W. Meier, Natural channel protein inserts and functions in a completely artificial, solid-supported bilayer membrane, *Scientific reports*, 3 (2013) 2196.
- [39] C. Nardin, S. Thoeni, J. Widmer, M. Winterhalter, W. Meier, Nanoreactors based on (polymerized) ABA-triblock copolymer vesicles, *Chemical Communications* (2000) 1433–1434.
- [40] A. Ranquin, W. Versées, W. Meier, J. Steyaert, P. van Gelder, Therapeutic nanoreactors: combining chemistry and biology in a novel triblock copolymer drug delivery system, *Nano letters*, 5 (2005) 2220–2224.
- [41] M. Grzelakowski, O. Onaca, P. Rigler, M. Kumar, W. Meier, Immobilized protein-polymer nanoreactors, *Small*, 5 (2009) 2545–2548.
- [42] D. Dobrunz, A.C. Toma, P. Tanner, T. Pfohl, C.G. Palivan, Polymer nanoreactors with dual functionality: simultaneous detoxification of peroxynitrite and oxygen transport, *Langmuir*, 28 (2012) 15889–15899.
- [43] K. Langowska, C.G. Palivan, W. Meier, Polymer nanoreactors shown to produce and release antibiotics locally, *Chemical Communications*, 49 (2013) 128–130.
- [44] K. Langowska, J. Kowal, C.G. Palivan, W. Meier, A general strategy for creating self-defending surfaces for controlled drug production for long periods of time, *Journal of Materials Chemistry B*, 2 (2014) 4684.
- [45] S. Ihle, O. Onaca, P. Rigler, B. Hauer, F. Rodríguez-Roperro, M. Fioroni, U. Schwaneberg, Nanocompartments with a pH release system based on an engineered OmpF channel protein, *Soft Matter*, 7 (2011) 532–539.

- [46] A. Graff, M. Sauer, P. van Gelder, W. Meier, Virus-assisted loading of polymer nanocontainer, *Proc. Natl. Acad. Sci. U.S.A.*, 99 (2002) 5064–5068.
- [47] H. Wang, T.-S. Chung, Y.W. Tong, K. Jeyaseelan, A. Armugam, Z. Chen, M. Hong, W. Meier, Highly permeable and selective pore-spanning biomimetic membrane embedded with aquaporin Z, *Small*, 8 (2012) 1185–90, 1125.
- [48] M. Grzelakowski, M.F. Cherenet, Y.-x. Shen, M. Kumar, A framework for accurate evaluation of the promise of aquaporin based biomimetic membranes, *Journal of Membrane Science*, 479 (2015) 223–231.
- [49] N. Uehlein, B. Otto, A. Eilingsfeld, F. Itel, W. Meier, R. Kaldenhoff, Gas-tight triblock-copolymer membranes are converted to CO₂ permeable by insertion of plant aquaporins, *Scientific reports*, 2 (2012) 538.
- [50] A. Graff, C. Fraysse-Ailhas, C.G. Palivan, M. Grzelakowski, T. Friedrich, C. Vebert, G. Gescheidt, W. Meier, Amphiphilic Copolymer Membranes Promote NADH:Ubiquinone Oxidoreductase Activity: Towards an Electron-Transfer Nanodevice, *Macromolecular Chemistry and Physics*, 211 (2010) 229–238.
- [51] D. Ho, B. Chu, H. Lee, C.D. Montemagno, Protein-driven energy transduction across polymeric biomembranes, *Nanotechnology*, 15 (2004) 1084–1094.
- [52] M. Lomora, M. Garni, F. Itel, P. Tanner, M. Spulber, C.G. Palivan, Polymersomes with engineered ion selective permeability as stimuli-responsive nanocompartments with preserved architecture, *Biomaterials*, 53 (2015) 406–414.
- [53] O. Onaca, P. Sarkar, D. Roccatano, T. Friedrich, B. Hauer, M. Grzelakowski, A. Güven, M. Fioroni, U. Schwaneberg, Functionalized nanocompartments (synthosomes) with a reduction-triggered release system, *Angewandte Chemie (Int. ed.)*, 47 (2008) 7029–7031.
- [54] R. Stoenescu, A. Graff, W. Meier, Asymmetric ABC-triblock copolymer membranes induce a directed insertion of membrane proteins, *Macromolecular bioscience*, 4 (2004) 930–935.
- [55] H.-J. Choi, C.D. Montemagno, Artificial organelle: ATP synthesis from cellular mimetic polymersomes, *Nano letters*, 5 (2005) 2538–2542.
- [56] V. Pata, N. Dan, The Effect of Chain Length on Protein Solubilization in Polymer-Based Vesicles (Polymersomes), *Biophysical Journal*, 85 (2003) 2111–2118.
- [57] G. Srinivas, D.E. Discher, M.L. Klein, Key roles for chain flexibility in block copolymer membranes that contain pores or make tubes, *Nano letters*, 5 (2005) 2343–2349.

- [58] R.G. Jones (Ed.), *Silicon-containing polymers: The science and technology of their synthesis and applications*, Kluwer Academic Publishers, Dordrecht, Boston, London, op. 2000.
- [59] J.N. Israelachvili, *Soft and Biological Structures*, in: *Intermolecular and Surface Forces*, Elsevier, 2011, pp. 535–576.
- [60] H. Aranda-Espinoza, H. Bermudez, F.S. Bates, D.E. Discher, Electromechanical Limits of Polymersomes, *Physical Review Letters*, 87 (2001) 208301.
- [61] D.E. Discher, A. Eisenberg, Polymer vesicles, *Science*, 297 (2002) 967–973.
- [62] Le Meins, J. -F., O. Sandre, S. Lecommandoux, Recent trends in the tuning of polymersomes' membrane properties, *The European Physical Journal E*, 34 (2011) 1–17.
- [63] G. Battaglia, A.J. Ryan, Bilayers and Interdigitation in Block Copolymer Vesicles, *Journal of the American Chemical Society*, 127 (2005) 8757–8764.
- [64] W.P. Meier, W. Knoll, *Polymer membranes/biomembranes*, Springer Science & Business Media, 2009.
- [65] A. Napoli, N. Tirelli, E. Wehrli, J.A. Hubbell, Lyotropic Behavior in Water of Amphiphilic ABA Triblock Copolymers Based on Poly(propylene sulfide) and Poly(ethylene glycol), *Langmuir*, 18 (2002) 8324–8329.
- [66] C. LoPresti, H. Lomas, M. Massignani, T. Smart, G. Battaglia, Polymersomes: nature inspired nanometer sized compartments, *Journal of Materials Chemistry*, 19 (2009) 3576–3590.
- [67] K. Schillén, K. Bryskhe, Y.S. Mel'nikova, Vesicles Formed from a Poly(ethylene oxide)–Poly(propylene oxide)–Poly(ethylene oxide) Triblock Copolymer in Dilute Aqueous Solution, *Macromolecules*, 32 (1999) 6885–6888.
- [68] R. Stoenescu, W. Meier, Asymmetric Membranes from Amphiphilic ABC Triblock Copolymers, *Molecular Crystals and Liquid Crystals*, 417 (2004) 185–191.
- [69] H. Bermudez, A.K. Brannan, D.A. Hammer, F.S. Bates, D.E. Discher, Molecular Weight Dependence of Polymersome Membrane Structure, Elasticity, and Stability, *Macromolecules*, 35 (2002) 8203–8208.
- [70] B.A. Lewis, D.M. Engelman, Bacteriorhodopsin remains dispersed in fluid phospholipid bilayers over a wide range of bilayer thicknesses, *Journal of Molecular Biology*, 166 (1983) 203–210.

- [71] Q. Chen, H. Schönherr, G.J. Vancso, Mechanical properties of block copolymer vesicle membranes by atomic force microscopy, *Soft Matter*, 5 (2009) 4944.
- [72] G. Srinivas, D.E. Discher, M.L. Klein, Self-assembly and properties of diblock copolymers by coarse-grain molecular dynamics, *Nature Materials*, 3 (2004) 638–644.
- [73] S. Jain, F.S. Bates, Consequences of Nonergodicity in Aqueous Binary PEO–PB Micellar Dispersions, *Macromolecules*, 37 (2004) 1511–1523.
- [74] H. Bermúdez, D.A. Hammer, D.E. Discher, Effect of Bilayer Thickness on Membrane Bending Rigidity, *Langmuir*, 20 (2004) 540–543.
- [75] K. Jaskiewicz, A. Larsen, I. Lieberwirth, K. Koynov, W. Meier, G. Fytas, A. Kroeger, K. Landfester, Probing Bioinspired Transport of Nanoparticles into Polymersomes, *Angewandte Chemie (Int. ed.)*, 124 (2012) 4691–4695.
- [76] M. Przybylo, J. Sýkora, J. Humpolíčková, A. Benda, A. Zan, M. Hof, Lipid Diffusion in Giant Unilamellar Vesicles Is More than 2 Times Faster than in Supported Phospholipid Bilayers under Identical Conditions, *Langmuir*, 22 (2006) 9096–9099.
- [77] K. Weiß, A. Neef, Q. Van, S. Kramer, I. Gregor, J. Enderlein, Quantifying the Diffusion of Membrane Proteins and Peptides in Black Lipid Membranes with 2-Focus Fluorescence Correlation Spectroscopy, *Biophysical Journal*, 105 (2013) 455–462.
- [78] G. Orädd, P.W. Westerman, G. Lindblom, Lateral diffusion coefficients of separate lipid species in a ternary raft-forming bilayer: a Pfg-NMR multinuclear study, *Biophysical Journal*, 89 (2005) 315–320.
- [79] G. Lindblom, Lipid Lateral Diffusion, in: G. Roberts (Ed.), *Encyclopedia of Biophysics*, Springer Berlin Heidelberg, 2013, pp. 1264–1268.
- [80] J.C.-M. Lee, M. Santore, F.S. Bates, D.E. Discher, From Membranes to Melts, Rouse to Reptation: Diffusion in Polymersome versus Lipid Bilayers, *Macromolecules*, 35 (2002) 323–326.
- [81] D.E. Discher, V. Ortiz, G. Srinivas, M.L. Klein, Y. Kim, D. Christian, S. Cai, P. Photos, F. Ahmed, Emerging applications of polymersomes in delivery: From molecular dynamics to shrinkage of tumors, *Polymers in Biomedical Applications*, 32 (2007) 838–857.

- [82] J. Liao, C. Wang, Y. Wang, F. Luo, Z. Qian, Recent Advances in Formation, Properties, and Applications of Polymersomes, *Current Pharmaceutical Design*, 18 (2012) 3432–3441.
- [83] A. Najer, D. Wu, D. Vasquez, C.G. Palivan, W. Meier, Polymer nanocompartments in broad-spectrum medical applications, *Nanomedicine*, 8 (2013) 425–447.
- [84] S. Rangelov, A. Pispas, Polymer and Polymer-Hybrid Nanoparticles: From Synthesis to Biomedical Applications, CRC Press, 2013.
- [85] G. Gunkel-Grabole, S. Sigg, M. Lomora, S. Lörcher, C.G. Palivan, W.P. Meier, Polymeric 3D nano-architectures for transport and delivery of therapeutically relevant biomacromolecules, *Biomaterials Science*, 3 (2015) 25–40.
- [86] P. Tanner, O. Onaca, V. Balasubramanian, W. Meier, C.G. Palivan, Enzymatic cascade reactions inside polymeric nanocontainers: a means to combat oxidative stress, *Chemistry - A European Journal*, 17 (2011) 4552–4560.
- [87] P. Tanner, V. Balasubramanian, C.G. Palivan, Aiding nature's organelles: artificial peroxisomes play their role, *Nano letters*, 13 (2013) 2875–2883.
- [88] B.A. Wallace, Gramicidin channels and pores, *Annual review of biophysics and biophysical chemistry*, 19 (1990) 127–157.
- [89] M. Lomora, Fabian Itel, I.A. Dinu, C. Palivan, Selective ion-permeable membranes by insertion of biopores into polymersomes, *Physical Chemistry Chemical Physics* (2015).
- [90] K. Renggli, P. Baumann, K. Langowska, O. Onaca, N. Bruns, W. Meier, Selective and responsive nanoreactors, *Advanced Functional Materials*, 21 (2011) 1241–1259.
- [91] M. Marguet, C. Bonduelle, S. Lecommandoux, Multicompartmentalized polymeric systems: towards biomimetic cellular structure and function, *Chemical Society Reviews*, 42 (2013) 512–529.
- [92] S.W. Cowan, R.M. Garavito, J.N. Jansonius, J.A. Jenkins, R. Karlsson, N. König, E.F. Pai, R.A. Paupit, P.J. Rizkallah, J.P. Rosenbusch, The structure of OmpF porin in a tetragonal crystal form, *Structure*, 3 (1995) 1041–1050.
- [93] P. Mörters, Y. Peres, O. Schramm, W. Werner, Brownian motion, Cambridge University Press, Cambridge, UK, New York, ©2010.
- [94] A. Einstein, R. Fürth, Investigations on the theory of Brownian movement, Dover Publications, New York, N.Y., 1956.

- [95] F. Itel, M. Chami, A. Najer, S. Lörcher, D. Wu, I.A. Dinu, W. Meier, Molecular Organization and Dynamics in Polymersome Membranes: A Lateral Diffusion Study, *Macromolecules*, 47 (2014) 7588–7596.
- [96] H.-J. Galla, W. Hartmann, U. Theilen, E. Sackmann, On two-dimensional passive random walk in lipid bilayers and fluid pathways in biomembranes, *The Journal of membrane biology*, 48 (1979) 215–236.
- [97] P.F.F. Almeida, W.L.C. Vaz, T.E. Thompson, Lateral diffusion in the liquid phases of dimyristoylphosphatidylcholine/cholesterol lipid bilayers: a free volume analysis, *Biochemistry*, 31 (1992) 6739–6747.
- [98] W.L. Vaz, F. Goodsaid-Zalduondo, K. Jacobson, Lateral diffusion of lipids and proteins in bilayer membranes, *FEBS Letters*, 174 (1984) 199–207.
- [99] P.F.F. Almeida, W.L.C. Vaz, Lateral diffusion in membranes, 1995.
- [100] L. Wawrezinieck, H. Rigneault, D. Marguet, P.-F. Lenne, Fluorescence Correlation Spectroscopy Diffusion Laws to Probe the Submicron Cell Membrane Organization, *Biophysical Journal*, 89 (2005) 4029–4042.
- [101] G.J. Schütz, H. Schindler, T. Schmidt, Single-molecule microscopy on model membranes reveals anomalous diffusion, *Biophysical Journal*, 73 (1997) 1073–1080.
- [102] T.V. Ratto, M.L. Longo, Anomalous Subdiffusion in Heterogeneous Lipid Bilayers, *Langmuir*, 19 (2003) 1788–1793.
- [103] M.J. Saxton, Lateral diffusion in an archipelago. Distance dependence of the diffusion coefficient, *Biophysical Journal*, 56 (1989) 615–622.
- [104] M.J. Saxton, A biological interpretation of transient anomalous subdiffusion. I. Qualitative model, *Biophysical Journal*, 92 (2007) 1178–1191.
- [105] M. Štefl, R. Macháň, M. Hof, Z-Scan Fluorescence Correlation Spectroscopy: A Powerful Tool for Determination of Lateral Diffusion in Biological Systems, in: C.D. Geddes (Ed.), *Reviews in Fluorescence 2009*, Springer New York, New York, NY, 2011, pp. 321–344.
- [106] P.G. Saffman, M. Delbrück, Brownian motion in biological membranes, *Proc. Natl. Acad. Sci. U.S.A.*, 72 (1975) 3111–3113.
- [107] P.G. Saffman, Brownian motion in thin sheets of viscous fluid, *Journal of Fluid Mechanics*, 73 (1976) 593.
- [108] Y. Chen, B.C. Lagerholm, B. Yang, K. Jacobson, Methods to measure the lateral diffusion of membrane lipids and proteins, *Methods*, 39 (2006) 147–153.

- [109] H. Qian, M.P. Sheetz, E.L. Elson, Single particle tracking. Analysis of diffusion and flow in two-dimensional systems, *Biophysical Journal*, 60 (1991) 910.
- [110] M.J. Saxton, K. Jacobson, Single-particle tracking: applications to membrane dynamics, *Annual review of biophysics and biomolecular structure*, 26 (1997) 373–399.
- [111] A. Kusumi, C. Nakada, K. Ritchie, K. Murase, K. Suzuki, H. Murakoshi, R.S. Kasai, J. Kondo, T. Fujiwara, Paradigm shift of the plasma membrane concept from the two-dimensional continuum fluid to the partitioned fluid: high-speed single-molecule tracking of membrane molecules, *Annual review of biophysics and biomolecular structure*, 34 (2005) 351–378.
- [112] D. Axelrod, D.E. Koppel, J. Schlessinger, E. Elson, W.W. Webb, Mobility measurement by analysis of fluorescence photobleaching recovery kinetics, *Biophysical Journal*, 16 (1976) 1055.
- [113] R. Rigler, Fluorescence correlations, single molecule detection and large number screening Applications in biotechnology, *Journal of Biotechnology*, 41 (1995) 177–186.
- [114] A.-L. Kuo, C.G. Wade, Lipid lateral diffusion by pulsed nuclear magnetic resonance, *Biochemistry*, 18 (1979) 2300–2308.
- [115] G. Lindblom, G. Orädd, Lipid lateral diffusion and membrane heterogeneity, *Biochimica et Biophysica Acta (BBA) - Biomembranes*, 1788 (2009) 234–244.
- [116] P. Devaux, H. McConnell, Lateral diffusion in spin-labeled phosphatidylcholine multilayers, *Journal of the American Chemical Society*, 94 (1972) 4475–4481.
- [117] Y.K. Shin, U. Ewert, D.E. Budil, J.H. Freed, Microscopic versus macroscopic diffusion in model membranes by electron spin resonance spectral-spatial imaging, *Biophysical Journal*, 59 (1991) 950.
- [118] D. Magde, E. Elson, W. Webb, Thermodynamic Fluctuations in a Reacting System—Measurement by Fluorescence Correlation Spectroscopy, *Physical Review Letters*, 29 (1972) 705–708.
- [119] D. Magde, E.L. Elson, W.W. Webb, Fluorescence correlation spectroscopy. II. An experimental realization, *Biopolymers*, 13 (1974) 29–61.
- [120] E.L. Elson, D. Magde, Fluorescence correlation spectroscopy. I. Conceptual basis and theory, *Biopolymers*, 13 (1974) 1–27.
- [121] K. Bacia, P. Schwille, A dynamic view of cellular processes by in vivo fluorescence auto- and cross-correlation spectroscopy, *Methods*, 29 (2003) 74–85.

- [122] E. Haustein, P. Schwille, Fluorescence Correlation Spectroscopy, in: R. Borsali, R. Pecora (Eds.), *Soft Matter Characterization*, Springer Netherlands, 2008, pp. 637-675.
- [123] E. Hermann, J. Ries, A. García-Sáez, Scanning Fluorescence Correlation Spectroscopy on Biomembranes, in: D.M. Owen (Ed.), *Methods in Membrane Lipids*, Springer New York, 2015, pp. 181-197.
- [124] J. Enderlein, I. Gregor, D. Patra, T. Dertinger, U.B. Kaupp, Performance of Fluorescence Correlation Spectroscopy for Measuring Diffusion and Concentration, *ChemPhysChem*, 6 (2005) 2324–2336.
- [125] J. Ries, P. Schwille, Fluorescence correlation spectroscopy, *Bioessays*, 34 (2012) 361–368.
- [126] R. Rigler, Ü. Mets, J. Widengren, P. Kask, Fluorescence correlation spectroscopy with high count rate and low background: analysis of translational diffusion, *European Biophysics Journal*, 22 (1993) 169–175.
- [127] J. Ries, P. Schwille, New concepts for fluorescence correlation spectroscopy on membranes, *Physical Chemistry Chemical Physics*, 10 (2008) 3487.
- [128] J. Enderlein, I. Gregor, D. Patra, J. Fitter, Statistical Analysis of Diffusion Coefficient Determination by Fluorescence Correlation Spectroscopy, *Journal of Fluorescence*, 15 (2005) 415–422.
- [129] N.O. Petersen, Scanning fluorescence correlation spectroscopy. I. Theory and simulation of aggregation measurements, *Biophysical Journal*, 49 (1986) 809.
- [130] T. Dertinger, von der Hocht, Iris, A. Benda, M. Hof, J. Enderlein, Surface sticking and lateral diffusion of lipids in supported bilayers, *Langmuir*, 22 (2006) 9339–9344.
- [131] N.L. Thompson, B.L. Steele, Total internal reflection with fluorescence correlation spectroscopy, *Nature protocols*, 2 (2007) 878–890.
- [132] A. Benda, M. Beneš, V. Mareček, A. Lhotský, W.T. Hermens, M. Hof, How To Determine Diffusion Coefficients in Planar Phospholipid Systems by Confocal Fluorescence Correlation Spectroscopy, *Langmuir*, 19 (2003) 4120–4126.
- [133] H.-T. He, D. Marguet, Detecting Nanodomains in Living Cell Membrane by Fluorescence Correlation Spectroscopy, *Annual review of physical chemistry*, 62 (2011) 417–436.
- [134] A.G. Lee, How lipids affect the activities of integral membrane proteins, *Biochimica et Biophysica Acta (BBA) - Biomembranes*, 1666 (2004) 62–87.

- [135] D.M. Engelman, Membranes are more mosaic than fluid, *Nature*, 438 (2005) 578–580.
- [136] O.S. Andersen, R.E. Koeppe, Bilayer Thickness and Membrane Protein Function: An Energetic Perspective, *Annual review of biophysics and biomolecular structure*, 36 (2007) 107–130.
- [137] P. Dalhaimer, F.S. Bates, H. Aranda-Espinoza, D. Discher, Synthetic cell elements from block copolymers – hydrodynamic aspects, *Comptes Rendus Physique*, 4 (2003) 251–258.
- [138] F.S. Bates, G.H. Fredrickson, Block copolymer thermodynamics: theory and experiment, *Annual review of physical chemistry*, 41 (1990) 525–557.
- [139] D. Wu, M. Spulber, F. Itel, M. Chami, T. Pfohl, C.G. Palivan, W. Meier, Effect of Molecular Parameters on the Architecture and Membrane Properties of 3D Assemblies of Amphiphilic Copolymers, *Macromolecules*, 47 (2014) 5060–5069.
- [140] J. Humpolíčková, E. Gielen, A. Benda, V. Fagulova, J. Vercammen, M. vandeVen, M. Hof, M. Ameloot, Y. Engelborghs, Probing Diffusion Laws within Cellular Membranes by Z-Scan Fluorescence Correlation Spectroscopy, *Biophysical Journal*, 91 (2006) L23.
- [141] O. Terreau, C. Bartels, A. Eisenberg, Effect of Poly(acrylic acid) Block Length Distribution on Polystyrene-*b*-poly(acrylic acid) Block Copolymer Aggregates in Solution. 2. A Partial Phase Diagram, *Langmuir*, 20 (2004) 637–645.
- [142] N.A. Lynd, A.J. Meuler, M.A. Hillmyer, Polydispersity and block copolymer self-assembly, *Progress in Polymer Science*, 33 (2008) 875–893.
- [143] N.A. Lynd, M.A. Hillmyer, Effects of polydispersity on the order-disorder transition in block copolymer melts, *Macromolecules*, 40 (2007) 8050–8055.
- [144] N.A. Lynd, M.A. Hillmyer, Influence of Polydispersity on the Self-Assembly of Diblock Copolymers, *Macromolecules*, 38 (2005) 8803–8810.
- [145] S. Förster, M. Zisenis, E. Wenz, M. Antonietti, Micellization of strongly segregated block copolymers, *The Journal of Chemical Physics*, 104 (1996) 9956.
- [146] J.E. Mark, H.R. Allcock, R. West, *Inorganic polymers*, 2nd ed., Oxford University Press, New York, 2005.
- [147] S. Egli, M.G. Nussbaumer, V. Balasubramanian, M. Chami, N. Bruns, C. Palivan, W. Meier, Biocompatible Functionalization of Polymersome Surfaces: A New Approach to Surface Immobilization and Cell Targeting Using Polymersomes, *Journal of the American Chemical Society*, 133 (2011) 4476–4483.

- [148] S. Egli, B. Fischer, S. Hartmann, P. Hunziker, W. Meier, P. Rigler, Towards Targeted Drug Delivery by Covalent Ligand-Modified Polymeric Nanocontainers, *Macromolecular Symposia*, 296 (2010) 278–285.
- [149] M.I. Angelova, D.S. Dimitrov, Liposome electroformation, *Faraday Discussion Chemical Society*, 81 (1986) 303–311.
- [150] S. Milon, R. Hovius, H. Vogel, T. Wohland, Factors influencing fluorescence correlation spectroscopy measurements on membranes: simulations and experiments, *Chemical Physics*, 288 (2003) 171–186.
- [151] C. Culbertson, Diffusion coefficient measurements in microfluidic devices, *Talanta*, 56 (2002) 365–373.
- [152] F. Heinemann, P. Schwille, Preparation of Micrometer-Sized Free-Standing Membranes, *ChemPhysChem*, 12 (2011) 2568–2571.
- [153] S. Ladha, A.R. Mackie, L.J. Harvey, D.C. Clark, E.J. Lea, M. Brullemans, H. Duclouhier, Lateral diffusion in planar lipid bilayers: a fluorescence recovery after photobleaching investigation of its modulation by lipid composition, cholesterol, or alamethicin content and divalent cations, *Biophysical Journal*, 71 (1996) 1364–1373.
- [154] T. Haefele, K. Kita-Tokarczyk, W. Meier, Phase behavior of mixed Langmuir monolayers from amphiphilic block copolymers and an antimicrobial peptide, *Langmuir*, 22 (2006) 1164–1172.
- [155] Y.A. Domanov, S. Aimon, Toombes, G. E. S., M. Renner, F. Quemeneur, A. Triller, M.S. Turner, P. Bassereau, Mobility in geometrically confined membranes, *Proc. Natl. Acad. Sci. U.S.A.*, 108 (2011) 12605–12610.
- [156] L.D. Frye, M. Edidin, The rapid intermixing of cell surface antigens after formation of mouse-human heterokaryons, *Journal of cell science*, 7 (1970) 319–335.
- [157] M. Edidin, Lipids on the frontier: a century of cell-membrane bilayers, *Nature Reviews Molecular Cell Biology*, 4 (2003) 414–418.
- [158] S. Ramadurai, A. Holt, V. Krasnikov, van den Bogaart, Geert, J.A. Killian, B. Poolman, Lateral Diffusion of Membrane Proteins, *Journal of the American Chemical Society*, 131 (2009) 12650–12656.
- [159] Anderson, Richard G W, K. Jacobson, A role for lipid shells in targeting proteins to caveolae, rafts, and other lipid domains, *Science*, 296 (2002) 1821–1825.

- [160] G. Adam, M. Delbrück, Reduction of dimensionality in biological diffusion processes, *Structural chemistry and molecular biology*, 198 (1968).
- [161] D. Axelrod, M.D. Wang, Reduction-of-dimensionality kinetics at reaction-limited cell surface receptors, *Biophysical Journal*, 66 (1994) 588–600.
- [162] M. Nallani, S. Benito, O. Onaca, A. Graff, M. Lindemann, M. Winterhalter, W. Meier, U. Schwaneberg, A nanocompartment system (Synthosome) designed for biotechnological applications, *Journal of Biotechnology*, 123 (2006) 50–59.
- [163] M. Sauer, T. Haefele, A. Graff, C. Nardin, W. Meier, Ion-carrier controlled precipitation of calcium phosphate in giant ABA triblock copolymer vesicles, *Chemical Communications* (2001) 2452–2453.
- [164] A. González-Pérez, K.B. Stibius, T. Vissing, C.H. Nielsen, O.G. Mouritsen, Biomimetic Triblock Copolymer Membrane Arrays: A Stable Template for Functional Membrane Proteins, *Langmuir*, 25 (2009) 10447–10450.
- [165] J.M. Dörr, M.C. Koorengel, M. Schäfer, A.V. Prokofyev, S. Scheidelaar, van der Crujisen, Elwin A W, T.R. Dafforn, M. Baldus, J.A. Killian, Detergent-free isolation, characterization, and functional reconstitution of a tetrameric K⁺ channel: the power of native nanodiscs, *Proc. Natl. Acad. Sci. U.S.A.*, 111 (2014) 18607–18612.
- [166] M.J. Borgnia, D. Kozono, G. Calamita, P.C. Maloney, P. Agre, Functional reconstitution and characterization of AqpZ, the E. coli water channel protein, *Journal of Molecular Biology*, 291 (1999) 1169–1179.
- [167] A. Baslé, R. Qutub, M. Mehrazin, J. Wibbenmeyer, A.H. Delcour, Deletions of single extracellular loops affect pH sensitivity, but not voltage dependence, of the Escherichia coli porin OmpF, *Protein engineering, design & selection PEDS*, 17 (2004) 665–672.
- [168] M. Erbakan, Y.-x. Shen, M. Grzelakowski, P.J. Butler, M. Kumar, W.R. Curtis, Molecular cloning, overexpression and characterization of a novel water channel protein from Rhodobacter sphaeroides, *PloS one*, 9 (2014) e86830.
- [169] P. Kask, R. Günther, P. Axhausen, Statistical accuracy in fluorescence fluctuation experiments, *European Biophysics Journal*, 25 (1997) 163-169.
- [170] M.K. Doeven, J.H. Folgering, V. Krasnikov, E.R. Geertsma, van den Bogaart, Geert, B. Poolman, Distribution, Lateral Mobility and Function of Membrane Proteins Incorporated into Giant Unilamellar Vesicles, *Biophysical Journal*, 88 (2005) 1134–1142.

- [171] Y. Gambin, R. Lopez-Esparza, M. Reffay, E. Sieracki, N.S. Gov, M. Genest, R.S. Hodges, W. Urbach, Lateral mobility of proteins in liquid membranes revisited, *Proc. Natl. Acad. Sci. U.S.A.*, 103 (2006) 2098–2102.
- [172] A. Naji, A.J. Levine, P.A. Pincus, Corrections to the Saffman-Delbrück mobility for membrane bound proteins, *Biophysical Journal*, 93 (2007) L49-51.
- [173] E.P. Petrov, P. Schwille, Translational Diffusion in Lipid Membranes beyond the Saffman-Delbrück Approximation, *Biophysical Journal*, 94 (2008) L41.
- [174] G. Guigas, M. Weiss, Influence of hydrophobic mismatching on membrane protein diffusion, *Biophysical Journal*, 95 (2008) L25-7.
- [175] L.D. Hughes, R.J. Rawle, S.G. Boxer, Choose your label wisely: water-soluble fluorophores often interact with lipid bilayers, *PloS one*, 9 (2014) e87649.
- [176] L. Saiz, M.L. Klein, Structural properties of a highly polyunsaturated lipid bilayer from molecular dynamics simulations, *Biophysical Journal*, 81 (2001) 204–216.
- [177] J.-L. Rigaud, D. Lévy, Reconstitution of Membrane Proteins into Liposomes, in: *Liposomes, Part B*, Elsevier, 2003, pp. 65–86.
- [178] F. Heinemann, S.K. Vogel, P. Schwille, Lateral Membrane Diffusion Modulated by a Minimal Actin Cortex, *Biophysical Journal*, 104 (2013) 1465–1475.
- [179] D.M. Cortes, E. Perozo, Structural dynamics of the *Streptomyces lividans* K⁺ channel (SKC1): oligomeric stoichiometry and stability, *Biochemistry*, 36 (1997) 10343–10352.
- [180] F. Itel, S. Al-Samir, F. Öberg, M. Chami, M. Kumar, C.T. Supuran, Deen, Peter M T, W. Meier, K. Hedfalk, G. Gros, V. Endeward, CO₂ permeability of cell membranes is regulated by membrane cholesterol and protein gas channels, *FASEB journal*, 26 (2012) 5182–5191.
- [181] A. Prilipov, P.S. Phale, P. Gelder, J.P. Rosenbusch, R. Koebnik, Coupling site-directed mutagenesis with high-level expression: large scale production of mutant porins from *E. coli*, *FEMS Microbiology Letters*, 163 (1998) 65–72.
- [182] K. Sakata, Y. Tahara, K. Morikawa, Y. Fujiyoshi, Y. Kimura, A method for observing cross-sectional views of biomembranes, *Ultramicroscopy*, 45 (1992) 253–261.
- [183] T. Steinberger, R. Macháň, M. Hof, Z-Scan Fluorescence Correlation Spectroscopy as a Tool for Diffusion Measurements in Planar Lipid Membranes, in: Y. Engelborghs, A.J. Visser (Eds.), *Fluorescence Spectroscopy and Microscopy*, Humana Press, Totowa, NJ, 2014, pp. 617–634.

Acknowledgments

First of all, I would like to thank my PhD supervisor Prof. Dr. Wolfgang Meier for the opportunity to do my PhD research in his group providing such a great working place to perform research at a high level.

I want to thank Prof. Dr. Nico Bruns for being my coexaminer of my thesis. Prof. Dr. Thomas Pfohl is kindly acknowledged for being the chair. I also would like to thank Prof. Dr. Cornelia Palivan for her great advice during my PhD and her writing skills. Especially, I appreciate the continuing support from Prof. Dr. Manish Kumar via email and Skype. He always helped me when I needed a second or third, independent opinion about polymer- and membrane protein-related problems. Dr. Mohamed Chami is highly appreciated for his patience doing cryo-TEM on many many samples and for preparing the nicest freeze fracture samples. I am also very grateful to Vesna Olivieri and Ursula Sauder for letting me using the TEM.

This work and other projects would have never been possible with the help of collaborators in Switzerland (Prof. Dr. Lucio Isa and Dr. Reinhard Kissner at ETH in Zurich; Prof. Dr. Sebastian Hiller at Biozentrum, Basel), in Germany (Prof. Dr. Gerolf Gros and Prof. Dr. Volker Endeward at MHH, Hannover; Prof. Dr. Ralf Kaldenhoff and Dr. Norbert Uehlein at TU-Darmstadt), in Denmark (Joachim Habel at Aquaporin A/S and University of Copenhagen) and in the USA (Prof. Dr. Manish Kumar at Penn State University, Pennsylvania).

I thank Jason, Gesine, Adrian Dinu and Adrian Najer for critical proof-reading parts of the thesis. I appreciate the hard work of polymer synthesis by Dalin, Sven, Sam and Adi. Without their help I could not have performed this work, and many other persons in the group either. These polymers are not just simply synthesized.

I am also thankful to my colleagues and friends in the group, for their friendship and great atmosphere not only in the labs but also during free-time. I cannot list all the names here, but everybody is on the list.

On a personal level I thank my parents, who supported me during my studies and to do whatever I wanted to do. Thanks for your support and open house. Finally, I am most thankful to Chatrina for patience, support and her time spending with me.

Thanks to all of you.